INVESTIGATION OF HIGH LYING STATES USING SINGLE NUCLEON TRANSFER REACTIONS

By

Gwang Ho Yoo

A DISSERTATION

Submitted to
Michigan State University
in partial fulfillment of the requirements
for the Degree of

DOCTOR OF PHILOSOPHY

Department of Physics and Astronomy

1992

ABSTRACT

INVESTIGATION OF HIGH LYING STATES USING SINGLE NUCLEON TRANSFER REACTIONS

By

Gwang Ho Yoo

The reactions (^{7}Li,^{6}Li), (^{7}Li,^{6}He), (^{7}Li,^{8}Li), (^{12}C,^{13}N) and (^{12}C,^{13}C) have been measured at 30 MeV/n on the targets ^{90}Zr, ^{91}Zr, ^{89}Y, ^{208}Pb, ^{209}Bi and ^{207}Pb in order to investigate high lying states. Particles were analyzed using the S320 magnetic spectrograph. In each reaction, the measured spectra were plotted both as a function of the reaction Q – value and as a function of the excitation energy. A preference for the excitation of high spin states with no spin flip was observed. Broad resonance like peaks were observed in both proton and neutron stripping reactions at excitation energies close to the excitation energy of the giant quadrupole resonance. Comparison of reaction Q – values and the excitation energy spectra suggests that these broad peaks are due to the excitation of single particle states rather than a collective giant resonance. The existence of an extra particle or hole outside closed shell nuclei does not change the strengths of these broad peaks significantly, but does change the excitation energies significantly in some cases. Shell model calculations carried out in the ^{208}Pb region support this conclusion. Substantial backgrounds were observed in these stripping reactions. Calculations of these underlying backgrounds were carried out with the Serber model and with a semi-classical theory developed

by Brink and Bonaccorso. The Serber model calculations do not match the shape of the experimental spectra except at the very high excitation energies ($>$ 35 MeV) in proton stripping. The Brink-Bonaccorso model, does match the shape of the experimental spectra for neutron stripping reactions very well although it does not agree with the shape for the proton stripping case. The Brink-Bonaccorso model, also, predicts that for these bombarding energies, only 20% of the continuum arises from projectile breakup and 80% arises from the excitation of compound states in the residual nucleus. Strong peaks observed the (^{12}C,^{13}C) reaction on both ^{90}Zr and ^{208}Pb region targets appear to arise from the mutual excitation of bound $2s_{1/2}$, $1p_{3/2}$ and $1d_{5/2}$ excited states in ^{13}C along with low lying states of the residual nuclei. Broad peaks are observed for the (^{12}C,^{13}N) reaction on the ^{208}Pb, ^{209}Bi and ^{207}Pb targets at excitation energies about 18 MeV. The origins of these structures are not understood clearly.

ACKNOWLEDGEMENTS

I would like to thank my advisor Professor G. M. Crawley for his guidance and direction. His constant advice and support played the most important role to complete this thesis. Professors P. Danielewicz, B. Lynch, P. Schroeder and D. Stump are also thanked for their guidance and support.

There are many people whom I would like to thank: Prof. J. Finck for his reading and correcting my writting, Dr. J. S. Winfield for his help to prepare the experiment and for many discussions about the analysis, Profs. D. Brink and A. Bonaccorso for their help to calculate the background for the continuum states, Prof. A. Brown for his help to understand and use the Shell Model code and Prof. D. Cha for the fruitful discussions about the contents of my thesis, Dr. S. Gales, Dr. N. Orr and J. Yurkon for their help during the experiment. L. Zhao is thanked for the discussions on several questions. This work would have been impossible without the help of these people.

I would also like to thank all my friends, K. Joh, J. Kim, J. Yee and D. Jeon for their encouragement to finish my work at the NSCL.

I owe a large debt to my family, especially my parents, my wife's parents and my brothers who loved, encouraged and helped me to study throughout the years. Finally, I am specially grateful to my two children, Sung Hyun and Seok Hyun, and my wife, Soo Gyung for their endless understanding, patience and love.

Contents

List of Tables

List of Figures

Chapter 1

Introduction

1.1 Motivation

The study of deep lying hole states and high lying particle states has been an interesting area of research and many investigations have been carried out particularly for nuclei near closed shells. These studies provide information on the strength distribution (position and width) of high lying single particle states, deep lying single hole states, and the mechanism that spreads these states. Such information is useful for calculations of more complicated excitations, such as giant resonances (GR) and multiple particle/hole excitations. The single particle transfer reaction is a simple method for studying hole states in heavy target nuclei compared to knock out reactions such as $(e, e'p)$ and $(p, 2p)$ which require coincidence measurements, and is the only way of observing particle states at high excitation in heavy nuclei. This method has proved successful particularly at lower excitation energy for light ion induced reactions such as (p,d), (^{3}He,^{4}He) and (^{4}He,^{3}He) [Kasa 83, Gerl 75, Mass 86]. These experiments found single particle and single hole state strengths ranging from discrete peaks at low excitation to large broad peaks at high excitation energy. The couplings to more complicated collective excitations such as phonon excitations were found to play a very important role in spreading the strength of the simpler states [Gale 85].

Unfortunately, in light ion reactions the poor peak to background ratio makes it difficult to use these reactions to study highly excited states. The major source of the background at high excitation energy is the breakup of the projectile. This background must be subtracted to obtain the strength of the peaks of interest, and has usually been estimated empirically. Several theories have been proposed to calculate the background. For example, the Serber Model [Serb 48] explains the background very well in light ion induced nuclear reactions, but it does not explain the background well in heavy ion induced reactions. A semi-classical theory developed by Brink and Bonaccorso [Bona 85, Bona 88] explains the shape of the background very well in a number of neutron stripping reactions, although it does less well in proton stripping reactions. Both of these models will be discussed in more detail in chap. 6 [Wu 78, Wu 79, Bona 91].

Heavy ion reactions at high energies are expected to be more selective of high spin states which might therefore become stronger relative to the background [Brin 72] than in light ion induced reactions. However, to make use of these reactions for studying high lying states, some questions remain to be answered. Recently, it has been reported in the ^{208}Pb(^{20}Ne,^{19}Ne) and the ^{90}Zr(^{20}Ne,^{19}Ne) reactions at 25, 30, 40 MeV/n [Fort 90, Fras 87] and in the ^{208}Pb(^{12}C,^{11}C) reaction at 40 MeV/n [Merm 88], that large broad peaks were observed at excitation energies which are close to the excitation energies of the giant quadrupole resonance (GQR), viz. 10.5 MeV for ^{208}Pb and 13.5 MeV for ^{90}Zr. A broad peak was observed at a similar energy in the (^{4}He,^{3}He) reaction at 46 MeV/n on a ^{208}Pb target [Mass 86] and in the (^{16}O,^{15}O) reaction at 20 MeV/n on a ^{197}Au target [Olme 78]. However, the broad peaks in the vicinity of the GQR were not observed in the (^{7}Li,^{6}Li) and (^{16}O,^{15}O) reactions at 20 MeV/n on a ^{208}Pb target [Becc 87, Olme 78] nor in the (^{4}He,^{3}He) reaction at 46 MeV/n on a ^{120}Sn target [Gale 85]. When these broad peaks are observed in transfer reactions,

they have excitation energies, widths and strengths consistent with the known GR states [Fort 90, Fras 87, Fras 89, Duff 86, Olme 78, Gale 91]. (Some experimental transfer reaction spectra with broad peaks are shown in fig. 1.1.) Whether these peaks are from the excitation of GR states or from broad single particle states is not clear.

The GR is known to be a $1p-1h$ excitation in which many nucleons are involved. Most information on GRs has been obtained through the inelastic scattering of light ions [Youn 76], and heavy ions [Fras87a, Suom 89, Suom 90]. So far the evidence for the excitation of GR states by transfer reactions is less convincing. According to RPA theory, however, closed shell nuclei may contain some admixtures of $p-h$ states in the ground state [Ring 80]. When a nucleon is transferred to these closed shell target nuclei, this nucleon may couple to the existing hole state in the target by a single step mechanism and thus excite a component of a GR. A similar processes of forming a GR may be possible by a pickup reaction on a closed shell target plus one nucleon [Fras 89, Chom 86]. The formation of a GR state in a transfer reaction was mentioned by Olmer et al. [Olme 78]. But the experimental data were not enough to provide a convincing identification of the broad peaks observed in the transfer reactions as GR states.

Giant resonance states and single particle states have different properties, and it may be possible to distinguish between them. In GR excitations, the motion is highly collective and many particles in the nucleus are involved. The excitation energies of GR states change very smoothly with the mass of the nucleus. On the other hand, for single particle states, only a few particles are involved and the excitation energies of similar single particle states may change substantially even for neighboring nuclei. For a closed shell target, both proposed explanations lead to similar behavior, therefore it is difficult to distinguish between these two explanations by measurements on only

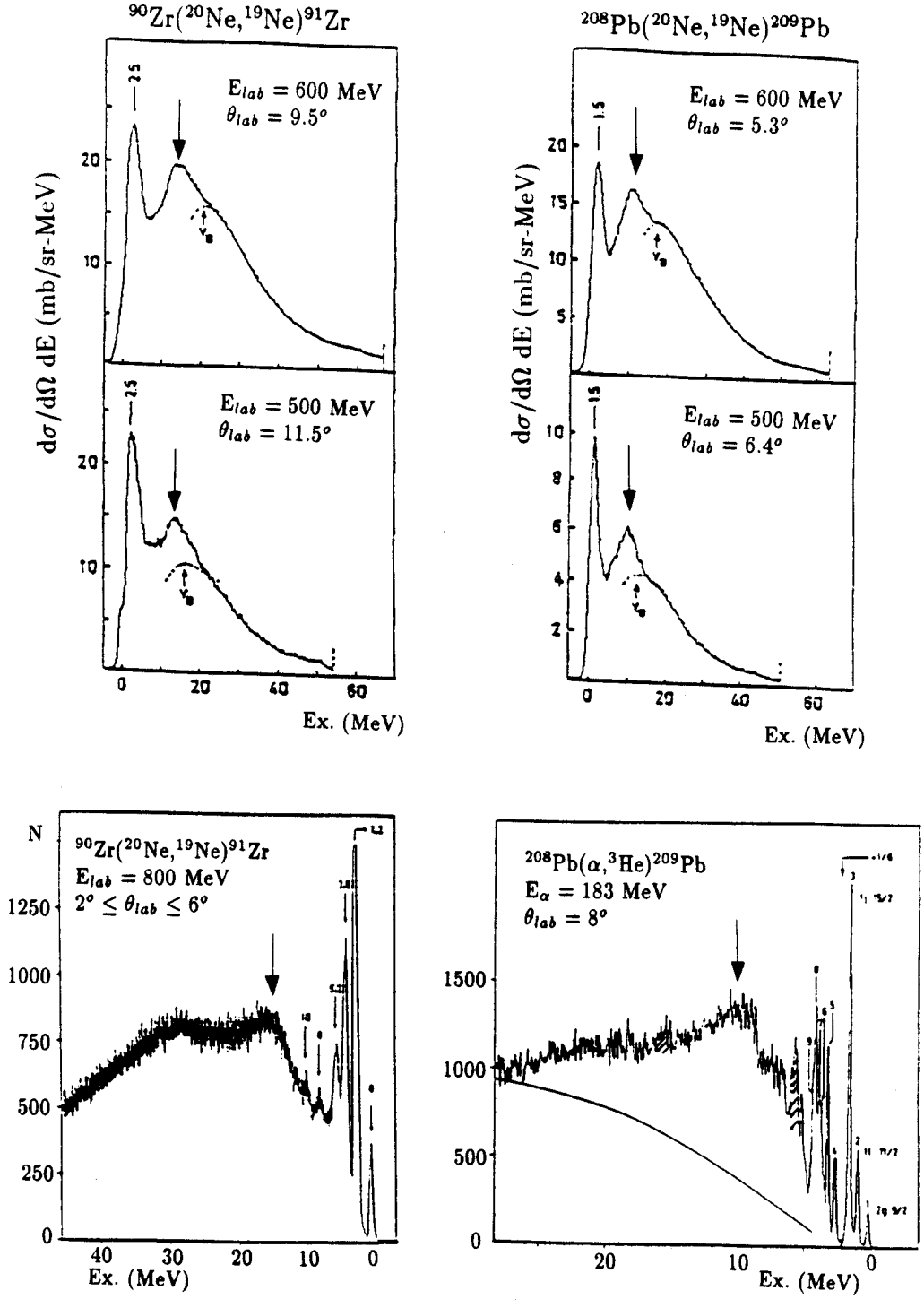

Figure 1.1: Broad peaks obtained by a neutron transfer reactions. The properties of the broad peaks (marked with arrows) are very similar to those of GR states [Fort 90, Fras 87, Mass 86].

closed shell targets. However, if the spectrum from a closed shell nucleus is compared with spectra from the same reaction for neighboring *even – odd* targets, one can distinguish the two models, because in this case one expects that the differences are large enough to be observable.

In this thesis, heavy ion transfer reactions have been investigated on even and odd A targets to try to resolve the question as to whether the broad peaks observed these reactions arise from GR excitation or from the excitation of single particle states. In addition, the underlying background observed in stripping reactions has been calculated using different models and the calculations have been compared to the experimental data.

1.2 Selection of Targets and Projectiles

The choice of targets was based on the following considerations. Consider a neutron stripping reaction on the *even – even* target ^{208}Pb leading to the residual nucleus ^{209}Pb. The low lying states formed in ^{209}Pb are the well known single neutron states which lie above the closed N=126 core. If the same reaction is carried out on the neighboring nucleus ^{209}Bi which has an extra $1h_{9/2}$ proton outside the Z=82 core, multiplets of states are formed from the coupling of the $1h_{9/2}$ proton with the aforementioned neutron states. These multiplets occur at about the same excitation energies in ^{210}Bi as the corresponding single neutron states in ^{209}Pb. However a different situation arises if a ^{207}Pb target is used. The ^{207}Pb nucleus has a $3p_{1/2}$ neutron hole state in the closed N=126 shell. Therefore the 0^+ ground state of ^{208}Pb is formed when a neutron is added to this hole. As a neutron is added to other higher lying neutron particle states, multiplets are produced due to the coupling of the $3p_{1/2}$ neutron hole with the neutron particle states. The excitation energies of these multiplets are

shifted to higher excitation approximately by the difference between the 0^+ ground state and the first multiplet. Such effects arise from rather general properties of single particle transfer reactions on neighboring nuclei. In contrast, the excitation energies of collective states like the GR change by much less than 0.1 MeV with a change of one in the mass of the target. Thus one may distinguish between collective and single particle states by measuring stripping reactions on ^{208}Pb, ^{209}Bi and ^{207}Pb. Similar behavior is expected for stripping reactions in the vicinity of closed shell target ^{90}Zr where one may perform a similar study using ^{90}Zr, ^{89}Y and ^{91}Zr targets.

Thus, reactions were measured for two *even – even* nuclei ^{208}Pb and ^{90}Zr and their neighboring nuclei, four *even – odd* nuclei ^{207}Pb, ^{209}Bi, ^{89}Y and ^{91}Zr as targets.

In choosing the projectiles, two conditions were considered. First, the ejectile excitations should be minimized to prevent the occurrence of spurious peaks in the spectrum from ejectile excitation. The problem of ejectile excitation may be reduced by using unbound or very weakly bound ejectiles such as *d*, ^{6}He, ^{6}Li, ^{8}Li and ^{13}N. Since the ejectiles excited above their "breakup threshold" decay into two or more fragments, they will not contaminate the spectrum at energies above this threshold. Second, the projectile energy should be high enough to excite the high lying states. However, as the projectile energy increases, the resolution becomes worse and the cross section for the breakup process increases faster with bombarding energy than the cross section for transfer reactions. To excite a high spin state, heavy ions are better than light ions, but the resolution is not as good as for light ions at the same projectile energy per nucleon. Thus, a compromise had to be made in choosing the projectiles and bombarding energies.

For the nucleon stripping reactions (^{7}Li,^{6}Li) and (^{7}Li,^{6}He), the projectile was chosen because the resultant ^{6}He and ^{6}Li ejectiles have threshold energies for breakup which are lower than the energies of their first excited states. In this case, one

expects ejectile excitation to be negligible. However projectile breakup still remains a dominant source of background at high excitation energies. The ^{7}Li beam is not suitable for measuring the proton pickup reaction (^{7}Li,^{8}Be), because ^{8}Be has a lifetime which is too short to be detected in the focal plane of the S320 spectrograph. Instead, the proton pickup reaction was measured with a ^{12}C beam, which again produces an ejectile ^{13}N for which the threshold energy for breakup is lower than the energy of the first excited state. For neutron pickup, both the (^{7}Li,^{8}Li) and (^{12}C,^{13}C) reactions were measured in order to estimate the contributions from ejectile excitation.

These reactions were measured at a projectile energy of 30 MeV/n because at this energy a large bump has already been seen in the ^{208}Pb(^{20}Ne,^{19}Ne) reaction [Fort 90].

1.3 Outline

In chapter 2, the experimental setup and procedures are described. These include the target preparation, detection system, electronics, and the method of calibration.

In chapter 3, shell model calculations useful for the description of one nucleon transfer reactions on ^{207}Pb and ^{209}Bi nuclei are presented. These calculations provide information on the energy levels of the multiplet states, such as the excitation energies, spectroscopic factors, and the shift of the centroid energy of the multiplets. The calculations are compared with the experimental data.

In chapter 4, the characteristics of the single particle states and GR states, and the method used to distinguish between the two states are described. The data obtained at the same kinematic conditions on *even – even* targets and *even – odd* targets for ^{90}Zr region and ^{208}Pb region are compared as a function of both the reaction Q – values and the excitation energies.

In chapter 5, the results for the one nucleon stripping reactions are presented. The

spectrum from the closed shell target nucleus is compared with the spectra from the neighboring targets. The relative strengths between the states are explained by the angular momentum transfer matching conditions. Evidence relevant to the nature of the broad peaks is presented.

In chapter 6, the background for the stripping reaction is described. Two theories for calculating the background: the Serber Model, and the Semi-Classical theory developed by Brink and Bonaccorso, are outlined and the corresponding calculations are compared with the experimental measurements. In addition, a test run for a coincidence measurement aimed at providing more information on the background is described.

In chapter 7, the results for the one nucleon pickup reactions are described. Ejectile excitation is shown to present significant problem for the interpretation of the neutron pickup reactions. The nature of the high lying peaks is discussed.

In chapter 8, a summary of this thesis and suggestions for future work are described briefly.

Chapter 2

Experimental Setup and Procedures

The transfer reactions (^{7}Li,^{6}Li), (^{7}Li,^{6}He), (^{7}Li,^{8}Li), (^{12}C,^{13}C) and (^{12}C,^{13}N) were carried out at a bombarding energy of 30 MeV/n using the K500 superconducting cyclotron at Michigan State University. The average beam current was between 10 and 20 particle nA (pnA). The targets used in this experiment, ^{89}Y, ^{90}Zr, ^{91}Zr, ^{207}Pb, ^{208}Pb and ^{209}Bi were all self supporting and had thicknesses of about 5 mg/cm^2. The thicknesses were chosen on the basis of the transfer reaction cross sections, counting rate, and the energy resolution for the given beams. The reaction products were analyzed with the S320 broad range magnetic spectrograph [S320 90] and detected by the focal plane detector system. In each reaction, the ejectiles were measured at the grazing angles to give large cross sections. The energy resolution was about 500 keV full width at half maximum (FWHM) for the ^{6}Li and ^{6}He spectra, and about 1 MeV FWHM for the ^{12}C, ^{13}C and ^{13}N spectra. In this chapter, the experimental equipment, procedures and analysis methods are described.

2.1 Target Preparations

Six targets, ^{89}Y (5.30 mg/cm^2, 100%), ^{90}Zr (5.06 mg/cm^2, 97.62%), ^{91}Zr (5.01 mg/cm^2, 88.5%), ^{207}Pb (4.95 mg/cm^2, 92.40%), ^{208}Pb (5.84 mg/cm^2, 99.14%) and ^{209}Bi (6.50 mg/cm^2, 100%) were used in this experiment. The ^{89}Y target was purchased from the Johnson Matthey Company. The original thickness of the yitrium target was 11.18 mg/cm^2 when it was purchased. A target of thickness, 5.3 mg/cm^2, was obtained by using a rolling machine. The thickness was determined by measuring the energy loss of α-particles emitted from an ^{241}Am source. The uniformity was $\pm$0.2 mg/cm^2 over the central region of the target. This method was verified by weighing the target. There was about a 10% difference between the two methods. This caused an uncertainty up to 10% in the absolute cross section.

The ^{209}Bi target was fabricated at Michigan State University using vacuum evaporation. When pure ^{209}Bi metal was heated in the furnace in a vacuum chamber, ^{209}Bi molecules evaporated and were deposited on a glass plate which was coated with detergent and placed about 15 cm above the ^{209}Bi source. The growth rate was dependent on the temperature of the furnace. The on-line measurement of the thickness of the target using a quartz crystal vibrator provided a rough indication of the thickness. The thickness was measured again after the target was floated off the glass slide. The exact thickness was obtained by measuring the energy loss of α-particles. The uniformity of the target was within $\pm$0.4 mg/cm^2.

The other targets, ^{90}Zr, ^{91}Zr, ^{207}Pb and ^{208}Pb were purchased from the Micro Matter Company. No noticeable sign of oxidation of the targets was observed in the data.

2.2 S320 Spectrograph

The reaction products were analyzed with the S320 magnetic spectrograph and charged particles were detected in a standard focal plane detector. This spectrograph has a K-parameter of 320, where K is defined by the equation $E/A = K(q/A)^2$, where E/A is the maximum allowable kinetic energy in Mev per nucleon, and q is the charge of a reaction product [S320 90]. The S320 spectrograph is designed to be operated in the dispersion matched mode. The kinematic effects due to the finite angular acceptance of the spectrograph are compensated by refocusing the quadrupole doublet according to the kinematic parameter of the reaction. The particles scattered from the target into a given solid angle and having the same momenta could be focused on the same position of the focal plane detector. The dynamic range in momentum covered by the spectrograph in a single setting is $\Delta P/P = 10\%$, the maximum solid angle is 0.67 msr and the angular range is from – 4 to 55 degrees. A schematic view of the S320 spectrograph is given in fig. 2.1 and some important parameters of the spectrograph are given in table. 2.1.

The S320 spectrograph is composed of a target chamber (or a scattering chamber), QQDMS (Quadrupole, Quadrupole, Dipole, Multipole (which is predominantly Octupole) and Sextupole) magnets and focal plane detectors. The target chamber is a precision scattering chamber with a sliding seal. The inner diameter is 39 cm and the inner height is 15 cm. The upper part of the chamber, including the lid, is braced to the wall and does not move. At the center, there is a target ladder with a circular platform. The target ladder can move up and down, and the ladder and the platform assembly may be rotated together independently of the spectrograph rotation. A total of 6 targets could be mounted in the target ladder at a same time. One target position was used for a scintillator of CsI crystal as a beam viewer. An-

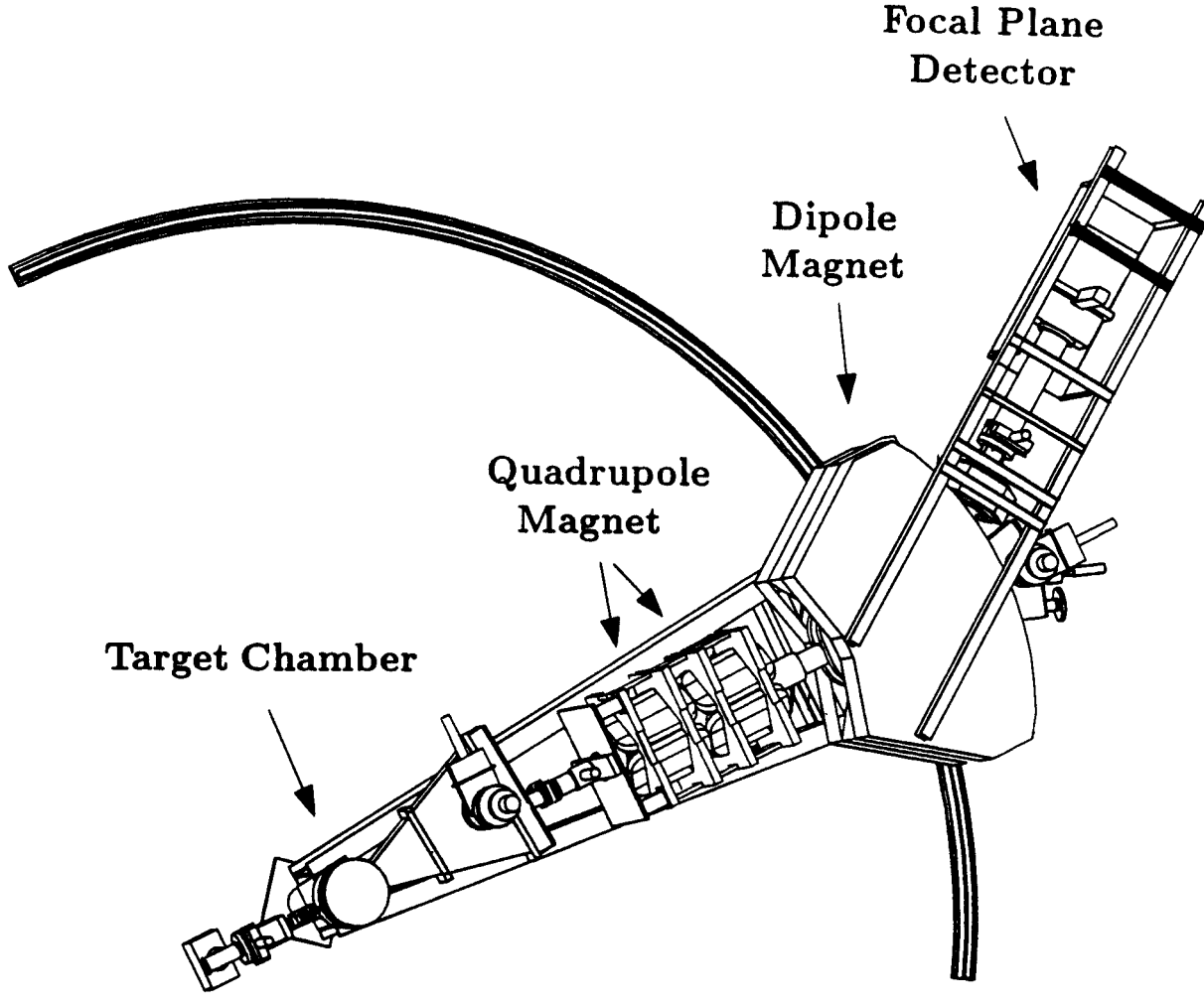

Figure 2.1: Schematic view of the S320 spectrograph.

Table 2.1: Parameters of the QQDMS S320 spectrograph.

Quad(Y) – Quad(X) – Dipole – Octupole – Sextupole	
Dispersion:	D = 1.6 cm/% ($\Delta p/p$)
Magnification:	Mx = −0.67 (D/M = 2.4)
	My = −2.5
Max. solid angle:	$\Delta\theta$ = 12 mr
	$\Delta\phi$ = 12 mr
	Ω = 0.67 msr
Beam spot on target (assumed):	
	0.5 mm incoherent width
	3 mm tall, dispersion matched
	2.4 mm dispersed beam width for 0.1% energy spread
Calculated line width (ray tracing):	
	$\Delta E/E$ = 0.1%, 0.8 mm
Range:	$(E_{max}-E_{min})/E$ = 20%
Focal plane:	Normal incidence, 18 cm long x 2.6 cm tall
Bend angle:	34.4°
Max rigidity:	$B\rho$ (max) = 2.57 T–m @ 1.47 T
	ρ (max) = 1.75 m
Central ray radius:	ρ (mean) = 1.70 m
Distance target → aperture:	1.965 m
Distance target → focal plane:	6.75 m
Distance target → scintillator:	7.12 m
Angular range:	−4° to 55°

other was used to hold a blank target to check the target frame contribution to the background, and a third one was used for a thin ^{12}C target for calibration. Therefore only three targets for reactions would be mounted at the same time in the ladder during the experiment. Two monitor detectors (bare photodiodes) were used. They were mounted on the lid of the chamber which is stationary and were located at a distance of 15 cm from the target. The distance between monitors was 1.5 inches and they were located at the lower left and lower right from the beam path. The aperture of the spectrograph is located at a distance of 196.5 cm from the target. Four different types of apertures, round holes of 8 mm and 25 mm diameter, a square 50 mm X 50 mm aperture and a 19 mm X 40 mm rectangular slit could be inserted remotely depending on the counting rate required.

There are two kinds of Faraday cups mounted in the S320 spectrograph. These cups stop the beam and accumulate the charge passing through the target. One is mounted in the wedge chamber for small angles, ranging from 1.5 to 9.5 degrees. The other one is mounted on the lid of the target chamber and is therefore independent of the spectrograph rotation. The minimum spectrometer angle such that this latter Faraday cup does not obscure the aperture is about $2.9 + W/2$ degrees, where W is the full opening angle of the spectrometer aperture. The biggest width of the aperture used in this experiment was 5 cm. In this case that W would be 1.46 degree and the minimum spectrometer angle possible would be 3.63 degree. Because the spectrometer angles used in the present experiments are 6 and 9 degrees, only the target chamber Faraday cup was used in this experiment.

The main role of the QQDMS magnet system is to separate the particles spatially on the focal plane where they are detected by a position sensitive detector according to the momentum and charge state of the particles. One of the quadrupole magnets focuses the particles in the Y – direction and the other one in the X – direction. The

dipole magnet bends the particles according to their magnetic rigidity $(B{\cdot}\rho = P/q)$, where P is the momentum and Q is the charge of the particle, B is the magnetic field and ρ is the orbit radius. The multipole and sextupole magnets are used to help focus the particles at the focal plane of the detector and to minimize the aberrations.

2.3 Focal Plane Detectors

The focal plane detection system of the S320 spectrograph is composed of three modular units: position sensitive counters, ion chambers, and scintillators. A schematic view of the detector system is given in fig. 2.2. A position sensitive single wire proportional counter (SWPC) is followed by two ionization chambers (IC), then another SWPC and scintillator (SCNT). All the gas detectors operate with the same gas volume and thus have the same pressures and are separated from the spectrometer vacuum by a Kapton window of thickness 25 microns which can hold a pressure difference of one atmosphere. Depending on the charges and the energies of the reaction products, different types of gases and pressures were used. For the ^{12}C beam, 100% isobutane gas was used at 70 torr, and for the ^{7}Li beam, a mixture of 20% of isobutane gas and 80% of freon gas was used at 140 torr. The mixed gas does not have as large a gain as the pure isobutane gas. However the uniformity in the mixed gas is better than that of pure Isobutane gas and less sensitive to poisoning. With the ^{7}Li beams, because there was no difficulty in particle identification, the mixed gas was used for better uniformity.

The SWPC detector enables one to obtain the position spectra using the charge division method (the relative ratio of the pulse heights from the two ends of the resistive wire). For precision measurement of the particle position, the gains of the amplifiers (front wire left and front wire right, back wire left and back wire right)

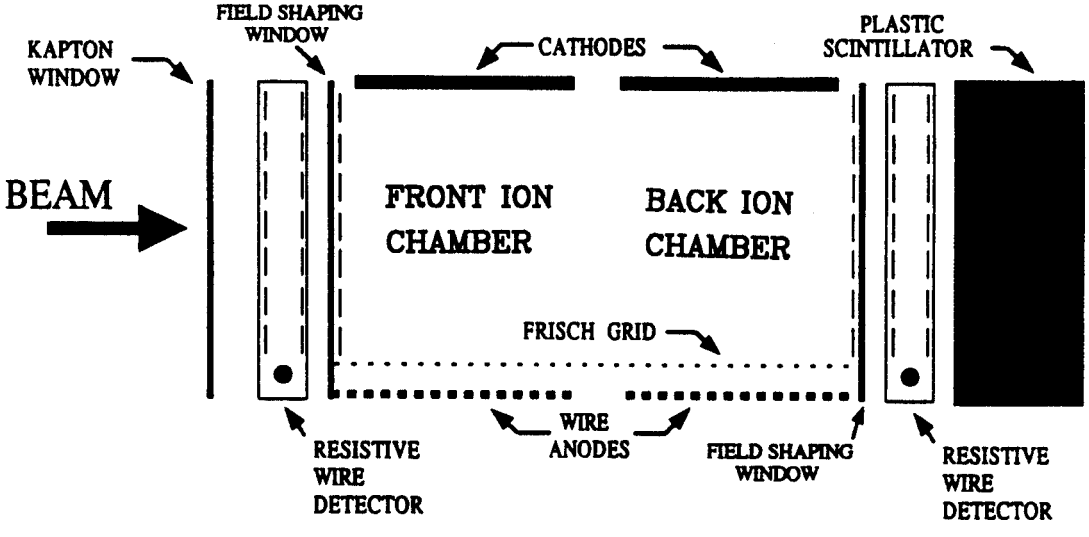

Figure 2.2: Schematic view of the focal plane detector [Moha 91].

were matched using a test signal. Adjustments for all the other amplifiers were also done before taking the data and the initial settings were not changed until the end of the experiment. A stopping scintillator is mounted behind the gas detectors. This is composed of a thin (0.51 mm) fast scintillator and thick (10 cm) slow scintillator. The output signal is the sum of the fast and slow scintillator signals and this signal was used as a start signal. The time of flight of the particles was obtained by measuring the difference between the cyclotron RF and the scintillator signal.

2.4 Electronics

The electronics used for the data taking is displayed in fig. 2.3. The same electronic setup is used for most experiments with the S320 spectrograph. Ten signals were obtained from the various detecting modules and were recorded after they were processed by the electronics. A S320 spectrograph event was normally defined by the total scintillator signal (fast + slow) above a constant fraction discriminator (CFD) level. The signals from the scintillator left and scintillator right passed through the coincidence checking circuit. When the two signals were above a CFD level and coincident, a true event was assumed and the output signal from the coincidence checking circuit was used as a start signal (or a S320 master signal). This signal was used to open the gates of the ADC and QDC modules, and as a start input of the TDC and the TAC. The signals detected from the two wire counters, two ion chambers and two monitors were digitized with an ORTEC AD811 analog to digital converter (ADC) and the signals obtained from the scintillator were digitized with a LECROY 2249W charge to digital converter (QDC). From the left and right signals from each wire counter, the position was calculated, and the difference between the two detected positions of the wires was used to measure the scattering angle relative to the central angle of the spectrograph. The TDC signals were used for the time of flight

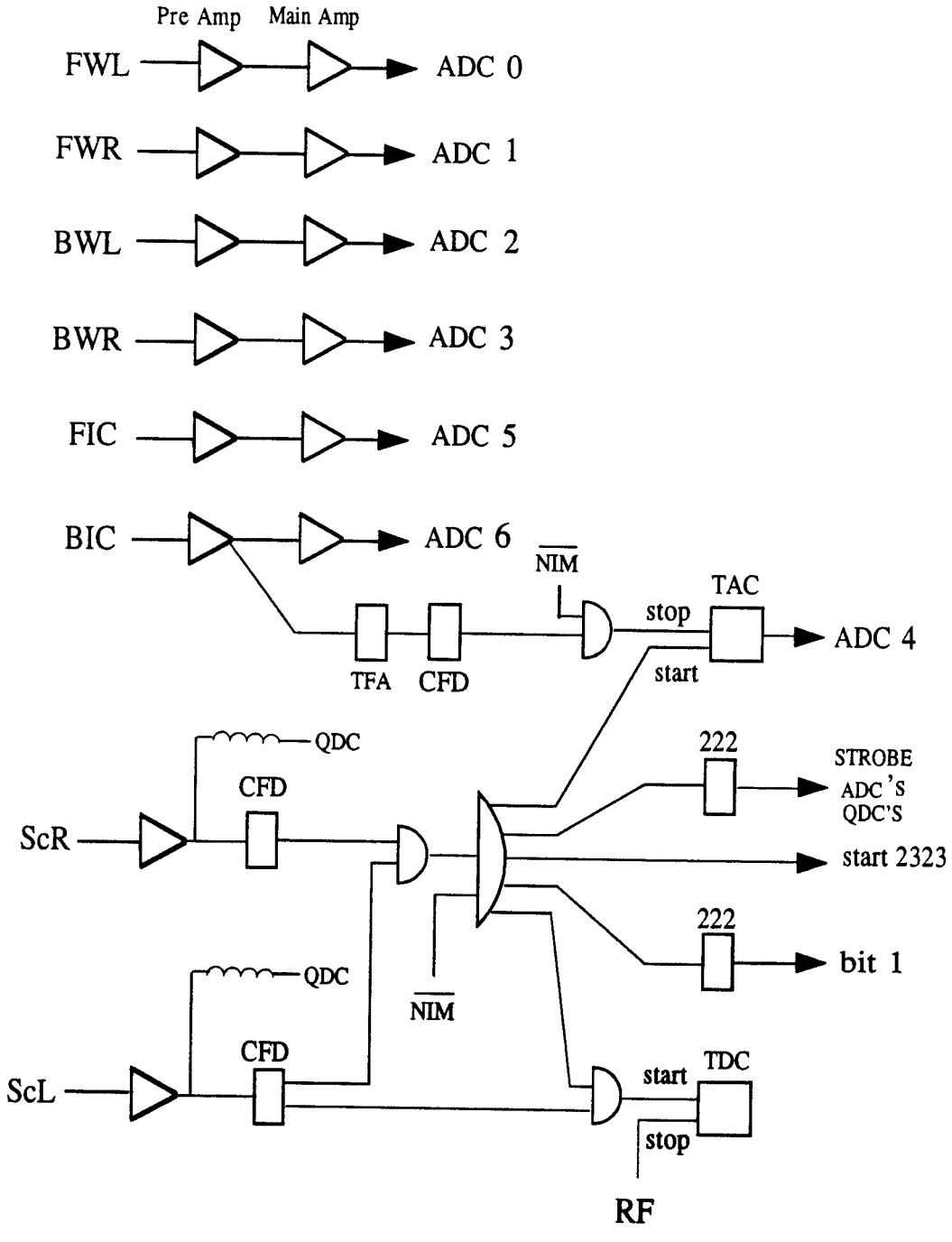

Figure 2.3: Schematic view of the S320 electronics [S320 90].

(TOF) information. For the TOF relative to the cyclotron RF, the TDC was started by either the left or the right scintillator delayed CFD output and was stopped by the cyclotron RF signal. A time to pulse height converter (TAC) signal was used to find the vertical position in the front ion chamber by measuring the drift time of the electrons. The TAC was started by the S320 master signal and stopped by one of the front ion chamber signals. The TAC signal was read by an ADC.

The signals which were digitized by ADC, QDC or TDC were recorded by the program ROUTER in the VME bus front ends based on multiple MC680x0 architecture processors as part of CAMAC data acquisition system [Fox 85, Fox 89, Sher 85]. The flow diagram of the data taking system is given in figs. 2.4 and 2.5 [Winf 91]. This system blocks the recorded events into 8192 byte buffers and then sends them back to the VAX/VMS system for on-line event recording and analysis. The buffered data are read by the program ROUTER and sent to specified subprocesses. There are three main subprocesses. One is a scaler display task which sums and displays scaler totals, and another is a tape writing task which writes the data buffers to tape. The other one is a data analyzing program, SARA [Sara 90], which identifies the particles and creates displays on the terminal. During the experiment, a fraction of the total data was displayed on the terminal and analyzed on-line as a check on the progress of the experiment.

2.5 Magnetic Field Setting

There are five magnets (QQDMS) which need to to be set to focus the particles on the focal plane. The functions of these magnets were described in section 2.2. The values for the field settings were obtained by executing the program *nscl_library* : [*setup.s*320]*s*320.*exe* with the inputs such as reaction formula, lab. angle, energy/n

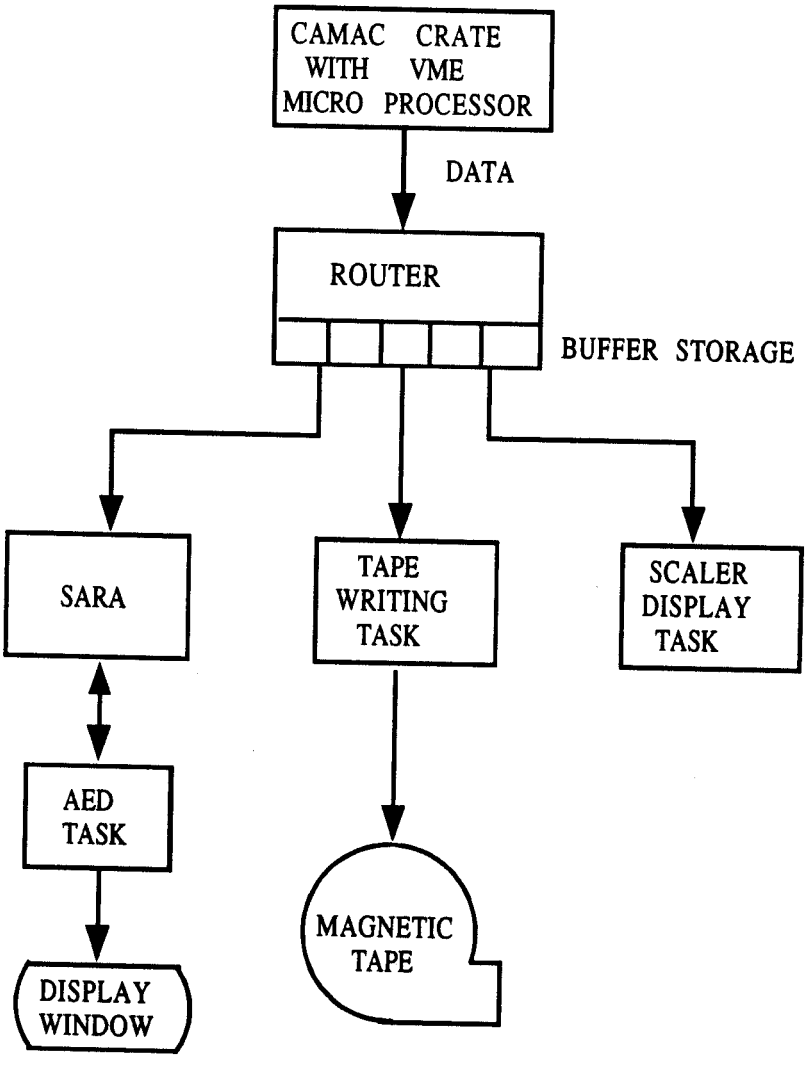

Figure 2.4: Flow diagram of on-line data taking system [Winf 91].

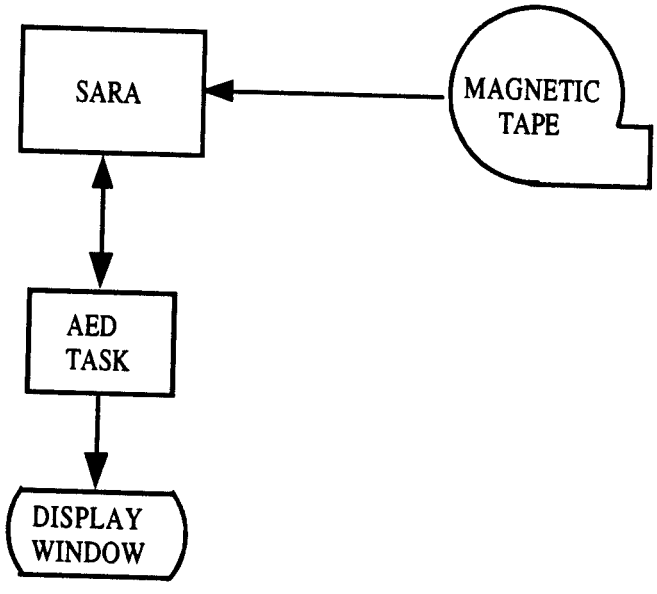

Figure 2.5: Flow diagram for off-line data taking system. [Winf 91]

and excitation energy of the residual nucleus. This program calculates the kinetic energies of the reaction products, magnetic fields of 5 magnets, grazing angles, C.M. angles for the given lab angles and time of flight. The masses of the particles were taken from the mass table of nscl_library : [mass86] mass86obj/lib. The magnetic fields were calculated with fully relativistic kinematics and were based on empirical calibrations. For each reaction, the fields were reset because of the different kinematics. The dipole field was measured with the SENTEC NMR system. When the dipole field strength was higher than 14 *kGauss* as was the case for the (^{7}Li,^{6}He) reaction, the field measured by the NMR probe was not very stable.

The calculated field settings focus the highest energy particles of interest on the middle of the focal plane single wire proportional counter (SWPC).

2.6 Particle Identification

The particle identification was done using the program *SARA* which allows gate and contour setting, and histogramming with or without conditions [Sara 90]. The gates can be set on the AED terminal by marking two points on a one dimensional histogram or by drawing a contour on a two dimensional plot which is composed of two parameters out of energy loss in ion chamber (ΔE), light out of scintillator (E), time of flight (TOF), and position in the focal plane (POS). The ion chamber was filled with a mixed gas of freon (80%) and isobutane (20%) at a pressure of 140 torr for the ^{7}Li beam and 100% isobutane gas at pressure of 70 torr for the ^{12}C beam. The energy loss in this chamber is proportional to Z^2/v^2, where Z is the charge state and v the velocity of a detected particle. The particles separate cleanly when Z is different at a similar energy per nucleon. TOF is proportional to M/Z where M is a mass of a particle. This permits good separation of a particle which has a different

mass from particles which have the same charge states. The program *SARA* was used for both on-line and off-line data analysis. In the on-line analysis, this program was used to display a sample of the collected data on the AED terminal. By setting the gates or contours on the spectra of the terminal while taking the data, spectra of specific reaction products could be checked to see if the data acquisition process was working correctly. In most of the reactions, two contours were used on the two dimensional spectra of $\Delta E.vs.E$ and $TOF.vs.POS$.

In the off-line analysis, clearer particle identification was possible. In the (^{7}Li,^{6}Li) reactions, because any single contour was not enough to separate ^{6}Li particles clearly, two contours on the $\Delta E.vs.E$ and $TOF.vs.POS$ spectra were used. The particles of charge state 3 were separated using the $\Delta E.vs.E$ spectrum and ^{6}Li particles were separated using the $TOF.vs.POS$ spectrum.

In the (^{7}Li,^{6}He) reactions, only ^{6}He, and ^3H which came from the direct breakup of ^{7}Li$\rightarrow^4$He + ^{3}H were detected. Because of big differences of Z^2/v^2 between the two particles, ^{6}He particles were cleanly separated in the $\Delta E.vs.E$ spectrum.

In the (^{12}C,^{13}C) reactions, because the magnetic rigidity (P/q) of ^{13}C is not much different from that of ^{12}C, the elastically scattered ^{12}C particles were also detected at the focal plane corresponding to excitation energies of about 25 MeV in the residual nuclei. Because the counting rate of elastically scattered ^{12}C particles was much larger than ^{13}C particles, the ^{12}C particles were blocked by using a "finger". The particle identification was done with two contours on the $\Delta E.vs.E$ and $TOF.vs.POS$ spectra.

In the (^{12}C,^{13}N) reactions, elastically scattered ^{12}C particles did not disturb the detection of ^{13}N particles and no blocking finger was used. The particle identification was done with the same method as for the ^{13}C particles. Some typical two dimensional spectra and contours for particle identifications are shown in fig. 2.6

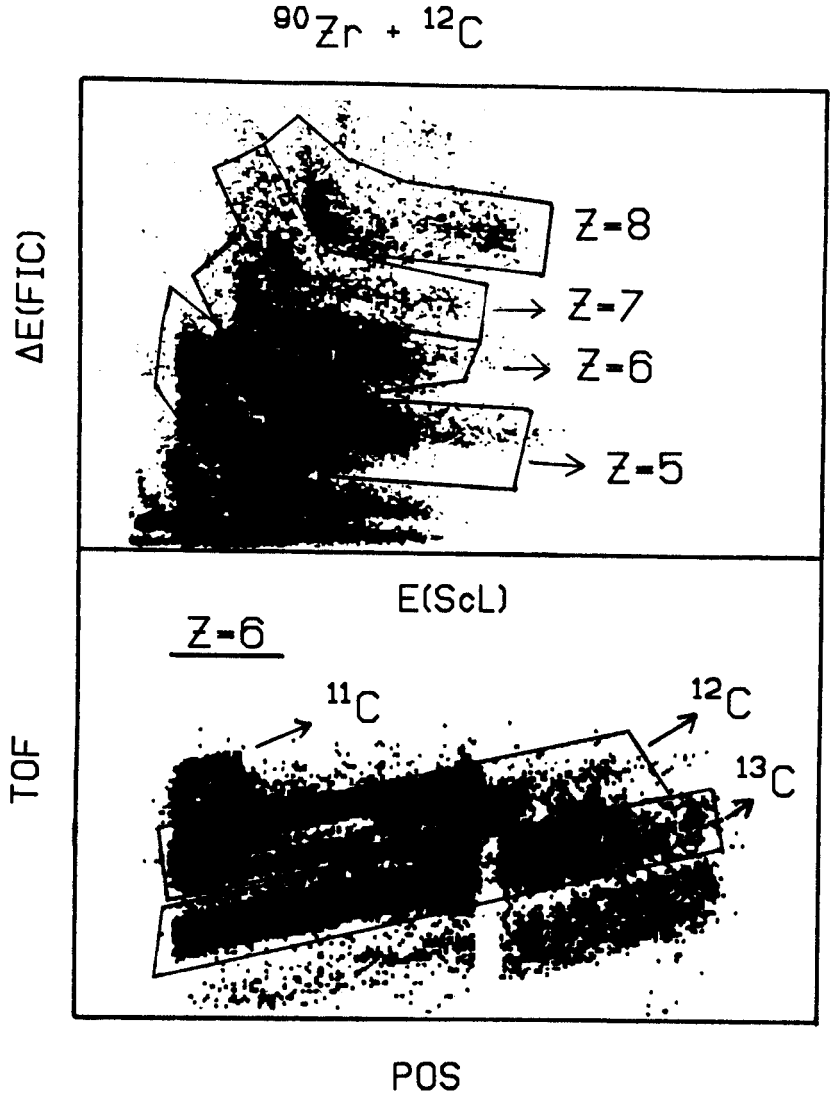

Figure 2.6: A sample of particle identification in two dimensional spectra for ^{90}Zr + ^{12}C reaction.

2.7 Energy Calibration

Energy calibration enables one to find the relation between the energies and the channel numbers of various particles detected in the focal plane detector. From magnetic rigidity, $B \cdot \rho = P/q$, the orbit radius ρ in a known magnetic dipole field B can be calculated for a detected particle of momentum P and charge state q. The orbit radius may be expressed in terms of a channel number using a simple polynomial of specified order. Normally a second order polynomial is sufficient. Then the relation between the calculated orbit radius ρ and the measured channel number x is given as

$$\rho = a + b \cdot x + c \cdot x^2. \tag{2.1}$$

To obtain the coefficients a, b and c at least 3 different settings of B and x are required. For the calibrations of this experiment, channel number x was obtained by changing the magnetic field B, with the same target at a fixed scattering angle. Once the calibration is done for a specified particle, the momentum and the related physical quantities can be extracted from the measured channel number, and this calibration may be applied to calibrations of energy spectra for other particles which have similar mass and energy. The calibration obtained for the ^{6}Li spectra may be applied to the calibration of ^{6}He or ^{8}Li spectra, but may not be acceptable for the calibration of ^{13}C or ^{13}N spectra because of the big differences in energies and momenta, and the nonlineality of the energy calibrations.

In this experiment, the ^{6}Li and ^{6}He spectra were calibrated using the reactions ^{12}C(^{7}Li,^{6}Li) and ^{12}C(^{7}Li,^{6}He). To minimize the uncertainty in the calibration due to the energy loss in the target, a very thin ^{12}C target (0.48 mg/cm^2) was used. For calibrations of ^{13}C and ^{13}N spectra, ^{12}C spectra on a target of ^{90}Zr of thickness 5.3 mg/cm^2 were used with elastic scattering reactions. The reason that ^{12}C spectra were

used instead of ^{13}C or ^{13}N spectra is that the ground state of ^{89}Zr or ^{89}Y was not separated cleanly from the excited states. The calibration coefficients were obtained by executing the program $NSCL\_LIBRARY : [SETUP.CALLIB]CAL88.EXE$. A detailed description is given in ref.[S320 90]. The fitted calibration curves for the ^{6}Li, ^{6}He and ^{12}C spectra are given in fig. 2.7.

The relativistic momentum P can be calculated for a given reaction, with known x, B and q. Then it is possible to predict the location or the channel number of a known state, or determine the excitation energy, reaction Q – value and particle's kinetic energy for a given channel number. To find the excitation energy corresponding to the ejectile's kinetic energy some relativistic kinematics are required. A diagram depicting the initial, intermediate, and final systems involved in the kinematics of transfer nuclear reaction is given in fig. 2.8. E_n, M_n and P_n are kinetic energy, mass and momentum of the n^{th} particle just before and after the reaction. It is assumed that the reaction happened at the middle of the target. As the particle's momentum and the position are measured after the reaction using the S320 spectrograph, it is necessary to compensate for the energy loss in the target. Thus the final form for the residual nucleus's excitation should be expressed in terms of the initial and final system's known parameters. The x and y – components of the momentum must be conserved, i.e.

$$P_1 = P_3 \cdot \cos\theta + P_4 \cdot \cos\psi, \tag{2.2}$$

$$P_3 \cdot \sin\theta = P_4 \cdot \sin\psi. \tag{2.3}$$

By eliminating the term which has ψ,

$$P_4^2 = P_1^2 + P_3^2 - 2P_1 \cdot P_3 \cdot \cos\theta, \tag{2.4}$$

$$P_1 = \sqrt{E_1^2 + 2M_1 \cdot E_1}, \tag{2.5}$$

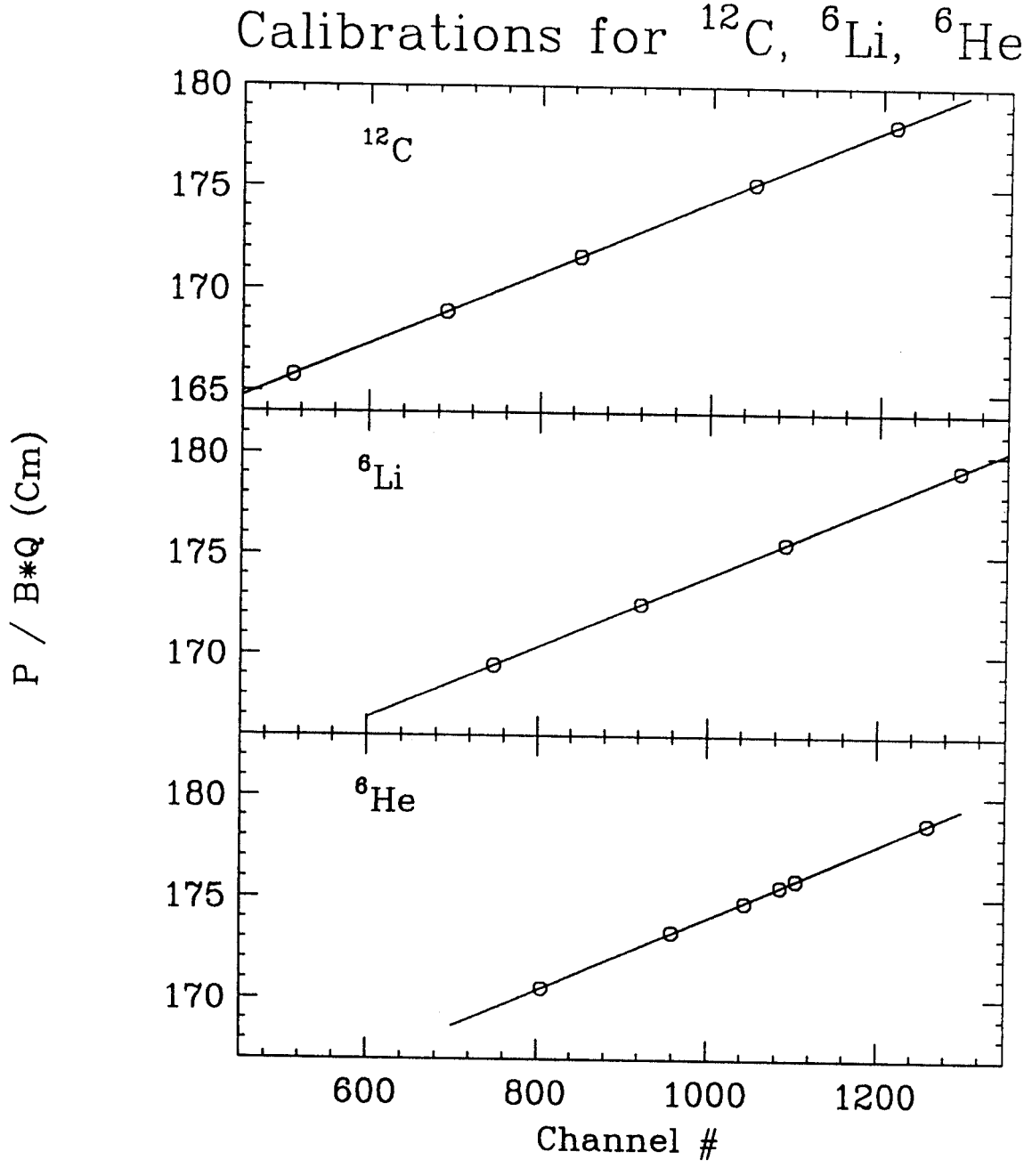

Figure 2.7: Calibrations on ^{12}C, ^{6}Li and ^{6}He particles. Uncertainty is about 0.1%.

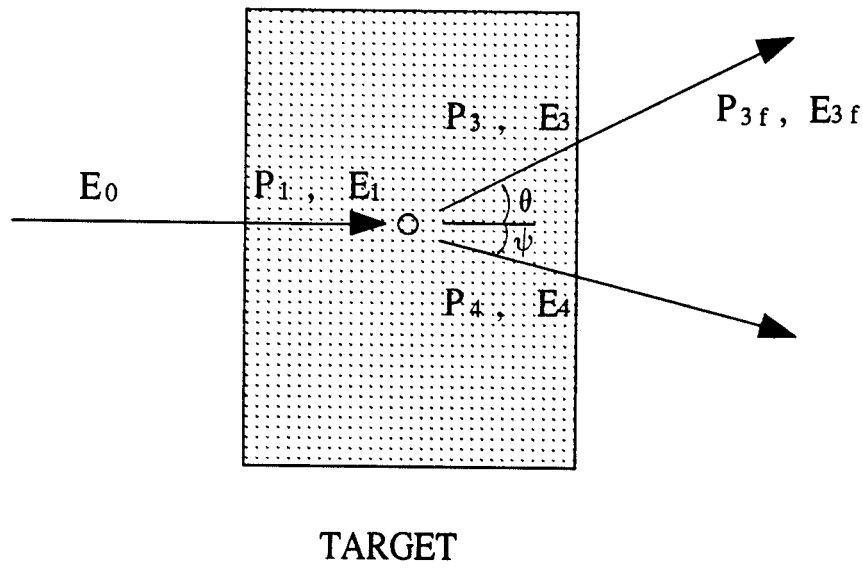

Figure 2.8: Schematic diagram depicting the kinematics in the target.

where $E_1 = E_0 - E_{lossin}$ and P_3 can be calculated easily using the measured channel number (ρ), E_{lossin}, $E_{lossout}$ and P_{3f},

$$P_{3f} = B \cdot \rho \cdot q/3.3356, \tag{2.6}$$

$$E_3 = E_{3f} + E_{lossout}$$

$$= \sqrt{P_{3f}^2 + M_3^2} - M_3 + E_{lossout}, \tag{2.7}$$

$$P_3 = \sqrt{{E_3}^2 + 2M_3 \cdot E_3}, \tag{2.8}$$

where momenta are expressed in a convenient unit (MeV/c) rather than an MKS unit, B is the magnetic field strength in kG, q is the charge state and ρ is the orbit radius in cm. E_{lossin} and $E_{lossout}$ are the incident particle and ejectile's energy loss in the first half and second half of the target. Now P_4 can be calculated from eq.2.4 by using P_1, P_3 and the scattering angle θ. The recoil energy is,

$$E_4 = \sqrt{P_4^2 + M_4^2} - M_4. \tag{2.9}$$

Then the excitation energy of the residual nucleus is

$$E_{ex} = E_0 - E_{3f} - E_4 + Q - E_{loss}, \tag{2.10}$$

where Q is a reaction Q – value and E_{loss} is the total energy loss in the target, sum of E_{lossin} and $E_{lossout}$. The energy losses in the targets were calculated by executing the program *nscl_library* : [*setup.eloss*]*donna.exe*. This program calculates the energy loss of any particles in any medium or series of media. The input parameters are, incident energy, proton number and nuclear mass of the projectile, and electron number, atomic mass, mass density and thickness of the target particles. In heavy targets, most of the energy loss is caused by inelastic collisions between the projectile and the atomic electrons of the target making an ionization or excitation of the target atoms. To determine the E_{lossin} and $E_{lossout}$, it was assumed that the reaction happened at the middle of the target. E_{lossin} is the energy loss of the projectile for the one half thickness of the target and $E_{lossout}$ is the energy loss of the ejectile for the other half thickness of the target. E_{lossin} is independent of residual nucleus's excitation, but $E_{lossout}$ is, because the kinetic energy of the ejectile, dependent on the excitation of the residual nucleus. In case when the residual nucleus was in an excited state after the reaction, $E_{lossout}$ was adjusted using the linear relation between the two cases of energy losses at $E = 0$ MeV and $E = 60$ MeV of a residual nucleus. Of course the exact excitation is not known in this step. But a small difference in excitation energy does not affect $E_{lossout}$ very much. If the excitation of the residual nucleus is E, then

$$E_{lossout,Ex=E} = E_{lossout,Ex=0.} + \frac{E}{60} \cdot (E_{lossout,Ex=60.} - E_{lossout,Ex=0.}). \qquad (2.11)$$

When the residual nucleus is in an excited state, the reaction Q – value is the sum of the excitation energy E and the reaction Q – value for the ground state of the residual nucleus,

$$Q = E + Q_{Ex=0.} . \qquad (2.12)$$

The calculated energy losses in the targets for the projectiles and the reaction products are given in table. 2.2.

Table 2.2: Energy losses of the reaction products in the targets at $E = 30$ MeV/n. Units are MeV. Numbers in parenthesis are target's thicknesses in mg/cm^2. Reac.Pro. represents "Reaction Products". Uncertainty is about 10%.

Target / Reac.Pro.	^{90}Zr (5.06)	^{91}Zr (5.01)	^{89}Y (5.30)	^{208}Pb (5.84)	^{209}Bi (6.50)	^{207}Pb (4.95)
^{7}Li	0.493	0.493	0.512	0.422	0.472	0.359
^{6}Li	0.440	0.437	0.457	0.382	0.426	0.322
^{6}He	0.199	0.198	0.204	0.172	0.191	0.146
^{12}C	1.976	1.973	2.052	1.690	1.888	1.439
^{13}C	2.134	2.109	2.214	1.800	2.012	1.531
^{13}N	2.903	2.900	3.006	2.467	2.736	2.099

The uncertainty of the calibration is about 0.15 MeV for ^{6}Li and ^{6}He, and about 0.3 MeV for ^{13}C and ^{13}N. The main uncertainties are from the inaccurate thickness of the target and the intrinsic uncertainty of the focal plane detecting system of S320 spectrograph. The final determination of the excitation energies was made by subtraction from the energy of the ground state which was set at $Ex. = 0$ MeV. The shifts to make $Ex. = 0.$ were less than 0.3 MeV for ^{6}Li and ^{6}He, and less than 0.5 MeV for ^{13}C and ^{13}N.

2.8 Cross Section Determination

The differential cross sections for the single nucleon transfer reactions were obtained by using the parameters measured in the laboratory frame. The formula used is

$$\frac{d\sigma}{d\Omega} = \frac{N_{spec}}{3.74 \cdot 10^{3}} \cdot \frac{Z \cdot m_t}{Q \cdot T} \cdot \frac{DTC}{\Delta\Omega}, \tag{2.13}$$

where N_{spec} is the number of the reaction products detected by the spectrograph per channel number, Z is the average charge number of the projectile after it passed through the target, Q is the integrated beam current in nC, m_t is the mass of the target nucleus in amu, T is the thickness of the target in mg/cm^2, $\Delta\Omega$ is the solid angle of the aperture in msr and DTC is the dead time correction coefficient. The cross sections are in mb/sr. The uncertainty for the cross section appears to be about 10% due to the the uncertainty of the target's thickness.

Chapter 3

Shell Model Analysis for ^{208}Pb Region Nuclei

3.1 Introduction

In single nucleon transfer reactions on targets which have an extra hole or particle outside a closed shell nucleus, the interaction between the transferred nucleon and the target's hole or particle is the main factor that splits the single particle states and produces a multiplet of states. At low excitation energies, the shift in excitation energy and a slight broadening of the peak due to this interaction were observed and discussed extensively on lead region nuclei using light ion transfer reactions [Alfo 70, Craw 73]. But at high excitation energies, the density of states is so high that individual states are not resolved. If the changes in excitation energies and widths of the multiplets due to the presence of an extra particle or hole can be predicted by theoretical methods, it would give us confidence in predicting the shifts in excitation energies at high excitation energy. One of the methods to calculate these changes is the shell model. This calculation provides us very useful information on the splitting of energy levels due to an extra particle or hole state, including the spectroscopic factors and the excitation energies by solving the Schrodinger equations for the given conditions assuming that nucleons inside the core nucleus are in the same average potential. From

this information, the shift and the broadening of the multiplet states from the single particle or single hole states can be obtained.

Shell model calculations have been very successful in the vicinity of the closed shell nuclei, especially in the lead region nuclei [Ma 73, Herl 72, Mcgr 75, Warb 91]. One problem with the shell model calculation is that there are many low lying single particle orbits which are potentially important. Thus very large matrices need to be diagonalized which requires too large a working area and cpu time for the available computers. Thus the number of particle states and hole states must be limited in these calculations.

For the chosen two target nuclei, ^{207}Pb and ^{209}Bi which have an extra single particle or hole outside the closed shell core nucleus ^{208}Pb, the energy levels and spectroscopic factors for the single nucleon stripping reactions were calculated. The purpose of the shell model calculation is to observe how the characteristics of the single particle states in the multiplet, such as excitation energies and spectroscopic factors, are changed by the presence of a single particle or hole outside a closed shell nucleus. But the single particle states at high excitation energies are not well known and it is therefore difficult to calculate the changes for the high lying particle states. But by calculating the changes for low lying particle states which are known well, one can assume that the results are applicable to high lying single particle states, since the interactions between the $p-p$ or $p-h$ states are not very dependent on the excitation energies.

3.2 Energy Level Calculations

For the single nucleon stripping reactions on targets of ^{207}Pb and ^{209}Bi, the energy levels, and their parameters such as excitation energies, wave functions and spectroscopic

factors were calculated using the NSCL version of the program OXBASH[OXBA 88]. This can handle up to 3 particle orbits and 4 hole orbits in both proton and neutron shells. The targets were assumed to be a composite of the ^{208}Pb core nucleus and a single proton particle for the ^{209}Bi nucleus or a single neutron hole for the ^{207}Pb nucleus. Energetically the highest 4 hole orbits and the lowest 3 particle orbits were considered to be the available particle and hole states both for proton and neutron shells. The experimental single particle energy levels in ^{208}Pb are given in fig. 3.1 [Ma 73]. (*proton particle* ; $1h_{9/2}, 2f_{7/2}$, $1i_{13/2}$, *proton hole* ; $1h_{11/2}, 3s_{1/2}$, $2d_{3/2}, 2d_{5/2}$, *neutron particle* ; $2g_{9/2}, 1i_{11/2}$, $1j_{15/2}$, *neutron hole* ; $1i_{13/2}, 3p_{1/2}$, $3p_{3/2}, 2f_{5/2}$)

The matrix elements of the Hamiltonian operator H between the many particle basis functions were obtained by using the second quantized operators a^+ and a [OXBA 88]. The Hamiltonian H can be written as

$$H = H_{core} + \sum_i \epsilon_i a_i^+ a_i + \sum_{i>j,k>l} v_{ijkl} a_i^+ a_j^+ a_k a_l, \tag{3.1}$$

where ϵ_i is the energy of a single particle state, and

$$v_{ijkl} = \langle ij|V|kl\rangle, \tag{3.2}$$

and $|ij\rangle$ is an antisymmetrized two particle m-scheme state. The values for the both ϵ_i and v_{ijkl} are inputs in the code OXBASH. The single particle energies ϵ_i are adjusted to fit the experiment and the two body terms v_{ijkl} were based on the Kuo-Herling G-matrix [Warb 91]. By applying this Hamiltonian operator to the wave function $|ij\rangle$ and diagonalizing the matrix elements, the eigenvalues and eigenfunctions can be obtained. Here, the eigenvalues are the energies of the final states.

In the ^{207}Pb$(+n)$ reaction, when the transferred neutron occupies one of the 3 neutron particle states, the neutron hole which is initially in the $3p_{1/2}$ state can be

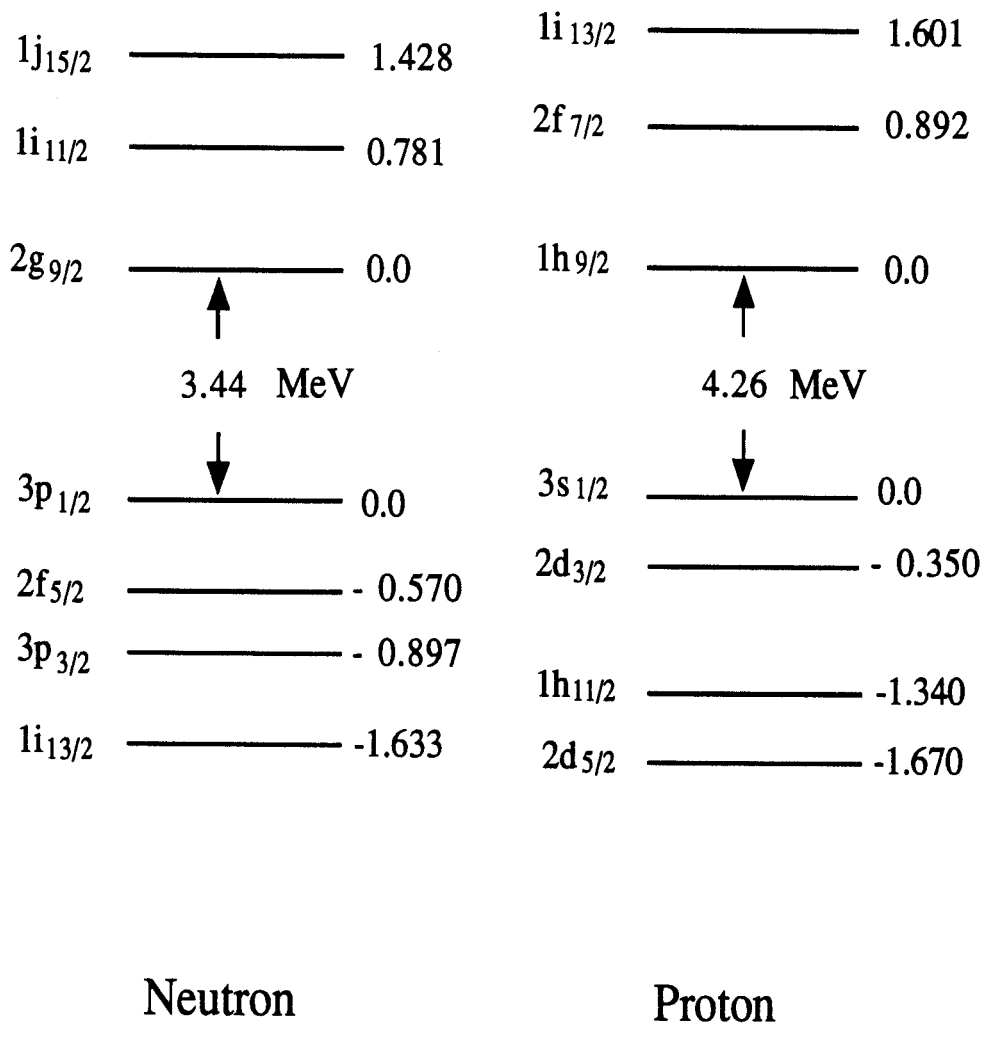

Figure 3.1: Experimental single particle and hole energy levels in ^{208}Pb [Ma 73]. In shell model calculation, the lowest 3 particle states and the highest 4 hole states for both proton and neutron shells were used.

located in any one of the 4 neutron hole states in the final state while the proton shell was assumed to remain closed. (The notation $(+n)$ stands for adding a neutron to the target by a neutron stripping reaction). So 12 combinations of one particle – one hole states were used in the calculations. If the neutron occupies the target's initial hole state $3p\frac{1}{2}^{-1}$, the neutron shell becomes a closed shell. In this case the proton shell was assumed either to be a closed shell or a proton can be excited to one of the 3 proton particle states from one of the proton hole states, which makes 13 (1+12) combinations. Thus a total of 25 combinations of particle and hole states were considered. Each combination has many different states due to the $p-h$ couplings.

The same procedures were also used for the other reactions. In the ^{209}Bi$(+n)$ reaction, since the target nucleus has a proton in the $1h_{9/2}$ orbit, the main interaction is between the transferred neutron and an outmost shell's proton. Three particle states are available for both proton and neutron shells, thus 9 combinations are allowed. In the ^{207}Pb$(+p)$ reaction, three proton particle states and 4 neutron hole states are available, thus total 12 combinations are allowed, where $(+p)$ represents adding a proton to the target by a stripping reaction. The main interaction comes from the coupling of the transferred proton and the target's neutron hole state. In the ^{209}Bi$(+p)$ reaction, there are two protons in proton particle states outside the closed ^{208}Pb core nucleus. A total of 9 combinations are possible.

3.3 Results and Discussions

The results for the energy levels are expressed as an excitation energy, spectroscopic factor S, j^π of the residual nucleus and a transferred nucleon's final orbit quantum numbers n, l and j. The cross section σ_f is defined as

$$\sigma_f = \sigma_{th} \cdot \frac{2J_f+1}{2J_i+1} S_f, \tag{3.3}$$

where σ_{th} is the cross section calculated theoretically and may be assumed to be constant for the same orbit. j_f and j_i are the total angular momentum of the final and initial state respectively, and S_f is the spectroscopic factor of the final state. The single particle states in the ^{209}Pb and ^{209}Bi nuclei are independently normalized to the experimental data, and the energy levels of each multiplet are plotted as a function of excitation energy after the strengths are normalized to those of the single particle states in the ^{209}Pb and ^{209}Bi nuclei (fig. 3.2). The average energies of each multiplet are obtained by averaging the energies weighted by the cross section. They are compared with the present experimental data, and the centroid energies are compared with the single particle states of the ^{209}Pb and ^{209}Bi nuclei in tables. 3.1 and 3.2, and fig. 3.3.

In the ^{207}Pb$(+n)$ reaction, the energy levels except the ground state are shifted to higher excitation, which agrees very well with the experimental result. The ground state is formed when a transferred neutron fills a target's hole, $3p_{1/2}$ state. As the final state is doubly closed, the shift of the ground state to lower energy (3.564 MeV) is much larger than in the $odd - odd$ (^{207}Pb$(+p)$ or ^{209}Bi$(+n)$) or non - closed $even - even$ (^{209}Bi$(+p)$) residual nuclei's ground states. The couplings between the neutron's particle state j^{π} and the ground state $3p_{\frac{1}{2}}^{-1}$ allow only two j_f of $j + \frac{1}{2}$ and $j - \frac{1}{2}$. Thus each multiplet is dominated by these two levels out of numerous levels which are not seen in the figure due to the very weak spectroscopic strengths.

In the ^{209}Bi$(+n)$ reaction, each multiplet is represented by many levels which have similar spectroscopic strengths, and the widths of the multiplets (about 500 keV) are somewhat bigger than those ($100 \sim 300$ keV) of the multiplets in the ^{207}Pb$(+n)$ reaction. The reason is that the ground state of ^{209}Bi, has a large angular momentum ($1h_{9/2}$) and the coupling with the neutron particle states allows many j_f ranging from $|j - \frac{9}{2}|$ to $j + \frac{9}{2}$. But the ground state is not shifted much (about 0.35 MeV) from

Figure 3.2: Energy levels obtained from shell model calculations. The relative strengths of single particle states of ^{209}Pb and ^{209}Bi are normalized to the experimental data of (^{7}Li,^{6}Li) or (^{7}Li,^{6}He) reaction. Each bar represents the strength of a specific configuration and the dashed lines are calculated spectra obtained using the gaussian distribution with the 0.3 MeV FWHM. The overall renomalization is arbitrary. The same colored lines originate from the same single particle state.

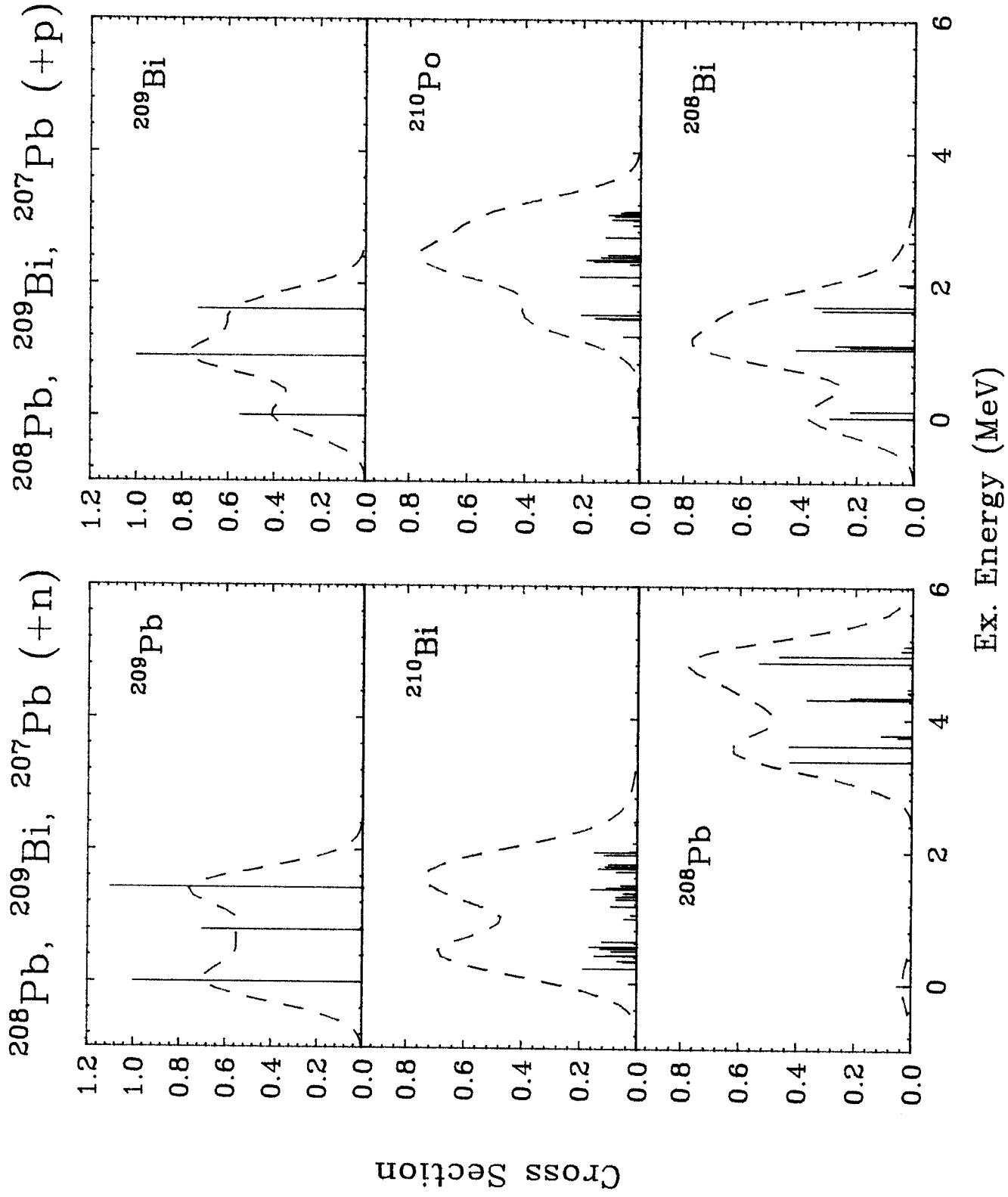
^{208}Pb, ^{209}Bi, ^{207}Pb (+n)
^{209}Pb
^{210}Bi
^{208}Pb
^{208}Pb, ^{209}Bi, ^{207}Pb (+p)
^{209}Bi
^{210}Po
^{208}Bi
Cross Section
Ex. Energy (MeV)

Figure 3.2

Table 3.1: Average excitation energies obtained using shell model calculations for the peaks 1, 2 and 3 of neutron stripping reactions on targets of ^{207}Pb and ^{209}Bi are shown with the experimental data. Each peak is a multiplet between target's state and single particle states where a neutron transferred. The values in parenthesis are the reaction Q – values for the corresponding excitation. Energy levels for the single particle states of the ^{208}Pb$(+n)$ reaction are also given to measure the energy shift from the particle - particle or particle - hole interactions. Experimental errors are about 0.15 MeV.

	Single State	Shell Model Calculations		This Experiment (^7Li, ^6Li)	
Peak #	$^{208}Pb(+n)$ (MeV)	$^{207}Pb(+n)$ (MeV)	$^{209}Bi(+n)$ (MeV)	$^{207}Pb(+n)$ (MeV)	$^{209}Bi(+n)$ (MeV)
1	0. (-3.313) $\nu(g_{9/2})$	3.557 (-3.400) $\nu(p_{1/2})^{-1} \otimes \nu(g_{9/2})$	0.414 (-3.060) $\pi(h_{9/2}) \otimes \nu(g_{9/2})$	3.30 (-3.11)	0.65 (-3.30)
2	0.779 (-4.092) $\nu(i_{11/2})$	4.281 (-4.164) $\nu(p_{1/2})^{-1} \otimes \nu(i_{11/2})$	1.201 (-3.832) $\pi(h_{9/2}) \otimes \nu(i_{11/2})$	4.14 (-4.02)	1.51 (-4.16)
3	1.423 (-4.736) $\nu(j_{15/2})$	4.939 (-4.712) $\nu(p_{1/2})^{-1} \otimes \nu(j_{15/2})$	1.760 (-4.406) $\pi(h_{9/2}) \otimes \nu(j_{15/2})$	4.70 (-4.58)	2.01 (-4.66)

Table 3.2: Average excitation energies obtained using shell model calculations for the peaks 1, 2 and 3 of proton stripping reactions on targets of ^{207}Pb and ^{209}Bi are shown with the experimental data. Each peak is a multiplet between target's state and single particle states where a proton transferred. The values in parenthesis are the reaction Q – values for the corresponding excitation energies. Energy levels for the single particle states of the ^{208}Pb$(+p)$ reaction are also given to measure the energy shift from the particle - particle or particle - hole interactions. Experimental errors are about 0.15 MeV.

	Single State	Shell Model Calculations		This Experiment (^7Li ,^6He)	
Peak	$^{208}Pb(+p)$ (MeV)	$^{207}Pb(+p)$ (MeV)	$^{209}Bi(+p)$ (MeV)	$^{207}Pb(+p)$ (MeV)	$^{209}Bi(+p)$ (MeV)
1	0. (-6.716) $\pi(h_{9/2})$	0.098 (-6.366) $\nu(p_{1/2})^{-1} \otimes \pi(h_{9/2})$	1.479 (-6.270) $\pi(h_{9/2}) \otimes \pi(h_{9/2})$	0.03 (-6.27)	1.39 (-6.38)
2	0.897 (-7.073) $\pi(f_{7/2})$	1.134 (-7.402) $\nu(p_{1/2})^{-1} \otimes \pi(f_{7/2})$	2.354 (-7.324) $\pi(h_{9/2}) \otimes \pi(f_{7/2})$	0.90 (-7.17)	2.12 (-7.11)
3	1.609 (-7.715) $\pi(i_{13/2})$	1.718 (-7.987) $\nu(p_{1/2})^{-1} \otimes \pi(i_{13/2})$	3.002 (-7.980) $\pi(h_{9/2}) \otimes \pi(i_{13/2})$	1.52 (-7.79)	2.73 (-7.72)

Figure 3.3: Comparison of shell model calculations with experimental spectra. Each vertical bar represents the strength of a specific configuration and the solid lines are experimental data and the dashed lines are calculated spectra obtained using the gaussian distribution with the 0.3 MeV FWHM. The same colored lines originate from the same single particle state. Calculated values are normalized to the experimental data. The average excitation energies of the shell model calculations for each multiplet are marked with short arrows on the horizontal - axis while the centroid of experimental peaks are marked with long arrows on the spectra.

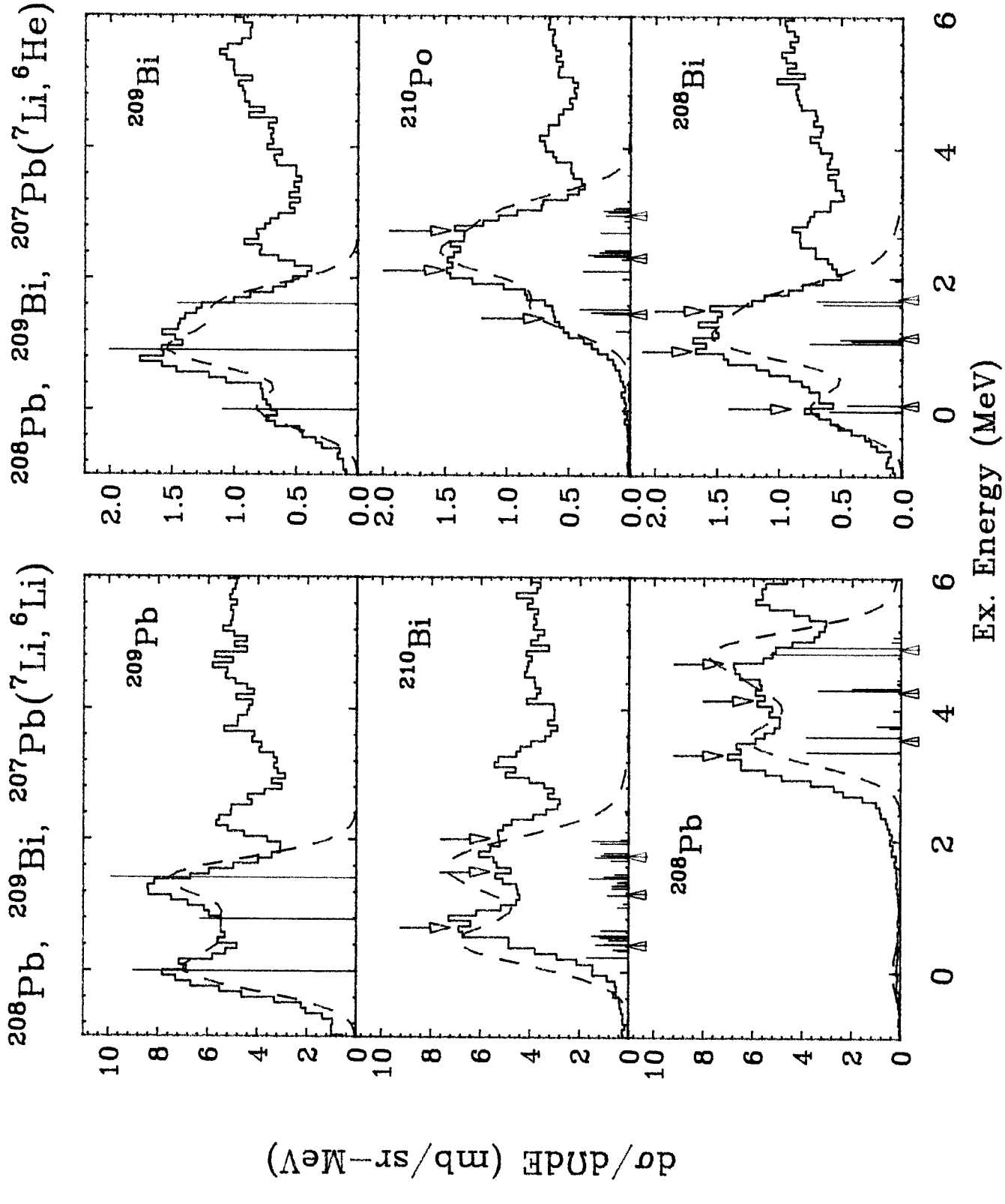
^{208}Pb, ^{209}Bi, ^{207}Pb(^{7}Li, ^{6}He)
^{209}Bi
^{210}Po
^{208}Bi
^{208}Pb, ^{209}Bi, ^{207}Pb(^{7}Li, ^{6}Li)
^{209}Pb
^{210}Bi
^{208}Pb
dσ/dΩdE (mb/sr−MeV)
Ex. Energy (MeV)

Figure 3.3

the centroid of the $\nu(1g_{9/2}) \otimes \pi(1h_{9/2})$ multiplet because of the weak strength of the $odd-odd$ coupling. Even if a single proton in the $2g_{9/2}$ state in the target can occupy any of its available states after the reaction, the most dominant state is the initial state. Similar phenomena are seen in proton stripping reactions. In the ^{207}Pb$(+p)$ reaction, two dominant levels appear in each multiplet as in the ^{207}Pb$(+n)$ reaction. Because of the very weak $odd-odd$ coupling strength between the $3p^{-1}_{1/2}$ state of ^{207}Pb and the proton's single particle states, the widths of the multiplets are about 70 keV and there is about a 0.1 MeV shift of the whole spectrum to higher excitation.

In the ^{209}Bi$(+p)$ reaction, due to the Pauli exclusion principle and the smaller $j-$values of the proton's single particle states, the numbers of energy levels dominantly contributing in each multiplet are less than those of the ^{209}Bi$(+n)$ reaction. Thus the widths, about 300 keV, of the multiplets are not as large as the widths of the multiplets in the ^{209}Bi$(+n)$ reactions, about 500 keV. The ground state of the $even-even$ residual nucleus ^{210}Po is shifted from the centroid of the $\pi(1h_{9/2})^2$ multiplet to lower energy by 1.34 MeV, due to the pairing interaction in the $\pi(1h_{9/2})^2$ $j = 0^+$ state. This shift is much larger than that of the ground state for the $even-odd$ residual nucleus of the ^{209}Bi$(+n)$ reaction, namely 0.36 MeV.

As is shown in fig. 3.2, even though the energy levels in the multiplets are spread up to 4 MeV, the relative excitation energies for the centroid of each multiplet do not differ significantly from those of the single particle states in the ^{209}Pb or ^{209}Bi nucleus (at most by a few hundred keV). When the reaction Q - values of the multiplets are compared with those of the single particle states, no significant differences are observed. However, when the excitation energies are compared, significant differences are observed in some cases. From these comparisons, it is evident that the existence of an extra hole or particle in the target does not change the reaction Q - values significantly, but it may change the excitation energies significantly.

Chapter 4

Single Particle States and Giant Resonance States

4.1 Introduction

In some recent heavy ion transfer experiments, broad peaks have been observed with properties (excitation energies, widths and strengths) which are similar to those of the giant quadrupole resonance (GQR) [Merm 87, Fras 87, Fort 90]. Whether these broad peaks are giant resonance (GR) states or simply broad single particle states is not clear and remains a question (see fig. 1.1). The possibility of GR excitation by transfer reactions was mentioned in a paper by Olmer et al.[Olme 78] and also by Frascaria et al. [Fras 89]. Broad peaks in single particle transfer reactions have been found in many nuclei over a wide range of the mass, from $A = 60$ to $A = 208$ [Fras 87, Duff 86, Fras 89, Fort 90, Gale 88].

This chapter attempts to address the nature of these broad peaks by discussing what differences one might expect in transfer reactions on different targets. For this purpose, 2 *even – even* nuclei targets, ^{90}Zr and ^{208}Pb, and their neighboring nuclei, 4 *even – odd* targets ^{91}Zr, ^{89}Y, ^{209}Bi and ^{207}Pb were chosen. The reason that these targets were chosen is described in section. 1.2.

In this chapter, the characteristics of single particle states and GR states, and the

method of distinguishing GR states from the single particle states are described.

4.2 Predictions for Single Particle States

A single particle state is a state in which a nucleon occupies one of the shells outside the non-excited core. The nucleon's orbit is characterized by shell model quantum numbers. A single particle state can be formed by adding a nucleon to an outer shell using a transfer reaction.

If this state couples with the target's ground state which has an extra hole or particle outside the closed shell core, a multiplet of states will be formed which are spread over a few MeV in excitation energy. The total cross sections for exciting the multiplet states in a transfer reaction will be nearly the same as the cross section of the single particle state. If the energies of the multiplet states are weighted by the spectroscopic factors, the centroid of the multiplet behaves in a systematic way from one nucleus to the next and it does not change significantly in absolute energy. Shell model calculations show that the change of the centroid is about a few hundred keV in the lead region [Ma 73] (and see chap. 3).

The excitation energy of a specific orbit's single particle state depends upon the ground state energy and may change significantly from one nucleus to the next. In neutron stripping reactions, a significant change in excitation energy is expected for similar single particle states between targets consist of a closed shell and targets which have a single neutron hole, such as ^{208}Pb and ^{207}Pb. The ground state energy of the ^{207}Pb$(+n)$ reaction is lower than the ground state energy of the ^{208}Pb$(+n)$ reaction by 3.43 MeV which is the difference in binding energy of the outmost neutron in ^{209}Pb and ^{208}Pb, where $(+n)$ denotes a neutron stripping reaction. Except for the ground state, the spectrum of the ^{207}Pb$(+n)$ reaction is shifted to higher excitation

energy compared to the spectrum of the ^{208}Pb$(+n)$ reaction. Similar results may be expected in proton stripping reactions for closed shell targets and targets which have a single proton hole, such as ^{90}Zr and ^{89}Y. The difference between the outmost proton's binding energy in ^{91}Nb and in ^{90}Zr is 3.2 MeV, and this shifts the spectrum of the ^{89}Y$(+p)$ reaction to higher excitation energy by about 3.2 MeV compared to the ^{90}Zr$(+p)$ reaction, where $(+p)$ represents a proton stripping reaction. Thus the excitation energies for similar single particle states may be changed significantly (up to 3 or 4 MeV) between two neighboring nuclei.

But the reaction Q – values for transferring a nucleon to the same shell of the neighboring nuclei are not very different from each other. At most a few hundred keV difference results from the coupling between a single particle state and a core state. For example, in neutron transfer reactions to the same $\nu(2g_{9/2})$ shells of the ^{208}Pb and ^{207}Pb targets, the difference between the two reaction Q – values is about 0.1 MeV, due to the coupling of $\nu(2g_{9/2}) \otimes \nu(3p_{1/2})^{-1}$. As was shown in the shell model calculations (chap. 3), $1p - 1p$ or $1p - 1h$ couplings convert the single particle state into a multiplet of $2j + 1$ states. Thus, for the single particle states, an extra hole or particle in the target changes the reaction Q – values by a few hundred keV at most.

These ideas may be applied to the broad peaks observed in single nucleon stripping reactions on targets of ^{90}Zr and ^{208}Pb region. If the broad peaks are single particle states, they should appear in the spectra of neighboring targets. There may be a slight broadening in the peaks but the total strength should be similar. The broad peaks shown in the ^{90}Zr$(+n)$ reaction [Fort 90, Fras 87] at excitation energy about 13.5 MeV should also appear in the ^{91}Zr$(+n)$ and ^{89}Y$(+n)$ reaction.

In the ^{91}Zr$(+n)$ reaction, the ground state will shift to lower energy by 1.34 MeV compared to the ground state of the ^{90}Zr$(+n)$ reaction. The broad peak is expected to appear at higher excitation energy than in the ^{90}Zr$(+n)$ reaction by 1.34 MeV,

where 1.34 MeV is the outmost neutron's binding energy difference between ^{92}Zr and ^{91}Zr.

Similarly in the ^{89}Y$(+n)$ reaction, the ground state of ^{90}Y will shift to lower energy compared to the ground state of the ^{90}Zr$(+n)$ reaction by about 0.39 MeV. The broad peak is expected to appear at about 0.39 MeV higher excitation energy than in the ^{90}Zr$(+n)$ reaction, where 0.39 MeV is the outmost neutron's binding energy difference between ^{90}Y and ^{91}Zr.

However, there should be no significant differences in reaction Q – values for the broad peaks in these reactions. If the spectrum of ^{90}Zr$(+n)$ reaction is compared to the spectra of the ^{91}Zr$(+n)$ and ^{89}Y$(+n)$ reactions as a function of reaction Q – values, all the broad peaks except the ground state are expected to appear at almost the same positions, within a few hundred keV.

Broad peaks observed in the ^{208}Pb$(+n)$ reactions [Fort 90, Merm 88, Mass 86] at excitation energy about 10 MeV should also appear in the ^{209}Bi$(+n)$ reaction and ^{207}Pb$(+n)$ reactions.

In the ^{207}Pb$(+n)$ reaction, the ground state will shift to lower energy by about 3.43 MeV compared to that of the ^{208}Pb$(+n)$ reaction. The broad peak is expected to appear at excitation energy higher than in the ^{208}Pb$(+n)$ reaction by about 3.43 MeV.

Similarly in the ^{209}Bi$(+n)$ reaction, the ground state will shift to lower energy but only by about 0.66 MeV. The broad peak is expected to appear at higher excitation energy than in the ^{208}Pb$(+n)$ reaction by about 0.66 MeV. But there will be no significant difference in reaction Q – values for the broad peaks in both reactions.

Schematic depictions of the prediction for the single particle model for single neutron transfer reactions on ^{208}Pb region targets are given in fig. 4.1. In this figure,

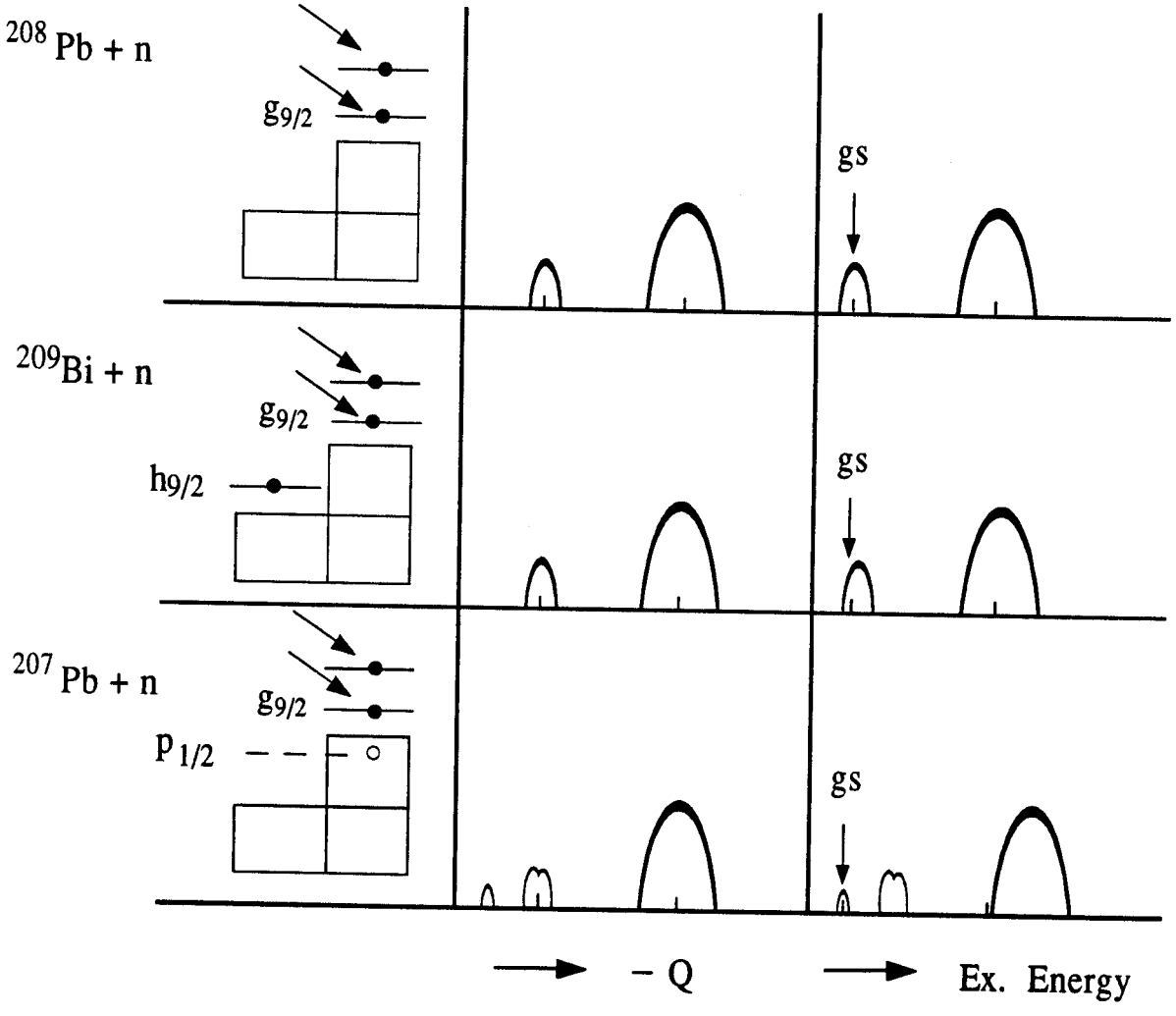

Figure 4.1: Predictions for the excitation energy shifts of single particle states in ^{208}Pb nucleus and its neighboring nuclei. If the broad peaks are GR states, they will have almost the same excitation energies.

only two peaks in the ^{208}Pb(+n) reaction are considered, the ground state where a neutron is transferred to the $2g_{9/2}$ shell, and a broad peak corresponding to some excited state. These peaks are expressed as a function of both the reaction Q – values and excitation energies. If the same procedures are applied to the ^{209}Bi(+n) reaction, the situation is very similar to the ^{208}Pb(+n) reaction. The two peaks, multiplets of the $\pi(h_{9/2})$ state and the same single particle states, appear at similar positions in both the reaction Q – value and excitation energy, with somewhat broad widths. In the ^{207}Pb(+n) reaction, the two doublets resulting from the couplings between the neutron hole state and the single particle states will appear at the same reaction Q – values. But the ground state will appear at lower energy by as much as the outmost neutron's binding energy difference between the ^{208}Pb and ^{209}Pb nuclei.

If all the peaks are compared as a function of reaction Q – values as in fig. 4.1.(a), they will appear at almost the same reaction Q – values except the ground state of the ^{207}Pb(+n) reaction. If they are compared as a function of excitation energies as in fig. 4.1.(b), the two peaks of the ^{207}Pb(+n) reaction will appear at higher excitation energies than the peaks of ^{208}Pb(+n) and the ^{209}Bi(+n) reactions.

In general, if the peaks, which are obtained by transferring a neutron to the same shell, have similar reaction Q – values but show a shift in excitation energies, then they can be assumed as single particle states. Whereas, if the broad peaks have the similar excitation energies whatever reaction Q – values they have, then the broad peaks can be assumed as GR states. This method may also be applied to the reactions with the ^{90}Zr region targets to distinguish GR state and single particle state.

4.3 Predictions for Giant Resonance States

A giant resonance is a highly collective mode of nuclear excitation in which many nucleons move together in a correlated way. The motion is so collective it may be treated as the oscillation of a liquid drop. The resonance in which neutrons and protons move in phase is an isoscalar resonance, while the one in which neutrons and protons move out of phase is an isovector resonance. Similarly, the one in which spin up and spin down nucleons move in phase yield S=0 modes (electric modes) and the one in which spin up and spin down nucleons move out of phase yield S=1 modes (spin flip, magnetic modes). Giant resonance have been observed in many nuclei [Youn 76, Woud 87].

The properties of GR such as excitation energies, widths and strengths change very smoothly as the nucleus's mass changes and the total cross section for the GR is generally large compared to the cross section for the typical single particle state. Microscopically, GR may be described as a coherent superposition of many $1p - 1h$ excitations resulting from applying the electromagnetic interaction force to the ground state [Woud 87]. A schematic representation for a single particle - hole transition between shell model states is shown in fig. 4.2 [Bert 81]. The transitions shown represent some of the collective vibrational modes that may occur by exciting one nucleon from the core to a higher orbit. The centroid of the GR peaks is dependent on the nucleus mass [Youn 76]. The centroid of the GQR excitation energy may be expressed approximately as $Ex = 63/A^{1/3}$ MeV, where A is the mass number [Bert 76, Youn 76]. A mass number difference of 2 or 3 in heavy nuclei does not shift the centroid energy of the GR significantly.

The giant quadrupole resonances obtained by inelastic scattering reactions in this experiment, using a ^{12}C beam at 30 MeV/n, on ^{90}Zr and ^{208}Pb region target nuclei are

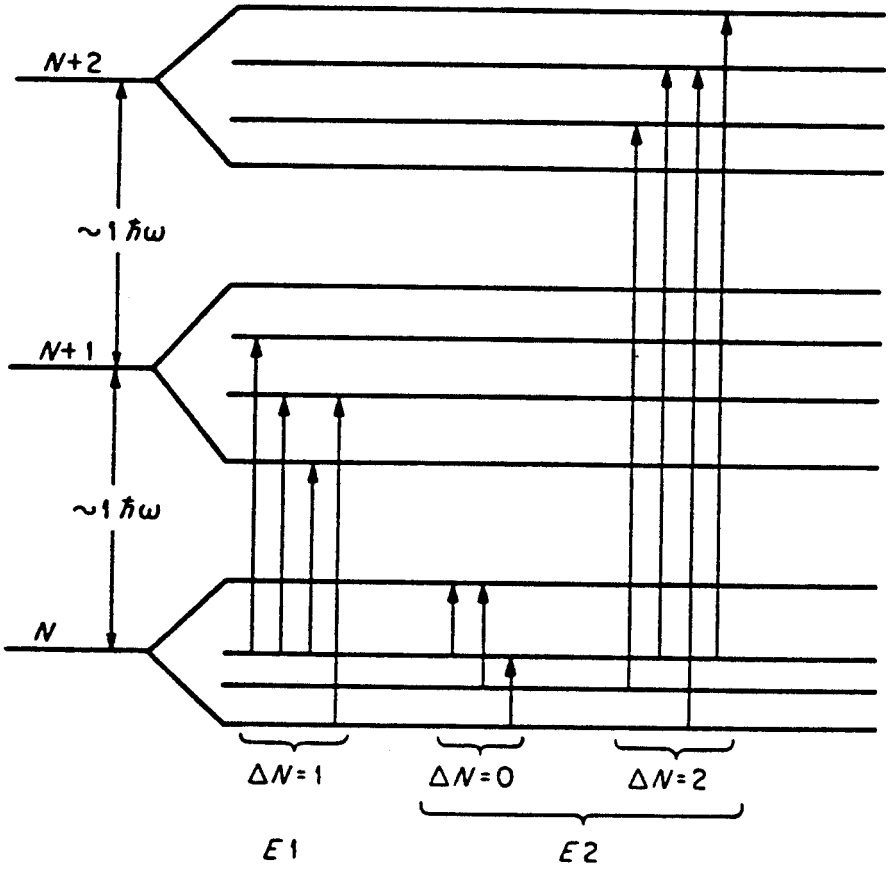

Figure 4.2: A schematic representation $E1$ and $E2$ single particle – hole transitions between the shell model states of a hypothetical nucleus.

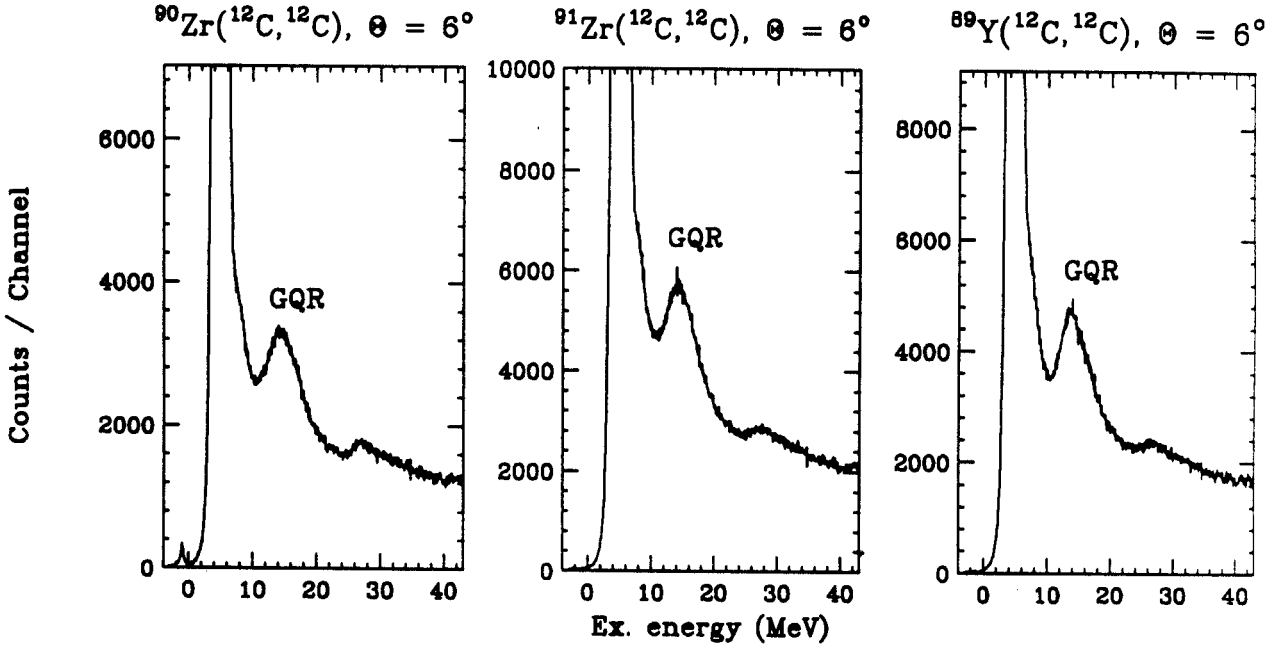

Figure 4.3: Giant resonances observed with inelastic scattering by a ^{12}C (E_{inc} = 30 MeV/n) beam on ^{90}Zr, ^{91}Zr and ^{89}Y nuclei. The excitation energies are about 13.5 MeV and the widths are about 6 MeV. Small peaks at about $Ex.$ ~ 27 MeV are not understood in this experiment. Similar peaks were observed on these nuclei in ref. [Ture 88, Yama 81, Bert81a].

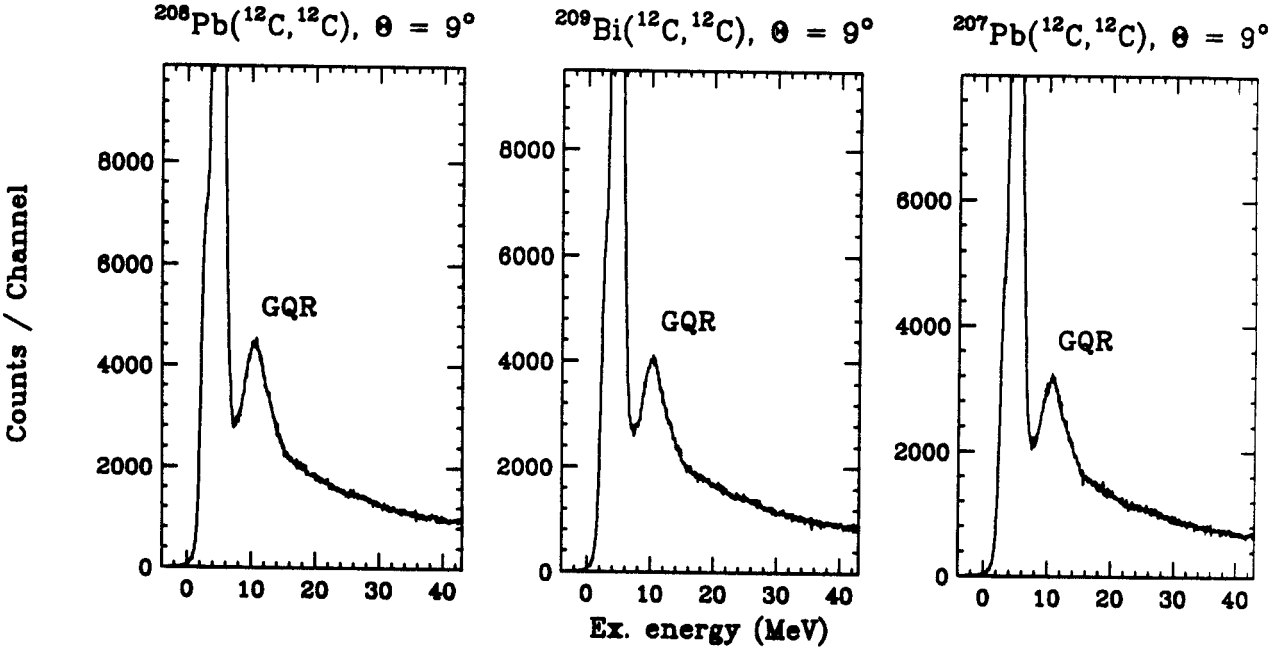

Figure 4.4: Giant quadrupole resonances observed with inelastic scattering by a ^{12}C (E_{inc} = 30 MeV/n) beam on ^{208}Pb, ^{209}Bi and ^{207}Pb nuclei. The excitation energies are about 10.5 MeV and the widths are about 6 MeV.

shown in figs. 4.3 and 4.4. From these figures, no recognizable differences are seen in the excitation energies and widths between the giant resonance peaks for neighboring nuclei.

Most of the studies of GRs to date have been done using inelastic scattering reactions. No GR has been observed using a transfer reaction. Theoretically, GR may be obtained through the two step processes by transfer reactions (inelastic scattering followed by transfer process). But GR with this mechanism seems to be very difficult to be produced at grazing angles with high incident beam energy. Another mechanism suggested [Chom 86, Fras 89] is that the particle – hole states are excited by a single step mechanism through particle or hole components in the ground state of the target nucleus. According to this explanation, for example, the giant quadrupole resonance in ^{208}Pb or ^{90}Zr would be formed by coupling the transferred neutron with a hole state of the appropriate j^{π} in the ^{208}Pb or ^{90}Zr target. It is suggested that the broad peaks shown in neutron stripping reactions on these targets might be produced by the giant resonance excitations.

If the broad peaks obtained by nucleon transfer reactions in any process (by one step or multi step process) are GR states, then the excitation energies of the peaks should be the same with those of the GR states formed by inelastic scattering reactions. There should be no noticeable differences in the excitation energies among the similar peaks obtained on targets of ^{208}Pb, ^{207}Pb and ^{209}Bi with single nucleon transfer reactions. One more nucleon or hole in heavy nuclei does not change the excitation energies of the GR significantly. If the spectra of single nucleon transfer reactions on these targets are compared as a function of excitation energy, the centroid of the peaks should appear with a few hundred keV deviations as in figure 4.1. The extra nucleon or hole in the target does not change the GR excitation energies (see figs. 4.3 and 4.4). The same results may be expected in a nucleon transfer reactions

on targets of ^{90}Zr, ^{91}Zr and ^{89}Y.

But, the cross section for the GR may vary dramatically depending on the structure of the target's ground state, angular momentum transfer matching conditions and on the number of the available configurations which can be coupled. For the nucleon stripping reactions on targets of ^{207}Pb and ^{89}Y which have a hole in the $p_{1/2}$ state, the contributions of the GR to the broad peaks are expected to be very small compared to the single particle states because only a few configurations are available. In this case the cross sections for the GR will be little larger than those of the nucleon stripping reactions on the closed shell targets ^{208}Pb and ^{90}Zr. For the same nucleon stripping reactions on targets of ^{209}Bi and ^{91}Zr which have no fixed hole in the ground states, no contribution of GR due to an extra particle to the broad peaks is expected. Thus the cross scections for the broad peaks are expected to be the same with those in the nucleon stripping reactions on the closed shell targets.

On the other hand, for the proton pickup reaction on the ^{209}Bi target which has a proton particle in the $h_{9/2}$ state, sevaral configurations are available for the GR. In this case the cross sections for the GR are expected to be somewhat larger than the cross section for the closed shell target ^{208}Pb. A similar phenomenon is expected for the neutron pickup reaction on the ^{91}Zr target which a neutron particle in $d_{5/2}$ state.

Chapter 5

Results of Single Nucleon Stripping Reactions

5.1 Introduction

In this chapter, the one nucleon stripping reactions (^{7}Li,^{6}Li) and (^{7}Li,^{6}He) at 30 MeV/n on targets of ^{90}Zr, ^{91}Zr, ^{89}Y, ^{208}Pb, ^{209}Bi and ^{207}Pb are discussed. In each reaction, the ejectiles were measured at grazing angles to obtain large cross sections and to avoid multi-step transfer processes. The ejectiles, ^{6}Li and ^{6}He, are so weakly bound that the threshold energies for breakup are lower than the first excited state's energies, and thus no ejectile excitations contribute to the energy spectra.

The spectra of the same reactions for the different targets are plotted as a function of both the excitation energies and reaction Q – values and the spectra from neighboring targets are compared. The purpose of the comparison is to observe the changes of the positions, widths and strengths of the peaks, and to understand the phenomena in the spectra due to the interactions between the single particle state and the target's ground state. In each energy spectrum there is substantial background at high excitation.

Strong peaks are observed when the final states have high spin and there is no spin-flip process. A preference for transfer to high spin and no spin-flip states is understood

due to the large angular momentum transfer from the incident projectile to the target at the grazing angle [Brin 72]. The selectivity for exciting high spin states has been observed in recent experiments which used (α,^{3}He) [Mass 86], (^{12}C,^{11}C), (^{12}C,^{11}B) [Merm 88], (^{20}Ne,^{19}Ne) [Fort 90], and (^{16}O,^{15}O) [Merm 87] reactions.

The angular momentum transfer in the (^{7}Li,^{6}Li) reaction at the grazing angle at a bombarding energy of 30 MeV/n on targets in the ^{90}Zr region is about $6\hbar$ and about $8\hbar$ on targets in the ^{208}Pb region. For the (^{7}Li,^{6}He) reaction under the same conditions, it is about $5\hbar$ and $8\hbar$ on the ^{90}Zr and ^{208}Pb region targets respectively. When a neutron or a proton which is initially in the $1p_{3/2}(l_i = 1, j_i = l_i + \frac{1}{2})$ state in the projectile ^{7}Li is transferred to the target nucleus, the favoured transfer appears where the final state has $j_f = l_f + \frac{1}{2}$, and $l_f - l_i$ is similar to the angular momentum transfer between the entrance channel and the exit channel.

5.2 ^{90}Zr, ^{91}Zr, ^{89}Y (^{7}Li, ^{6}Li) Reactions

The energy spectra for (^{7}Li, ^{6}Li) reactions on the targets of ^{90}Zr, ^{91}Zr and ^{89}Y at E_{inc} = 30 MeV/n are shown in fig. 5.1. The dotted lines represent the background drawn by hand and the arrows at the bottom represent the centroid of the peaks analyzed. The peaks which have the same peak number are formed by transferring a neutron to the same orbit. The ejectile, ^{6}Li was measured at the grazing angle θ_{lab} = 6°. Parameters for the peaks are shown in table 5.1. In fig. 5.2, they are plotted as a function of both the excitation energies of the residual nuclei, and the reaction Q - values.

Eight peaks at low excitation (less than 10 MeV) are observed in each reaction. The first four peaks at low excitation in the ^{90}Zr(^{7}Li, ^{6}Li) reaction are well resolved, but the peaks are not so clearly resolved in the ^{91}Zr(^{7}Li, ^{6}Li) and ^{89}Y(^{7}Li, ^{6}Li)

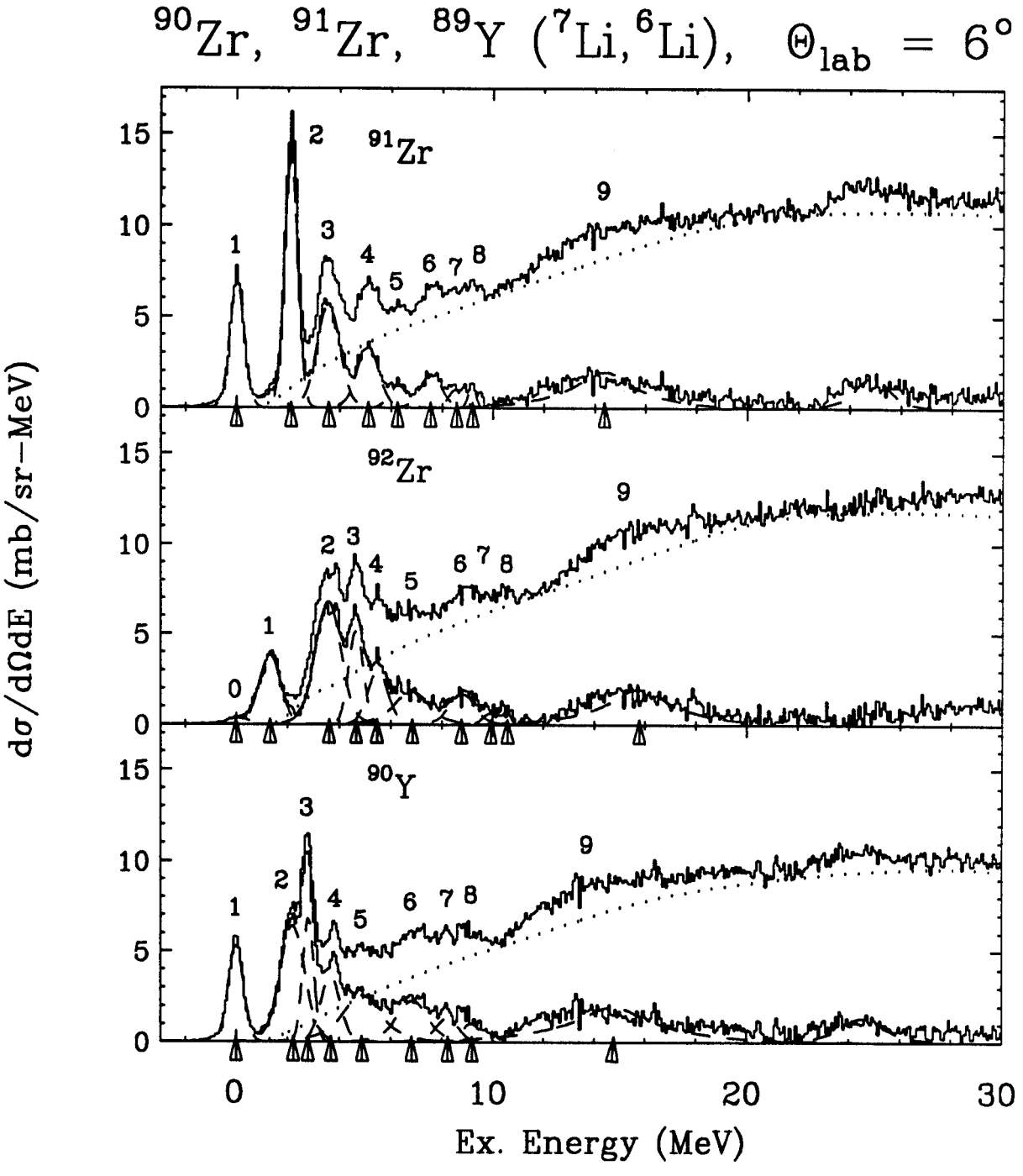

Figure 5.1: Energy spectra from ^{90}Zr, ^{91}Zr, ^{89}Y (^{7}Li, ^{6}Li) reactions (E_{inc} = 30 MeV/n). The dotted lines represent the background and the under lying spectra are obtained after the background is subtracted. Arrows at the bottom of each spectrum represent the centroid of the peaks.

Table 5.1: Excitation energies for the resolved peaks for (^{7}Li, ^{6}Li) reactions on targets of ^{90}Zr, ^{91}Zr and ^{89}Y. Γ is the full width at half maximum, Q is the reaction Q-Value for a corresponding excitation energy and the units are MeV. The uncertainty is about 0.15 MeV. σ is the cross section in mb/sr and the uncertainty is about 20%. Peak 0 in the spectrum is the ground state which is shifted to lower energy due to the $p-p$ interaction.

	^{90}Zr(^{7}Li,^{6}Li)^{91}Zr				^{91}Zr(^{7}Li,^{6}Li)^{92}Zr				^{89}Y(^{7}Li,^{6}Li)^{90}Y			
Peak #	Ex.	Γ	- Q	σ	Ex.	Γ	- Q	σ	Ex.	Γ	- Q	σ
0					0.00	0.6	-1.39					
1	0.00	0.7	0.06		1.34	0.9	-0.05		0.1	0.7	0.49	
2	2.13	1.0	2.19		3.60	1.2	2.21		2.22	1.1	2.61	
3	3.58	1.0	3.64		4.67	0.9	3.28		2.84	0.8	3.23	
4	5.12	1.0	5.18		5.53	1.0	4.14		3.70	1.1	4.09	
5	6.29	1.2	6.35		6.83	1.6	5.44		4.92	1.6	5.31	
6	7.58	1.2	7.64		8.84	1.2	7.45		6.87	1.4	7.26	
7	8.57	0.7	8.63		9.97	0.8	8.58		8.25	1.0	8.64	
8	9.20	0.5	9.26		10.63	0.5	9.24		9.19	0.7	9.58	
9	14.40	6.0	14.46	8.0	15.80	6.0	14.41	8.3	14.0	6.0	14.39	9.9

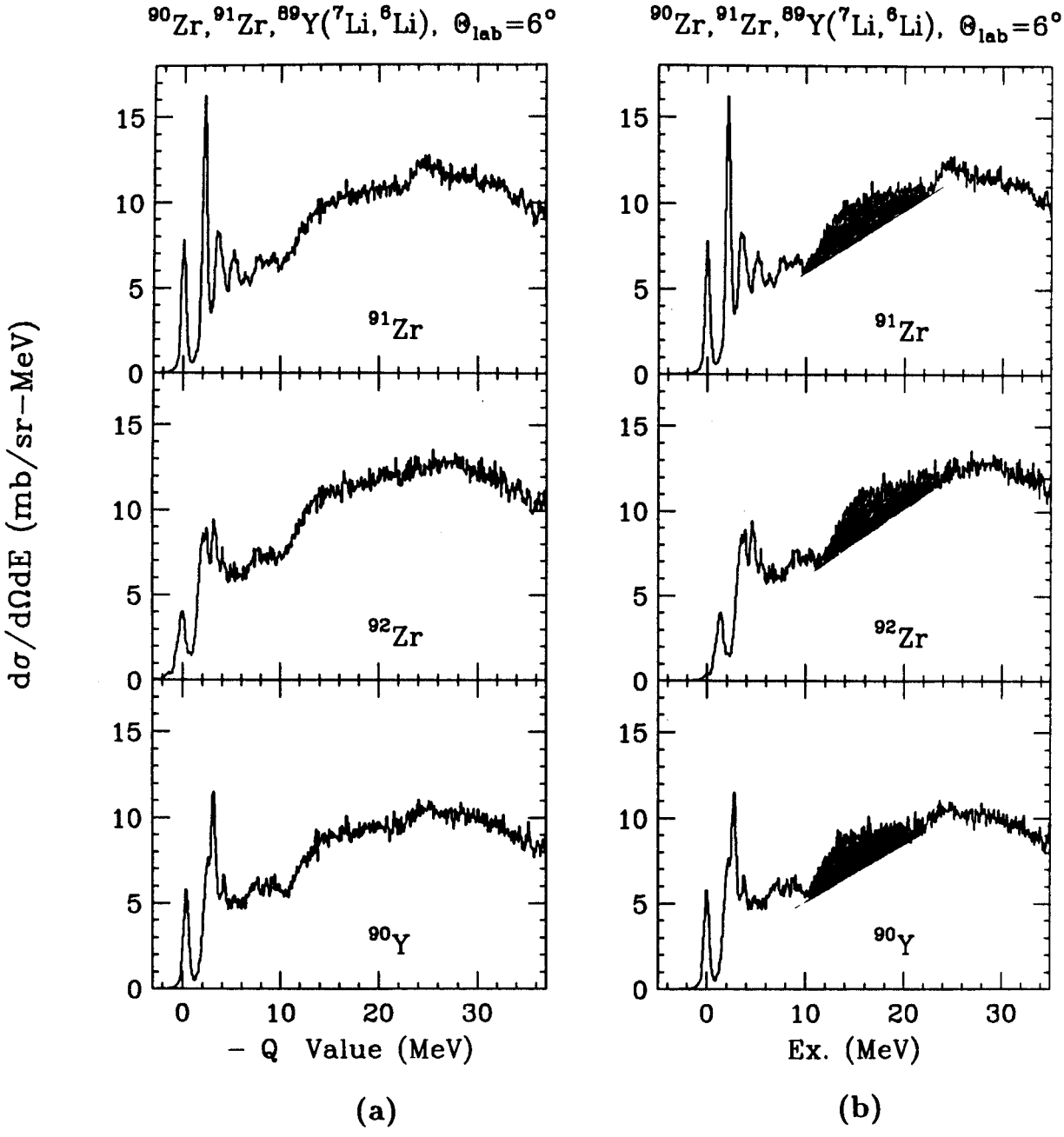

Figure 5.2: Comparison of the neutron transfer spectra on ^{90}Zr region nuclei. Spectra are plotted as functions of reaction Q – values and excitation energies. Broad peaks above the assumed background are shaded to help to compare the positions and cross sections.

reactions. Two broad peaks are seen at excitation energies about 14 MeV and 24 MeV.

The ^{90}Zr target has a j^{π}=0^{+} ground state. If the core nucleus ^{90}Zr remains in the ground state after the reaction, then in the residual nucleus ^{91}Zr, only the single particle states are formed by the transfer reaction. The single particle states of ^{91}Zr at low excitation are 0.0 MeV ($2d_{5/2}$), 1.2 MeV ($3s_{1/2}$), 2.04 MeV ($2d_{3/2}$), 2.17 MeV ($1h_{11/2}$) and 2.2 MeV ($1g_{7/2}$). But the ground state of the core may be broken and the core states may couple with the single particle states and split the single energy level into many levels [Zism 73].

The ^{89}Y target nucleus has one less proton in the $2p_{1/2}$ shell than the ^{90}Zr nucleus and can be regarded as a composite of ^{90}Zr and a proton hole state $(2p_{1/2})^{-1}$. The ^{91}Zr target nucleus has one extra neutron in the $1d_{5/2}$ shell compared to the ^{90}Zr nucleus and may be treated as a composite of ^{90}Zr and a neutron particle state ($1d_{5/2}$). When a neutron is transferred to the target nucleus, the residual nucleus's wave function may be written as

$$|^{91}\ Zr\rangle = |^{90}\ Zr\rangle \mid n\rangle, \tag{5.1}$$

$$|^{92}\ Zr\rangle = |^{90}\ Zr\rangle \mid \nu(d_{5/2})\rangle \mid n\rangle, \tag{5.2}$$

$$|^{90}\ Y\rangle = |^{90}\ Zr\rangle \mid \pi(p_{1/2})^{-1}\rangle \mid n\rangle, \tag{5.3}$$

where $\mid n\rangle$ is the transferred neutron's particle state. As the interesting physical quantities are obtained from the comparison of each reaction, only the relative values will be compared in the analysis. So the common term, $|^{90}\ Zr\rangle$ may be neglected in the residual nucleus's wave function for simplicity. Then the couplings of the core state with the neutron's single particle states may be simplified without losing any important physical characteristics. In many experiments, the Q – value of the centroid of the particle states, weighted by spectroscopic factor, shifts about 0.2 to 0.3 MeV

due to a single particle or a hole state [Hodg 80].

In the ^{90}Zr(^{7}Li, ^{6}Li) reaction, the first four peaks are strongly populated, where the main contribution comes from a single state in each peak. The favoured angular momentum transfer in this reaction is about $6\hbar$ and a transition with no spin-flip is more favoured. The ground state $2d_{5/2}(l_f = 2, j_f = l_f + \frac{1}{2})$ is strongly populated, but a single particle state $3s_{1/2}$ (1.21 MeV, $l_f = 0, j_f = \frac{1}{2}$) is so weak due to the small angular momentum transfer compared to the favoured angular momentum transfer and the small value of $2j+1$ that it is not seen at all. The second peak at 2.13 MeV is composed of $2d_{3/2}$ (2.04 MeV, $l_f = 2, j_f = l_f - \frac{1}{2}$), $1h_{11/2}$ (2.17 MeV, $l_f = 5, j_f = l_f + \frac{1}{2}$) and $1g_{7/2}$ (2.20 MeV, $l_f = 4, j_f = l_f - \frac{1}{2}$), where $1h_{11/2}$ is probably the most dominant because of a similar angular momentum transfer to the favoured angular momentum transfer $6\hbar$ and no spin-flip process. These 3 states are not resolved in this experiment. The third and fourth peaks (3.58 MeV and 5.12 MeV) probably have a contribution mainly from the $1h_{11/2}$ state, and a little from the $1g_{7/2}$ state [Bing 70]. The first four peaks are resolved clearly, because the density of states is small in this excitation energy region and the transfer conditions favour only one state in each peak. But, as the excitation energy increases, the density of states become larger and the states overlap each other. Thus peaks 5 to 8 show up very weakly above the substantial underlying background and the components are not well known.

In the ^{91}Zr(^{7}Li, ^{6}Li) reaction, the spectrum is similar to the spectrum of ^{90}Zr(^{7}Li,^{6}Li) reaction. But the relative strengths and positions are changed a little due to the couplings of single particle states with the target's $\frac{5}{2}^+$ state. The ground state of ^{92}Zr(0^+) is shifted to lower energy by about 1.34 MeV from the strong 4^+ state which corresponds to the ground state of the ^{90}Zr(^{7}Li,^{6}Li) reaction where a neutron is transferred to the $2d_{5/2}$ state. This is caused by the coupling between the two neutrons in the $\frac{5}{2}^+$ state. If a neutron is transferred to the $2d_{5/2}$ state, then there will be two neutrons

in the same state. Because of the two identical particles in the same state, only even values of j are allowed and the possible states are 0^+ (ground state), 2^+ (0.93 MeV) and 4^+ (1.50 MeV). The first peak has $j^\pi = 0^+$ which is the ground state and the second peak (1.34 MeV) is a mixture of 2^+, 0^+ and 4^+ states, where the 4^+ state is the most prominent. The $(2j_f + 1)$ dependence of stripping reaction cross section is a probable explanation for the weak ground state population. The two neutrons in the same shell are very similar to the two protons in the same shell, as in the ^{209}Bi(^{7}Li,^{6}He) reaction. Shell model calculations for the two protons in the $1h_{9/2}$ state in ^{210}Po show that the ground state, 0^+, is shifted to lower energy by 1.33 MeV (see chap. 3), which is a very similar value to the 1.34 MeV shift of the ground state for the two neutrons in the $2d_{5/2}$ state. The reaction Q – values of the centroid of the peaks, except the ground state, are shifted very little from the reaction Q – values of the similar peaks seen in the ^{90}Zr(^{7}Li,^{6}Li) reaction (fig. 5.2). In most of the cases, except for peaks 4 and 5, the differences of the reaction Q – values from the ^{90}Zr(^{7}Li, ^{6}Li) reaction are less than 0.5 MeV. For peaks 4 and 5, the differences are about 1 MeV. This is probably caused by the insufficient energy resolution, rather than a particle – particle interaction. All the peaks in the spectrum of the ^{92}Zr nucleus are broadened because of the couplings with the $1d_{5/2}$ state of the ^{91}Zr nucleus. However, the total strengths of the peaks in the ^{92}Zr spectrum are not very different from those in the ^{91}Zr spectrum, within 10% in most of the cases. The peaks beyond peak 4 are not clearly resolved as in the ^{91}Zr spectrum.

In the ^{89}Y(^{7}Li,^{6}Li) reaction, the spectrum is similar to the previous two spectra. The ground state of ^{89}Y is $\frac{1}{2}^-$. A neutron transferred to a $2d_{5/2}$ state couples with the $\frac{1}{2}^-$ state of the target, and produces 2^- and 3^- states, which are present in peak 1. These two states are not resolved due to the small energy difference ($\sim$ 0.2 MeV). The reaction Q – value of the centroid of these two peaks is shifted from that of

the ^{90}Zr(^{7}Li,^{6}Li) reaction by about 0.4 MeV. All the peaks in this reaction, except peak 1, are broadened and overlap with their neighboring states due to the couplings between the single particle states and a proton hole state, $\pi(2p_{1/2})^{-1}$. These coupling strengths are not big enough to change the shape of the peak, as is shown in peak 1. But it makes the states overlap with each other, and thus the peaks beyond peak 4 are not resolved clearly.

In fig. 5.2, all 3 spectra are plotted as functions of reaction Q – values and excitation energies. At high excitation, two broad peaks are seen in all 3 reactions at about $Ex. \sim 14$ MeV and ~ 24 MeV.

The broad peaks seen at $Ex. \sim 14$ MeV, are so broad that it is difficult to compare the centroid of the peaks. Instead, the starting points of the peaks are compared. In the figure expressed in reaction Q – values, the broad peaks in all 3 reactions appear almost at the same positions and the deviations are less than 0.3 MeV. But in the figure expressed in excitation energies, the peak in the ^{91}Zr(^{7}Li,^{6}Li) reaction is shifted to higher excitations by 1.5 MeV compared to the peak in the ^{90}Zr(^{7}Li,^{6}Li) reaction, while the peak in the ^{89}Y(^{7}Li,^{6}Li) reaction is shifted to lower energy by about 0.3 MeV. The broad peaks have very similar reaction Q – values but have different excitation energies, which shows that the peaks have the characteristics of single particle states rather than those of GR states.

The other peaks are seen at excitation energies about $23 \sim 26$ MeV. Broad peaks at similar excitation energies were also observed in the ^{90}Zr(^{20}Ne,^{19}Ne) reactions at E_{inc} =25, 30 and 40 MeV/n [Fras 87, Fort 90], where the excitation energies are somewhat dependent on the incident projectile's energies. One of the possible explanations is that they are from the projectile direct breakup processes. Consider the ^{90}Zr(^{7}Li,^{6}Li) reaction. The threshold energy for breakup of ^{7}Li $\rightarrow$ ^{6}Li + n is 7.25 MeV and the recoil energy of ^{90}Zr is about 0.2 MeV for elastic scattering of ^{7}Li

at 6°. Thus the kinetic energy of ^{6}Li from the breakup process may be as large as 202.55 MeV, which corresponds to 7.15 MeV excitation energy in ^{91}Zr where the kinetic energy of ^{6}Li from the transfer reaction of ^{90}Zr(^{7}Li, ^{6}Li)^{91}Zr$_{gnd}$ is 209.7 MeV. In many experiments the centroid of the peak of the breakup particles has been observed at the energy corresponding to the incident beam velocity, but always less than the beam velocity [Wu 78, Mats 80]. The energy corresponding to the beam velocity for ^{6}Li is 180 MeV, which corresponds to 29.7 MeV in excitation energy. This excitation energy is higher than the observed peak by about 5 MeV so that it is unlikely this peak is from the projectile breakup process. This remains a puzzle.

5.3 ^{208}Pb, ^{209}Bi, ^{207}Pb (^{7}Li, ^{6}Li) Reactions

The energy spectra for the (^{7}Li, ^{6}Li) reactions on targets of ^{208}Pb, ^{209}Bi and ^{207}Pb are shown in fig. 5.3. Parameters for the peaks are given in table 5.2. In fig. 5.4, they are compared as a function of both the excitation energies and the reaction Q – values. The scattered ejectile, ^{6}Li was measured at the grazing angle. Eight peaks were resolved at low excitation in each spectrum. Two broad peaks at excitation energies about 10 MeV and 20 MeV are observed in all 3 reactions.

The ^{208}Pb nucleus is a doubly closed shell nucleus and has $j^{\pi} = 0^{+}$ in its ground state. The single particle states formed by a neutron stripping reaction on the ^{208}Pb target are 0.0 MeV ($2g_{9/2}$), 0.78 MeV ($1i_{11/2}$), 1.42 MeV ($1j_{15/2}, 3d_{5/2}$) and 2.49 MeV (mainly $2g_{7/2}$) at low excitation. The ^{209}Bi nucleus has one more proton in the $1h_{9/2}$ shell than the ^{208}Pb nucleus, and the ^{207}Pb nucleus has one less neutron in the $3p_{1/2}$ shell than the ^{208}Pb nucleus. For neutron stripping reactions on these targets, the residual nuclei's wave functions may be written as

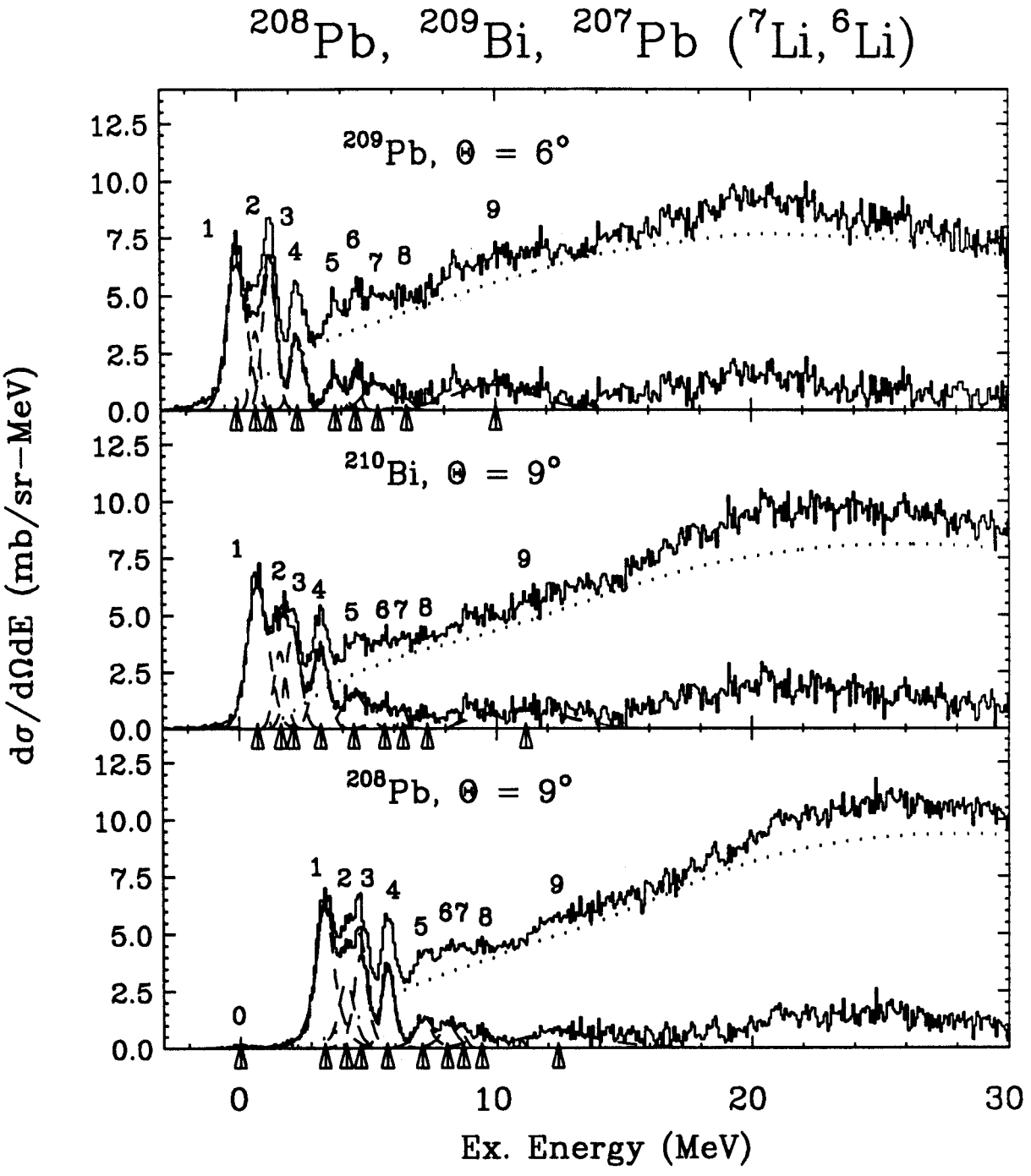

Figure 5.3: Energy spectra from ^{208}Pb, ^{209}Bi, ^{207}Pb (^{7}Li, ^{6}Li) reactions (E_{inc} = 30 MeV/n). The dotted lines represent the background and the under lying spectra are obtained after the background is subtracted. Arrows at the bottom of each spectrum represent the centroid of the peaks.

Table 5.2: Excitation energies for the resolved peaks for the (^{7}Li, ^{6}Li) reactions on targets of ^{208}Pb, ^{209}Bi and ^{207}Pb. Γ is the full width at half maximum, Q is the reaction Q – value for a corresponding excitation energy and units are MeV. The uncertainty is about 0.15 MeV. σ is the cross section in mb/sr and the uncertainty is about 20%. Peak 0 in the spectrum is the ground state which is shifted to lower energy due to the $p-p$ interaction.

	^{208}Pb(^{7}Li,^{6}Li)^{209}Pb				^{209}Bi(^{7}Li,^{6}Li)^{210}Bi				^{207}Pb(^{7}Li,^{6}Li)^{208}Pb			
Peak #	Ex.	Γ	- Q	σ	Ex.	Γ	- Q	σ	Ex.	Γ	- Q	σ
0									0.00	1.2	-0.12	
1	0.00	1.1	3.13		0.65	1.0	3.30		3.30	1.0	3.18	
2	0.78	0.6	3.91		1.51	0.7	4.16		4.14	0.8	4.02	
3	1.32	0.7	4.45		2.01	0.8	4.66		4.70	0.8	4.58	
4	2.39	0.7	5.52		3.06	0.8	5.71		5.75	0.7	5.63	
5	3.78	0.8	6.91		4.36	1.0	7.01		7.13	1.0	7.01	
6	4.60	0.7	7.73		5.56	1.0	8.21		8.10	1.0	7.98	
7	5.44	1.0	8.57		6.29	0.7	8.94		8.68	0.8	8.56	
8	6.61	0.7	9.74		7.20	1.0	9.85		9.39	1.0	9.27	
9	10.0	5.0	13.13	4.6	11.01	5.0	13.66	4.4	13.29	5.0	13.17	3.5

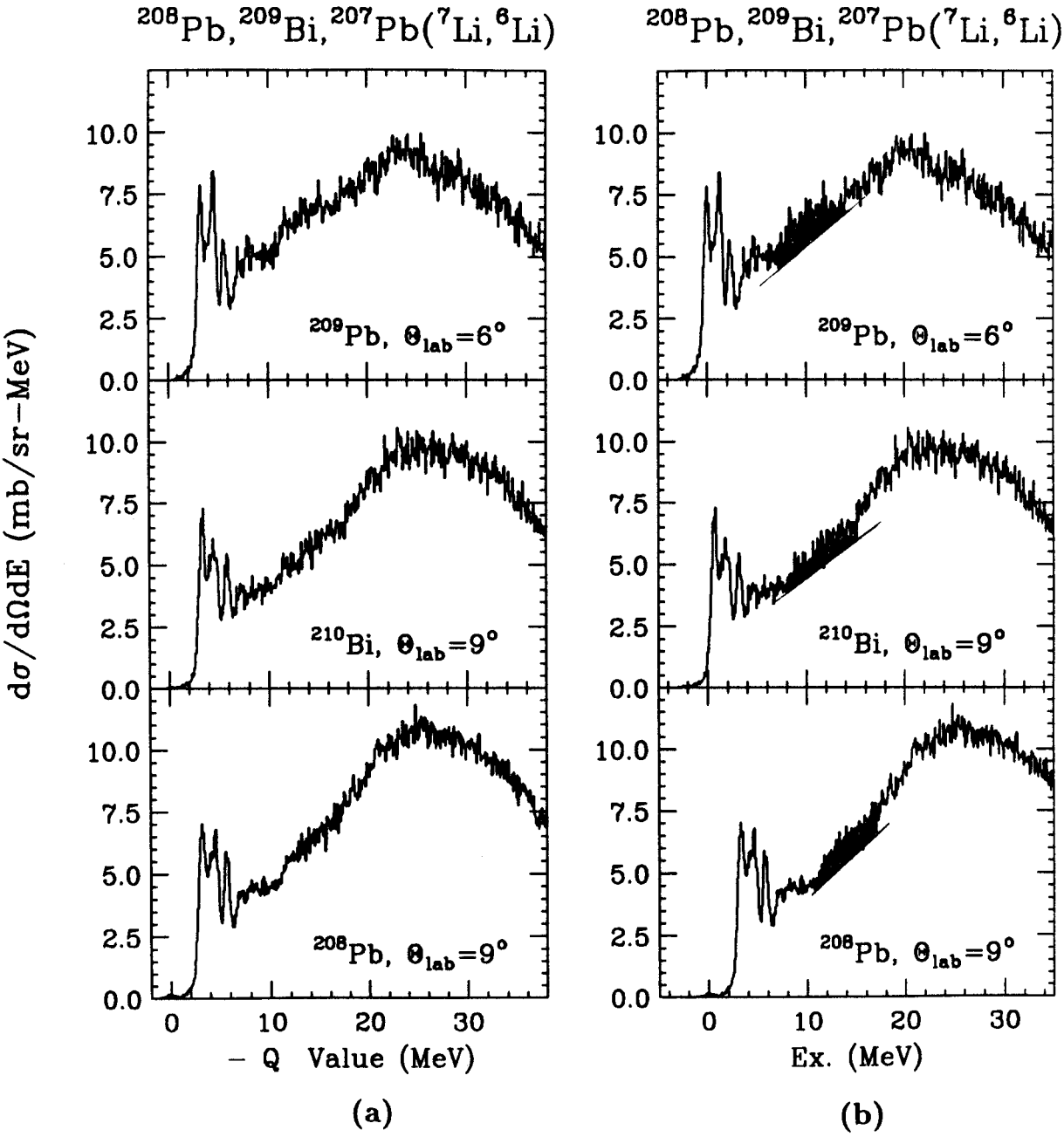

Figure 5.4: Comparison of the neutron transfer spectra on ^{208}Pb region nuclei. Spectra are plotted as functions both of reaction Q – values and excitation energies. Broad peaks above the assumed background are shaded to help to compare the positions and cross sections.

$$|^{209}\,Pb\rangle = |^{208}\,Pb\rangle \mid n\rangle, \tag{5.4}$$

$$|^{210}\,Bi\rangle = |^{208}\,Pb\rangle \mid \pi(h_{9/2})^{+}\rangle \mid n\rangle, \tag{5.5}$$

$$|^{208}\,Pb\rangle = |^{208}\,Pb\rangle \mid \nu(p_{1/2})^{-1}\rangle \mid n\rangle. \tag{5.6}$$

The common term $|^{208}\,Pb\rangle$ may be neglected for simplicity as in the previous section, because the physics of interest results from the comparisons of the spectra for the different targets.

In the ^{208}Pb(^{7}Li, ^{6}Li)^{209}Pb reaction, the ground state ($2g_{9/2}$, peak 1) and the third peak (1.33 MeV, mainly $1j_{15/2}, 3d_{5/2}$) are strongly populated, whereas the second (0.78 MeV, $1i_{11/2}$) and the fourth peaks (2.24 MeV, mainly $2g_{7/2}$) are relatively weakly populated. The relative intensities of these peaks can be explained by a combination of angular momentum transfer and spin-flip processes. In this reaction, the favoured angular momentum transfer for good matching is about $8\hbar$ and no spin-flip is favoured [Merm 88]. If these two matching conditions are applied to the first four peaks, the relative populations can be understood easily. In fig. 5.3, the ground state of ^{209}Pb ($2g_{9/2}$, $l_f = 4$, $j_f = l_f + \frac{1}{2}$) which is formed by a no spin-flip transition, is stronger than the fourth peak (2.24 MeV, $2g_{7/2}$, $l_f = 4$, $j_f = l_f - \frac{1}{2}$) which is formed by a spin-flip transition. The second peak (0.78 MeV, $1i_{11/2}$, $l_f = 5$, $j_f = l_f - \frac{1}{2}$) is relatively weak compared to the third peak, mainly a $1j_{15/2}$ state (1.33 MeV, $l_f = 6$, $j_f = l_f + \frac{1}{2}$), which has a similar orbital angular momentum but is formed by a no spin-flip transition. In these two cases, the spin-flip processes played an important role in the transition strengths. Above 4 MeV of excitation energy, peaks are not resolved as individual states but appear as a combination of many single states above the substantial background.

In the ^{209}Bi(^{7}Li, ^{6}Li)^{210}Bi reaction, the kinematics and the transfer matching

conditions are very similar to those of the ^{208}Pb(^{7}Li,^{6}Li) reaction, except that ^{209}Bi has one more proton in the $1h_{9/2}$ shell than ^{208}Pb. This $\pi(1h_{9/2})$ state couples with the single particle states of the ^{209}Pb nucleus and forms multiplets. The 1^- ground state of ^{210}Bi results from one of the couplings between the $\pi(1h_{9/2})$ state and the $\nu(2g_{9/2})$ state, whereas the other coupled states, arising from the coupling of these two states, make a large peak at 0.65 MeV (peak 1), a composite of many states. The ground state is very weak and it is not seen as a separated peak. Peak 2 is also not seen as a separated peak due to the overlap with peaks 1 and 3. Peak 3 is somewhat broader than the comparable peak in the ^{209}Pb nucleus. The strengths for peaks 2 and 3 are almost the same as those of the comparable peaks in ^{209}Pb. Overall, the shape of the spectrum looks very similar to that of the ^{209}Pb nucleus except that the spectrum is shifted to higher excitation energy by about 0.65 MeV.

If the spectra are plotted as functions of reaction – Q values as in fig. 5.4.(a), the centroid of the each peak in ^{210}Bi appears at almost the same position as the comparable peak in ^{209}Pb. The existence of an extra proton in the ^{209}Bi target changed the widths of some peaks slightly, but the total strength of the comparable peaks remained the same. In chap. 3, the contribution of an extra particle or hole in the target to the transition probability of each final state is discussed. For the three lowest orbits ($2g_{5/2}$, $1i_{11/2}$, $1j_{15/2}$), the average excitation energies for the $[\nu(2g_{9/2}) \otimes \pi(1g_{9/2})]$, $[\nu(1i_{11/2} \otimes \pi(1g_{9/2})]$ and $[\nu(1j_{15/2}) \otimes \pi(1g_{9/2})]$ multiplets due to coupling with the target's $1h_{9/2}$ state are calculated using the shell model (see chap. 3). The excitation energies and reaction Q – values of the centroid are compared with the experimental measurements for the 3 multiplets after the energies of individual states in each multiplet are weighted by their cross sections (see tables 3.1, 3.2 and fig. 3.3). The results show that the shell model calculations agree with this experiment very well and one extra proton outside the closed shell of a heavy nucleus does not change

the reaction Q – values much, at most by 0.3 MeV at low excitation.

In the ^{207}Pb(^{7}Li, ^{6}Li)^{208}Pb reaction, the conditions are the same as with the ^{208}Pb(^{7}Li,^{6}Li) reaction, except that ^{207}Pb has a neutron hole state in the $3p_{1/2}$ shell. The 0^+ ground state of ^{208}Pb results when a transferred neutron fills the $3p_{1/2}$ hole state. This state is shifted by about 3.3 MeV to lower energy from peak 1, a composite of 5^- and 4^- states resulting from the couplings between $3p_{1/2}$ and $2g_{9/2}$ states (fig. 5.4). This 3.3 MeV is very similar to the outmost neutron's binding energy difference (3.43 MeV) between the ^{208}Pb and ^{209}Pb nuclei. The ground state is extremely weakly populated compared to the other states. This is because first this transition involves a spin-flip process, and second the angular momentum transfer, $1\hbar$, is much smaller than the favoured angular momentum transfer, $7\hbar$.

At about 10 MeV excitation energy in all 3 spectra, broad peaks whose nature has been questioned are seen. In the present experiment, these peaks are very weak compared to the data obtained by using the ^{20}Ne or ^{12}C beam [Fort 90, Merm 88]. However, the peaks may still be recognized above the large underlying background. The starting points of the peaks are compared. All 3 broad peaks appeared at almost the same reaction Q – values. But, when expressed in excitation energies, the peak of ^{209}Bi(^{7}Li,^{6}Li) reaction is shifted to higher excitation by about 0.6 MeV and the peak of ^{207}Pb(^{7}Li,^{6}Li) reaction is shifted to higher excitation by 3.5 MeV. The broad peaks have same reaction Q – values, but have different excitation energies. The result of this comparison also suggests that the peaks have the characteristics of single particle states.

At about 20 MeV of excitation energy in the ^{209}Pb and ^{210}Bi nuclei, another broad peaks are observed. The peak is seen at about 25 MeV excitation energy in the ^{208}Pb nucleus. The broad peaks at these excitation energies are also observed in the experiments of ^{208}Pb(^{20}Ne,^{19}Ne) with E_{inc} = 40 MeV/n and ^{208}Pb(^{36}Ar,^{35}Ar) with

E_{inc} = 41 MeV/n [Chom 90]. However the reaction Q - values of these broad peaks are nearly the same (within 1 MeV difference). From the comparison of the excitation energies and the reaction Q - values, these peaks show the characteristics of single particle states rather than GR states. The energy of the beam velocity of the projectile breakup particles (180 MeV, ^{6}Li) corresponds to 26.6 MeV excitation energy in ^{209}Pb. The excitation energy of the centroid is somewhat higher (by $\sim$ 6.6 MeV) than the beam velocity. In light ion projectile breakup experiments [Wu 79, Mats 78, Mats 80], the projectile breakup processes are peaked at near or smaller than the energy of the beam velocity. Thus it seems unlikely that these broad peaks are from the projectile breakup processes. As in the previous section for (^{7}Li,^{6}Li) reactions on ^{90}Zr regions targets, their nature is not clearly understood.

5.4 ^{90}Zr, ^{91}Zr, ^{89}Y (^{7}Li, ^{6}He) Reactions

The energy spectra for the (^{7}Li,^{6}He) reactions on targets of ^{90}Zr, ^{91}Zr and ^{89}Y with E_{inc} = 30 MeV/n are given in fig. 5.5. The ^{6}He particles were measured at the grazing angle θ_{lab} = 6°. Parameters for the peaks are given in table 5.3. Eight peaks are resolved at low excitation. In the ^{6}He nucleus, as the threshold energy for breakup into ^{5}He + n is smaller than the excitation energy for the first excited state, no ejectile excitation is possible. All the peaks, except peak 1, appear above a substantial background in all three reactions. In fig. 5.6, they are compared as a function of both the excitation energies of the residual nuclei, and the reaction Q - values.

In the ^{90}Zr(^{7}Li,^{6}He)^{91}Nb reaction, peak 1 is strongly populated. This peak is a composite of the two states which are not resolved, the $1g_{9/2}$ (0.0 MeV) and $2p_{1/2}$ (0.105 MeV) states [Fink 73, Knop 70, Vour 69]. The main contribution to the peak

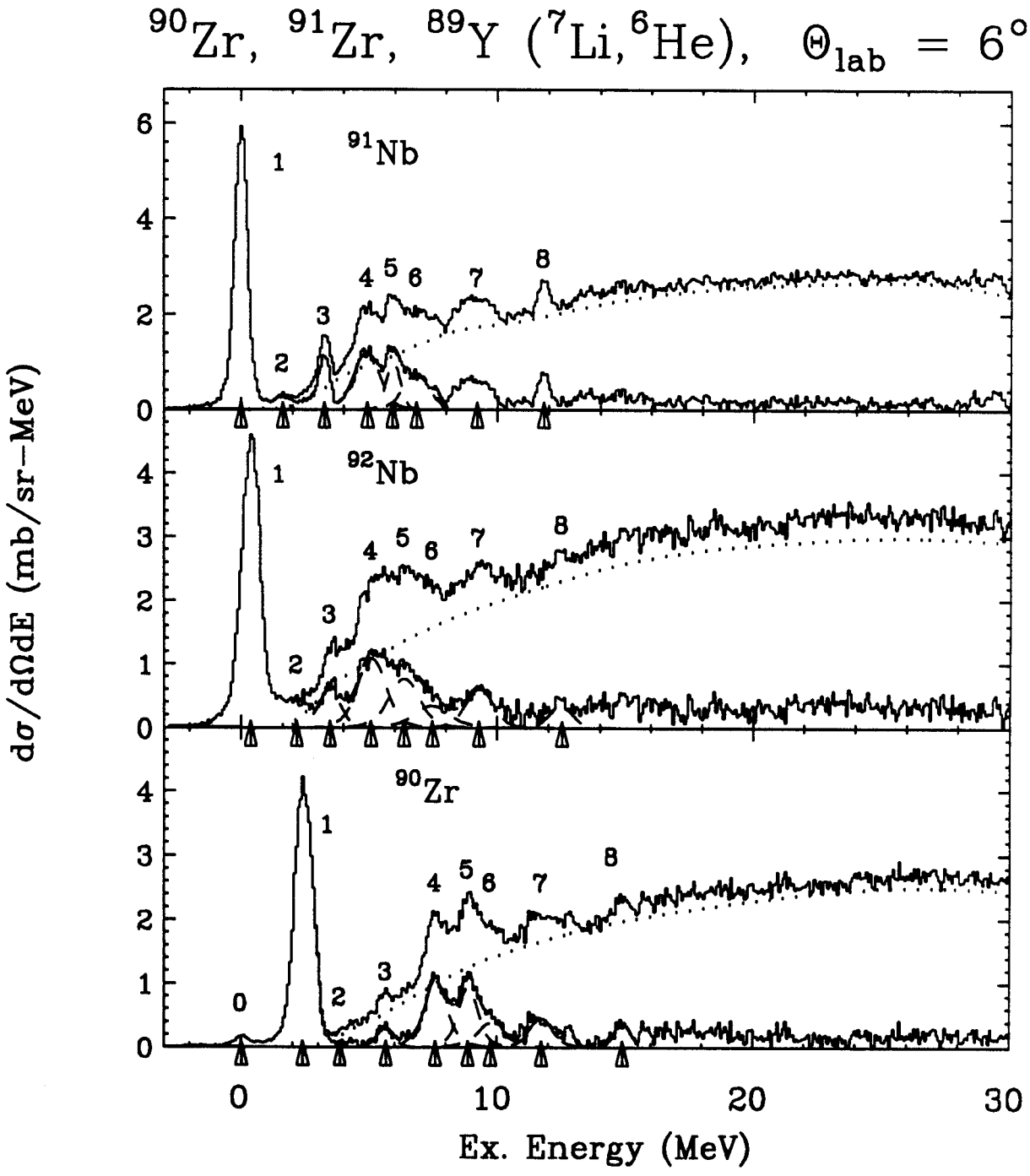

Figure 5.5: Energy spectra of ^{90}Zr, ^{91}Zr, ^{89}Y (^{7}Li, ^{6}He) reactions (E_{inc} = 30 MeV/n). The dotted lines represent the background and the under lying spectra are obtained after the background is subtracted. Arrows at the bottom of each spectrum represent the centroid of the peaks.

Table 5.3: Excitation energies for the resolved peaks for (^{7}Li, ^{6}He) reactions on targets of ^{90}Zr, ^{91}Zr and ^{89}Y. Γ is the full width at half maximum, Q is the reaction Q-Value for a corresponding excitation energy and units are MeV. The uncertainty is about 0.15 MeV. σ is the cross section in mb/sr and the uncertainty is about 20%. Peak 0 in the spectrum is the ground state which is shifted to lower energy due to an extra hole state.

	^{90}Zr(^{7}Li,^{6}He)^{91}Nb				^{91}Zr(^{7}Li,^{6}He)^{92}Nb				^{89}Y(^{7}Li,^{6}He)^{90}Zr			
Peak #	Ex.	Γ	- Q	σ	Ex.	Γ	- Q	σ	Ex.	Γ	- Q	σ
0									0.00	0.86	1.62	
1	0.00	0.8	4.82		0.42	1.0	4.53		2.44	1.0	4.06	
2	1.67	0.6	6.49		2.22	0.5	6.35		4.13	0.5	5.75	
3	3.13	0.6	7.95		3.48	0.9	7.61		5.75	0.9	7.37	
4	4.93	1.2	9.75		5.13	1.2	9.26		7.75	1.3	9.37	
5	5.96	0.8	10.78		6.39	1.3	10.52		9.02	1.3	10.74	
6	6.85	1.2	11.67		7.48	1.5	11.61		9.91	1.3	11.53	
7	9.10	3.0	13.92	.72	9.35	3.0	13.48	.79	11.88	3.0	13.50	.68
8	11.86	0.6	16.68		12.52	0.8	16.65		15.02	1.0	16.64	

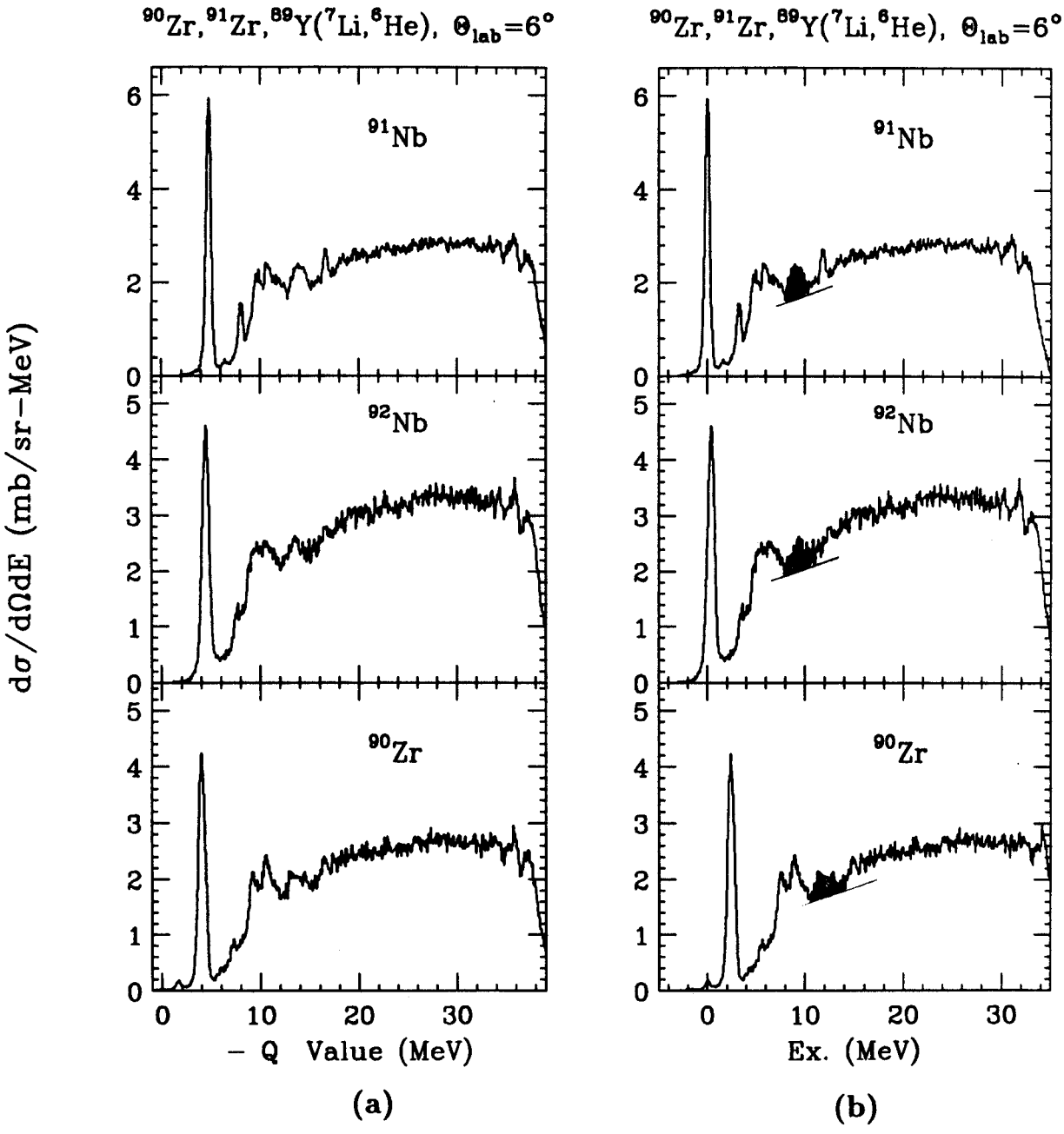

Figure 5.6: Comparison of the proton transfer spectra on ^{90}Zr region nuclei. Spectra are compared as functions of reaction Q – values and excitation energies. Peaks 7 above the assumed background are shaded to help to compare the positions and cross sections. Note that the small peaks near 32 MeV excitation energy arise from end effects in the counter. Similar effects are seen in many other spectra.

is very likely from the $1g_{9/2}$ state. The ^{90}Zr target's ground state has $j^{\pi} = 0^{+}$, a mixture of about 65% of $\pi(2p_{1/2})^{2}$, which is a closed shell, and about 35% of $\pi(2p_{1/2})^{-2}\pi(1g_{9/2})^{2}$, which has two proton holes in the $2p_{1/2}$ state and two proton particles in the $1g_{9/2}$ state [Baym 58]. Defining the closed shell as $\mid 0\rangle$, the ground state of the ^{90}Zr target can be represented by

$$|^{90}\ Zr\rangle_{0+} = \sqrt{0.65}\mid 0\rangle + \sqrt{0.35}[\pi(2p_{1/2})^{-2}\pi(1g_{9/2})^{+2}]\mid 0\rangle. \qquad (5.7)$$

The ground state of the ^{91}Nb nucleus, $j^{\pi} = \frac{9}{2}^{+}$ is formed when a proton is transferred to the $1g_{9/2}$ shell and can be written as

$$|^{91}\ Nb\rangle_{9/2^{+}} = \sqrt{0.65}[\pi(1g_{9/2})]\mid 0\rangle + \sqrt{0.35}[\pi(2p_{1/2})^{-2}\pi(1g_{9/2})^{+3}]\mid 0\rangle. \qquad (5.8)$$

The first excited state $j^{\pi} = \frac{1}{2}^{-}$ (0.105 MeV) results when a proton is transferred to the $2p_{1/2}$ shell and forms a state with the combination $[\pi(2p_{1/2})^{-1}\pi(1g_{9/2})^{+2}]\mid 0\rangle$ [Knop 70]. The weak population of this state may be explained by using the two matching conditions for transfer reactions. First a spin-flip process is involved in a transition to the $2p_{1/2}$ state, whereas it is not involved in a transition to the $1g_{9/2}$ state. It was evident in neutron stripping reactions that a non spin-flip transition is preferable to a transition where a spin-flip process is involved. Secondly, the favoured angular momentum transfer, $5\hbar$ is much larger than that of a transition to $2p_{1/2}(l = 1)$, while the angular momentum transfer to the ground state $(2g_{9/2}, l = 4)$ is closer to the favoured transfer condition.

In reactions with low incident energies, the angular momentum mismatch between the entrance and exit channel is small and the favoured angular momentum transfer becomes small, and thus the relative ratio of the population for the $2p_{1/2}$ state will be increased. In the ^{90}Zr(^{3}He,d) experiment done at an incident energy of 6 MeV/n, where the favoured momentum transfer is about $2\hbar$, the $2p_{1/2}$ state is much more strongly excited than in the present reaction [Knop 70].

Peak 3 (3.25 MeV), which is strongly populated, is mainly a $2d_{5/2}$ state. The angular momentum transfer to this $2d_{5/2}$ state is $2\hbar$ and no spin-flip process is involved, while the angular momentum transfer to the ground state is $4\hbar$ and no spin-flip is involved. The smaller angular momentum transfer is a good reason for the relatively weaker strength for peak 3 than that of the ground state. Peaks of 4, 5 and 6 are the sum of many single particle states which were resolved as separate states in a low energy experiment [Zism 73].

A large peak is seen at 9.1 MeV (peak 7). When the reaction Q – value and the excitation energy are compared with those of peaks 7 of other spectra, peaks 7 appeared at similar reaction Q – values but different excitation energies. The comaprison suggests that peaks 7 seem to be single particle states. The sharp peak seen at 11.9 MeV (peak 8) is an isobaric analog state [Fink 73]. No recognizable peak is observed above 12 MeV. The spectrum stays fairly flat from 15 MeV excitation energy up to about 30 MeV excitation energy.

One spectrum was measured out to 50 MeV excitation energy (see fig. 6.4). No large broad peak is observed at around 13 MeV of excitation energy in this reaction, whereas a large broad peak was observed in neutron stripping reactions on the ^{90}Zr region targets. This suggests that the broad peaks seen in (^{7}Li,^{6}Li) reactions are from one step processes rather than multi-step processes. If they were made by multi-step processes (GR excitation followed by transfer reaction), they also should be seen in (^{7}Li,^{6}He) reactions, because the cross sections and mechanisms for both reactions are very similar.

In the ^{91}Zr(^{7}Li, ^{6}He) reaction, the proton single particle states form multiplets when coupled with the target's ground state $\nu(d_{5/2})$. For example, the $\pi(g_{9/2})$ state couples with the $\nu(d_{5/2})$ state and forms a $(\pi(g_{9/2}), \nu(d_{5/2}))$ multiplet with j^π ranging from 2^+ to 7^+, which makes up most of peak 1. Similarly, $\pi(p_{1/2})$ couples with $\nu(d_{5/2})$

and forms a $(\pi(p_{1/2}), \nu(d_{5/2}))$ multiplet, 2^- and 3^-, which is a small fraction of peak 1. The ground state of the ^{92}Nb nucleus, $j = 7^+$ is so weakly excited that it is not separated from peak 1. The centroid of peak 1 is positioned at an excitation energy of 0.42 MeV, 0.3 MeV lower than the comparable peak in the ^{90}Zr(^{7}Li,^{6}Li) reaction, due to the coupling between the $\pi(g_{9/2})$ and $\nu(d_{5/2})$ states.

Peak 2 and peak 3 appear to be weaker than the corresponding peaks in the ^{90}Zr(^{7}Li,^{6}He) reaction. This results from the broadening of the peaks due to the couplings with the $\nu(d_{5/2})$ state. Overall, all the peaks, except peak 1 in this spectrum, are broadened and the ratio of peak to background is not as good as in the ^{91}Nb spectrum. Peak 8, which is very sharp in ^{91}Nb, is almost hidden in the background and is not seen clearly. The interactions between the $\nu(2d_{5/2})$ state and the proton's single particle state are very similar to the interactions between the $\pi(2g_{9/2})$ state and the neutron single particle states in the ^{209}Bi(^{7}Li,^{6}Li) reaction. Peak 7 which is shifted to higher excitation energy by 0.25 MeV from the comparable peak of ^{91}Nb appears to be the sum of many single particle states.

In the ^{89}Y(^{7}Li, ^{6}He)^{90}Zr reaction, the spectrum is very similar to that of the ^{90}Zr(^{7}Li,^{6}He) reaction except that the ground state is shifted to lower energy. As the ground state of ^{89}Y is $j^\pi = \frac{1}{2}^-$, proton single particle states couple with this state to form multiplets. The ground state of the residual nucleus ^{90}Zr is formed when a transferred proton fills the $2p_{1/2}$ hole state. This transition is very similar to that of the ^{207}Pb$(+n)$ reaction where the ground state is formed when a neutron fills the neutron hole state, $\nu(3p_{1/2})$. In both cases, the ground states are very weakly excited because of small values of $2j + 1$, and the poor transfer matching conditions.

Peak 1 is a composite of many states and is mainly populated when a proton is transferred to the $1g_{9/2}$ shell. This $1g_{9/2}$ state couples with the $\pi(2p_{1/2})^{-1}$ state and forms 4^- and 5^- states, where the 5^- state is more strongly populated. The reaction

Q – value difference between the ground states of the ^{90}Zr(^{7}Li,^{6}He) and ^{89}Y(^{7}Li,^{6}He) reactions is 3.2 MeV, which is the same as the proton's binding energy difference in ^{90}Zr and ^{91}Nb nuclei. While in peaks 1 of these two reactions, a difference in reaction Q – value of about 0.76 MeV is observed. This results from the coupling between the $\pi(1g_{9/2})$ and $\pi(2p_{1/2})^{-1}$ states in the ^{89}Y(+p) reaction, but the strengths of peaks 1 in each of the 3 spectra are almost the same. Similar differences are also observed in peaks 2 and 3.

Peak 7 is seen with the same strength as in the other two reactions but is shifted to higher excitation as in peaks 1. The interactions between the proton single particle states and the proton hole state does not change the positions of the peaks plotted versus reaction Q – values significantly as were expected from the shell model calculations. The deviations of the peaks in reaction Q – values ranged from 0. to 0.9 MeV for the peaks in the ^{91}Nb spectrum.

5.5 ^{208}Pb, ^{209}Bi, ^{207}Pb (^{7}Li, ^{6}He) Reactions

The spectra for the (^{7}Li, ^{6}He) reactions on targets of ^{208}Pb, ^{209}Bi and ^{207}Pb with E_{inc} = 30 MeV/n are shown in fig. 5.7. The ejectile, ^{6}He was measured at the grazing angle, $\theta_{lab} = 9^{o}$. Parameters for the peaks are given in table 5.4. Seven peaks are resolved at low excitation energies in each spectrum and they are plotted as a function of both excitation energies and reaction Q – values in fig. 5.8. All the peaks are seen above a substantial underlying background.

In the ^{208}Pb(^{7}Li,^{6}He)^{209}Bi reaction, the first 4 single particle states $1h_{9/2}$ (ground state), $2f_{7/2}$ (0.71 MeV), $1i_{13/2}$ (1.4 MeV) and $2f_{5/2}$ (2.63 MeV), and 3 composite states at excitation energies 4.03 MeV, 5.22 MeV and 8.35 MeV are resolved. The ground state ($j^{\pi} = \frac{9}{2}^{-}$) of ^{209}Bi is not separated clearly from peaks 2 and 3 which have

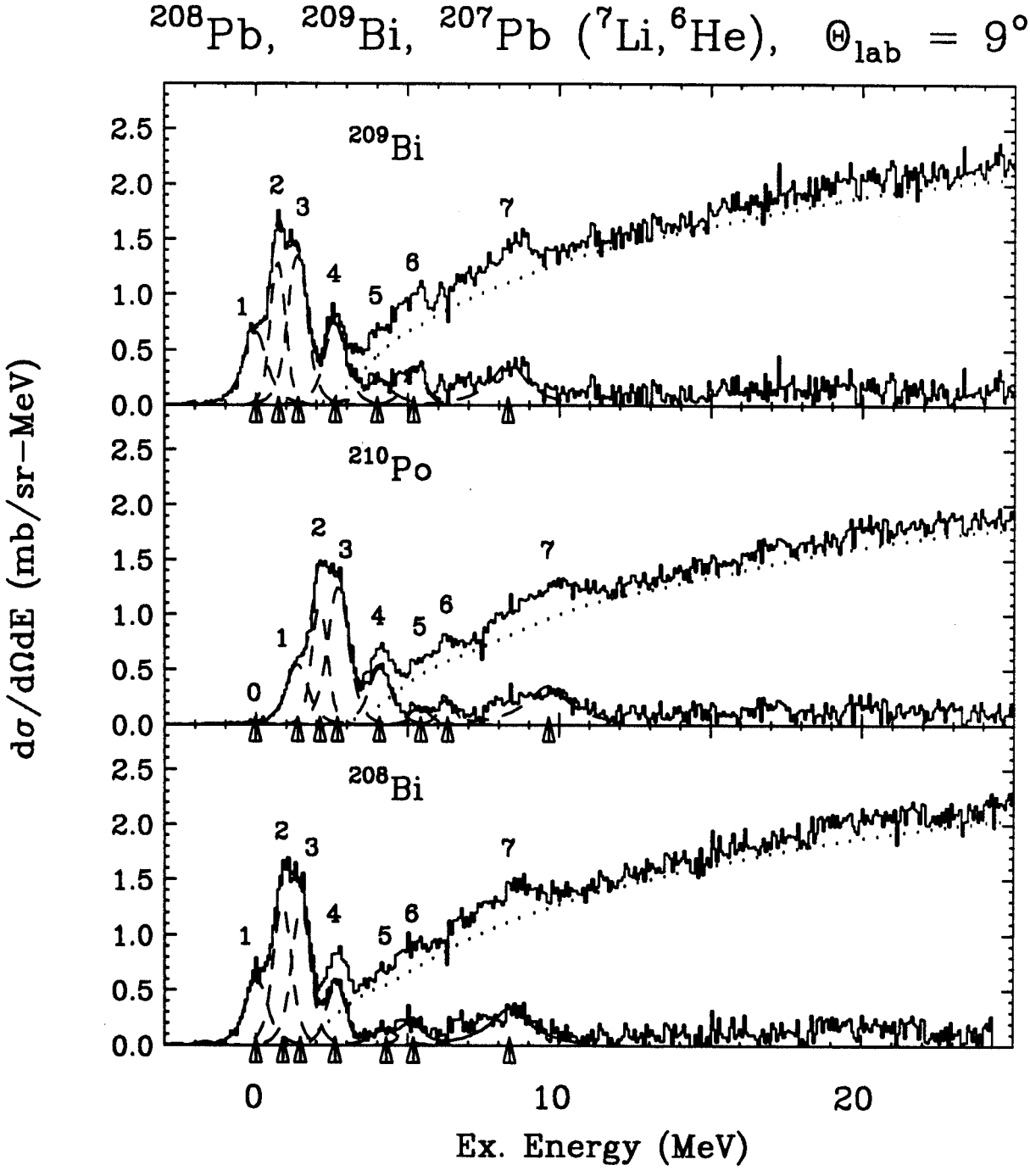

Figure 5.7: Energy spectra of ^{208}Pb, ^{209}Bi, ^{207}Pb (^{7}Li, ^{6}He) reactions (E_{inc} = 30 MeV/n). The dotted lines represent the background and the under lying spectra are obtained after the background is subtracted. Arrows at the bottom of each spectrum represent the centroid of the peaks.

Table 5.4: Excitation energies for the resolved peaks for (^{7}Li, ^{6}He) reactions on targets of ^{208}Pb, ^{209}Bi and ^{207}Pb. Γ is the full width at half maximum, Q is the reaction Q – Value for the corresponding excitation energy and units are MeV. The uncertainty is about 0.15 MeV. σ is the cross section in mb/sr and the uncertainty is about 20%. Peak 0 in the spectrum is the ground state which is shifted to lower energy due an extra hole state.

	^{208}Pb(^{7}Li,^{6}He)^{209}Bi				^{209}Bi(^{7}Li,^{6}He)^{210}Po				^{207}Pb(^{7}Li,^{6}He)^{208}Bi			
Peak #	Ex.	Γ	- Q	σ	Ex.	Γ	- Q	σ	Ex.	Γ	- Q	σ
0					0.00	0.3	4.99					
1	0.00	0.8	6.18		1.39	0.8	6.38		0.03	0.9	6.30	
2	0.71	0.6	6.89		2.12	0.7	7.11		0.90	0.9	7.17	
3	1.40	0.7	7.58		2.73	0.7	7.72		1.52	0.6	7.79	
4	2.63	0.8	8.81		4.10	1.0	9.09		2.70	1.0	8.97	
5	4.03	1.1	10.21		5.48	0.8	10.47		4.30	1.0	10.57	
6	5.22	0.8	11.40		6.32	0.7	11.31		5.20	0.9	11.47	
7	8.35	4.0	14.53	.71	9.66	4.0	14.65	.80	8.41	4.0	14.68	.75

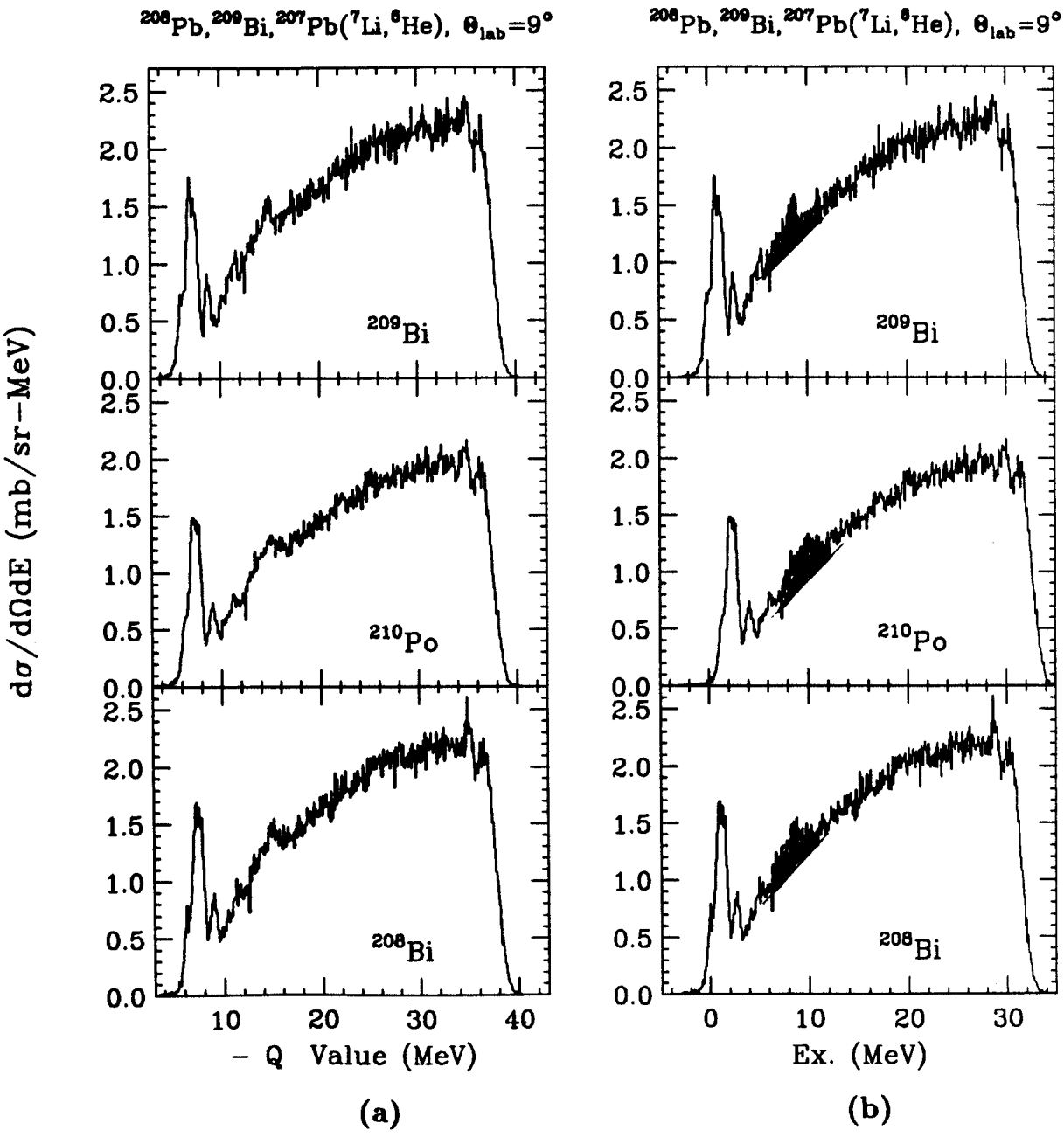

Figure 5.8: Comparison of the proton transfer spectra on ^{208}Pb region nuclei. Spectra are compared as functions of reaction Q - values and excitation energies. Peaks 7 above the assumed background are shaded to help to compare the positions and corss sections.

$j^\pi = \frac{7}{2}^-$ and $\frac{13}{2}^+$ respectively. It was extracted only by using a curve fitting program. Peak 4 appears above a substantial background and is separated clearly from peaks 2 and 3. The relative strengths of these single particle states may be explained by using the two matching conditions which were described in previous sections.

The ground state, $1h_{9/2}$, has a high angular momentum $5\hbar$ and a spin-flip is involved in the transition, whereas peak 3, $1i_{13/2}$, has a similar value of angular momentum $6\hbar$ but no spin-flip is involved. The favoured angular momentum transfer between the entrance channel and exit channel of this reaction is about $6\hbar$. Thus peak 3, which has $l = 6$ and no spin-flip transition is stronger than the ground state.

As another example, consider peak 2 and peak 4, which have the same angular momentum. Peak 2 ($2f_{7/2}$), which has an angular momentum $l = 3$ with no spin-flip transition, is more strongly populated than peak 4 ($2f_{5/2}$), which has the same angular momentum $l = 3$ with a spin-flip process. In this case, the difference between the two transition strengths results only from the spin-flip process. Similar examples explaining the relative transition strength using the matching conditions for transfer processes were given for the (^{12}C,^{11}B) and (^{16}O,^{15}N) reactions on the ^{208}Pb target [Merm 88].

In the ^{209}Bi(^{7}Li,^{6}He)^{210}Po reaction, the energy spectrum of ^{210}Po is very similar to that of the ^{208}Pb(^{7}Li,^{6}He) reaction. The target has one more proton in the $1h_{9/2}$ state than the ^{208}Pb nucleus and this state couples with the proton single particle states and makes many multiplets. When a proton is transferred to the $1h_{9/2}$ state, as there are two protons in the same state, only even value of j (from 0^+ to 8^+) are allowed. The ground state of ^{210}Po ($j = 0^+$) is very weakly populated due to a small value of $2j + 1$, and it is shifted to lower energy by 1.39 MeV from the centroid of the $(\pi(1h_{9/2}), \pi(1h_{9/2}))$ multiplet. Comparing the spectrum with that of

the ^{208}Pb(^{7}Li,^{6}He) reaction as a function of the reaction Q – values in fig. 5.8, no significant difference is seen between the two spectra except that peak 7 of ^{210}Po is slightly wider. Even the relative strengths of the peaks between the two spectra are almost the same. Thus there is evidence that an extra proton in the $1h_{9/2}$ state does not change the shape of the spectrum either at low excitation or at high excitation.

For the lowest 3 single particle states ($1h_{9/2}, 2f_{7/2}$ and $1i_{13/2}$), the excitation energy for the centroid of each multiplet coupled with the target's state ($1h_{9/2}$) were calculated in chap. 3 using the shell model. The relative values for the excitation energies of the centroid of the multiplets weighted by a cross section have very similar values to those of the single particle states before they are split even though the multiplet states are spread over 3~4 MeV in excitation energy (see table 3.2 and fig. 3.3). The comparison of the experimental values to the shell model calculations shows that they agree within 0.3 MeV. As the interactions between the two states are not very dependent on their excitation energies, these calculations for low excitation states can be applied to high excitation states, and the shift of excitation energies in high lying single particle states due to the $1h_{9/2}$ proton state may be assumed to be about 0.3 MeV.

In the ^{207}Pb(^{7}Li,^{6}He)^{208}Bi reaction, the proton single particle states couple with the target state ($3p_{1/2}$), and forming a doublet. For example, the single particle state, $1h_{9/2}$, couples with the $3p_{1/2}$ state to form 4^+ and 5^+ states, where the ground state is 5^+. The energy difference between the 4^+ and 5^+ states is so small that they are not separated in this spectrum. Not only the $1h_{9/2}$ state but also other single particle states are split into two states with small gaps [Alfo 70]. The centroid excitation energies of these multiplets at low excitation and the relative strengths between the states are not changed much compared to the spectra of the ^{209}Bi and ^{210}Po nuclei. Only the broad peak 7 (8.41 MeV) of the ^{208}Bi nucleus becomes slightly broader

compared to the same peak(7) in the ^{209}Bi nucleus, but has almost the same width as peak 7 in the ^{210}Po nucleus.

Overall, the spectrum of the ^{207}Pb(^{7}Li,^{6}He) reaction is almost the same as those of the same reactions on targets of ^{208}Pb and ^{209}Bi, even at high excitation. The shell model calculations, weighted by a cross section, for proton stripping on the ^{207}Pb target are given in table 3.2, and the results show that the relative excitation energies of the centroid of the multiplets are not changed much from the energies of the single particle states.

Broad peaks are seen at excitation energies of 8.35, 9.66 and 8.41 MeV in the spectra of the ^{208}Pb, ^{209}Bi and ^{207}Pb(^{7}Li,^{6}He) reactions respectively. The peak from the ^{209}Bi target is shifted to higher excitation energy by about 1.3 MeV compared to the other two peaks. But the reaction Q – values of the centroid for these broad peaks are all within 0.3 MeV. The comparison shows that these broad peaks have the characteristics of single particle states rather GR states.

Chapter 6

Analysis of Background

6.1 Introduction

In single particle stripping reactions there is a substantial background at high excitation. In many cases, this background is so strong that the extraction of information at high excitation is difficult. One major possible source of the background at high excitation in single particle stripping reactions is breakup of the projectile. The projectile breakup processes may be divided into sequential and direct processes according to the time scale of the reaction. In sequential breakup, which has a relatively long life time, the ejectile is produced in a particle unstable state which will subsequently decay. In direct breakup on the other hand the projectile breaks up into a few fragments due to the interaction with the target nucleus with a corresponding nuclear reaction time. From now on, the discussion of the direct breakup will be limited to the process of projectile breakup into two fragments.

In a direct breakup process the fragments are related to the projectile and hence exhibit the properties of the projectile [Meij 85]. In the past the background was often estimated empirically and only occasionally was calculated theoretically. There are several theories to calculate the background from a projectile breakup processes such as the Serber Model [Serb 48], the Quasi Free Breakup Model, the Distorted Wave

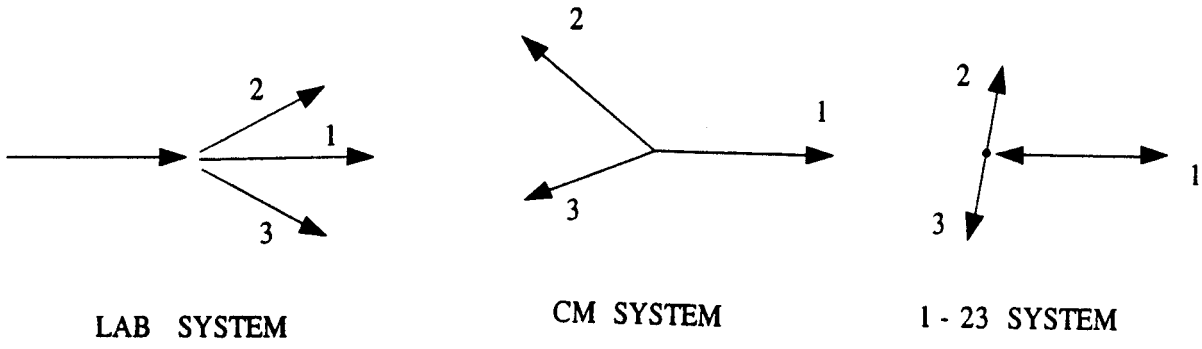

Figure 6.1: Schematic diagram for the projectile direct breakup processes with 3 body kinematics

Breakup Model [Meij 85] and a semi-classical theory to calculate the background from a single particle transfer to continuum states developed by Bonaccorso and Brink [Bona 85, Bona 87, Bona 88]. We chose two theories, the Serber Model which is based on the geometrical structures of the nucleus to find a nucleon stripping cross section and has been used commonly in the past, and a semi-classical theory developed by Brink and Bonaccorso, which calculates a transition cross section of a single particle from a bound state in the projectile to a continuum states of the target.

6.2 Projectile Breakup Background

6.2.1 3 - Body Kinematics of Projectile Direct Breakup Process

In direct breakup processes in which the projectile breaks up into 2 fragments, there are 3 fragments in the final state. The schematic representation for the 3 body motion due to the projectile breakup

$$a + A \longrightarrow 1 + 2 + 3 \tag{6.1}$$

is given in fig. (6.1), where A is the target and is represented as 3 in the final state. In center of mass frame (CM), the projectile breakup cross section can be expressed as functions of the parameters such as momenta, masses, and angles given in these two motions. If a single fragment only is measured, the parameters of this cross section can be changed into the single fragment's parameters by averaging the contribution from the other fragment's parameters.

From Fermi's golden rule, the transition probability per unit time from the initial state $\mid i\rangle$ to the final state $\mid f\rangle$ may be written as

$$R_{fi} = \frac{2\pi}{\hbar} \mid M_{fi} \mid^2 \rho(E_f), \tag{6.2}$$

where $\mid M_{fi} \mid^2$ is a transition matrix element and $\rho(E_f)$ is the number of final states with energy E_f. Then the transition cross section per unit solid angle and per unit energy is

$$\begin{aligned} d\sigma &= \frac{R_{fi}}{v_i} \\ &= \frac{2\pi}{\hbar}\frac{\mu_i}{p_i} \mid M_{fi} \mid^2 \rho(E_f), \end{aligned} \tag{6.3}$$

where μ_i and p_i are the reduced mass and momentum of the entrance channel in the CM frame, respectively.

The three particles in the final state have 9 degrees of freedom, but 3 of them can be eliminated due to momentum conservation. Then the cross section in the phase space of 6 independent variables can be written as [Ohls 65, Meij 85]

$$\begin{aligned} \rho(E_f) &= \frac{d\vec{p}_{1-23}d\vec{p}_{2-3}}{(2\pi\hbar)^9}(2\pi\hbar)^3\delta(E_{tot} - E_{1-23} - E_{2-3}) \\ &= \frac{p^2_{1-23}p^2_{2-3}dp_{1-23}dp_{2-3}d\Omega_{1-23}d\Omega_{2-3}}{(2\pi\hbar)^6}\delta(E_{tot} - E_{1-23} - E_{2-3}) \end{aligned}$$

$$= \frac{2}{(2\pi\hbar)^6}(\mu_{1-23}\mu_{2-3})^{\frac{3}{2}}[E_{1-23}(E^c_{tot}-E_{1-23})]^{\frac{1}{2}}dE_{1-23}dE_{2-3}\cdot$$
$$d\Omega_{1-23}d\Omega_{2-3}\delta(E_{tot}-E_{1-23}-E_{2-3})$$
$$= \rho_1(E_{1-23})d\Omega_{1-23}dE_{1-23}d\Omega_{2-3}dE^c_{tot}, \tag{6.4}$$

where E_{1-23} and E^c_{tot} are the kinetic energies in CM frame, and

$$E_{1-23} = \frac{p^2_{1-23}}{2\mu_{1-23}},$$
$$E^c_{tot} = \frac{p^2_{1-23}}{2\mu_{1-23}}+\frac{p^2_{2-3}}{2\mu_{2-3}} = E_{1-23}+E_{2-3}. \tag{6.5}$$

If eq. (6.4) is averaged over the solid angle Ω_{2-3} and integrated by E^c_{tot}, then the result is

$$\rho_1(E_{1-23})dE_{1-23}d\Omega_{1-23} = \frac{2}{(2\pi\hbar)^6}\left(\frac{m_1m_2m_3}{M}\right)^{\frac{3}{2}}[E_{1-23}(E^c_{tot}-E_{1-23})]^{\frac{1}{2}}\cdot$$
$$dE_{1-23}d\Omega_{1-23}, \tag{6.6}$$

where M is $m_1+m_2+m_3$. The relation of the phase space between the CM frame and the laboratory frame is

$$dE^l_1d\Omega^l_1 = \left(\frac{E^c_1}{E^l_1}\right)^{\frac{1}{2}}dE^c_1d\Omega^c_1, \tag{6.7}$$

where c and l denote CM frame and laboratory frame respectively, E^c_1 is $E_{1-23}(m_2+m_3)/M$ and E^l_1 is the kinetic energy of the fragment 1.

Now the phase space factor $\rho_1(E_{1-23})$ in the CM frame may be expressed as the phase space factor for the single measurement in the laboratory frame, $\rho_1(E^l_1)$ [Ohls 65],

$$\rho_1(E^l_1)dE^l_1d\Omega^l_1d\Omega^l_2 = \frac{2}{(2\pi\hbar)^6}\frac{M^{\frac{1}{2}}(m_1m_2m_3)^{\frac{3}{2}}}{(m_2+m_3)^2}\sqrt{E^l_1}\cdot$$
$$\left(\frac{m_2+m_3}{M}E^c_{tot}-E^l_1+2a_1\sqrt{E^l_1}\cos\theta^l_1-a^2_1\right)^{\frac{1}{2}}\cdot dE^l_1d\Omega^l_1d\Omega^l_2, \tag{6.8}$$

where θ_1^l is scattering angle of fragment 1 in the laboratory system, and a_1 is $(\frac{m_1 V_{CM}^2}{2})^{\frac{1}{2}}$, where V_{CM} is the velocity of the center of mass.

If eq. (6.8) is substituted into eq. (6.3) and integrated about Ω_2^l, then the differential cross section for the single measurement of the projectile breakup fragment can be expressed as functions of E_1^l and θ_1^l ,

$$\frac{d^2\sigma}{d\Omega_1 dE_1} = \frac{8\pi^2 m_a}{\hbar^2 k_a} \mid M_{fi} \mid^2 \rho(E_1^l), \tag{6.9}$$

where a subscript "a" denotes projectile. For the measurement of the two fragments 1 and 2 in coincidence, the phase space factor and the cross section are

$$\rho_1(E_1^l) = \frac{1}{(2\pi\hbar)^6} \frac{m_1 m_2 m_3 p_1 p_2}{m_2 + m_3 - m_2 \frac{\vec{p}_2 \cdot (\vec{P} - \vec{p}_1)}{p_2^2}}, \tag{6.10}$$

and

$$\frac{d^2\sigma}{d\Omega_1 d\Omega_2 dE_1} = \frac{2\pi m_a}{\hbar^2 k_a} \mid M_{fi} \mid^2 \rho(E_1^l), \tag{6.11}$$

where $\vec{P}$ is the incident particle's momentum. The detailed derivation may be found in previous reports [Ohls 65, Fuch 82].

Now the phase space factor is known explicitly, but the transition matrix still must be formulated. To calculate the projectile breakup cross section for the (^{7}Li,^{6}Li) and (^{7}Li,^{6}He) reactions, eq. (6.8) will be used as the phase space factor with the Serber Model for the transition matrix. In the case of the coincidence measurement of $^7\text{Li} \longrightarrow {}^6\text{He} + p$, eqs. (6.10) and (6.11) will be used for the cross section with the Serber Model transition matrix.

6.2.2 Projectile Breakup Cross Section Calculations Using Serber Model

In calculating the projectile breakup cross sections of ^{7}Li into ^{6}He + p and ^{6}Li + n using the Serber Model [Serb 48], it is assumed that one of the nucleons in the pro-

jectile is stripped off by the collision and the ejectile continues to move with its same momentum $\vec{p}_x$ as at the moment of the breakup. The target is assumed to play no role except to breakup the projectile at the collision, and is assumed to be transparent to the breakup fragments. The coulomb and spin-spin interactions between the target and the projectile are neglected. The residual nucleus and the ejectile are assumed to remain in their ground states after the breakup processes. In this model the probability of observing a particle with momentum $\vec{p}_x$ is given by $|M_{fi}|^2 = P(\vec{p}_x) \sim |\phi(\vec{p})|^2$, where $|\phi(\vec{p})|^2$ is the Fourier transform of the relative wave function between the two constituents in the projectile and $\vec{p}$ is the ejectile's internal momentum in the projectile.

Using eq. (6.9) from the previous section, the differential cross section for observing a fragment from the breakup process with energy E_x can be written as

$$\frac{d^2\sigma}{d\Omega_x dE_x} = N_x R_t R_p \frac{m_a}{\sqrt{2m_a E_a}} |\phi(\vec{p})|^2 \rho(E_x), \tag{6.12}$$

$$\phi(\vec{p}) = \frac{1}{(2\pi\hbar)^{\frac{3}{2}}} \int \phi(r) exp(-\frac{i}{\hbar}\vec{p}\cdot\vec{r}) d^3r, \tag{6.13}$$

where N_x, R_t, R_p and $\rho(E_x)$ are the normalization constant, target's radius, projectile's radius and density of the final states respectively, m_a and E_a are the mass and kinetic energy of projectile, and $\vec{p} = \vec{p}_x - \vec{p}_o$ where $\vec{p}_x$ is an observed final momentum of the ejectile and $\vec{p}_o$ is its initial momentum in the projectile, corresponding to the beam velocity and

$$|\vec{p}|^2 = |\vec{p}_o|^2 + 2m_x E_x - 2|\vec{p}_o|\sqrt{2m_x E_x} \cdot cos\theta_x, \tag{6.14}$$

where m_x and θ_x are the ejectile's mass and scattering angle.

A wave function of the Eckart form [Lim 73]

$$\phi(r) = C \left(\frac{\alpha}{2\pi}\right)^{\frac{1}{2}} \frac{e^{-\alpha r}}{r} (1 - e^{-\beta r})^4 \tag{6.15}$$

is used for the relative wave function of the constituents in the projectile, where $\alpha = \sqrt{2\mu\epsilon}/\hbar$ with μ and ϵ being the reduced mass and separation energy, and C is a normalization constant. The constant β is determined to give the best fit to the experimental data. In this analysis $\beta = 1.0$ is used. By substituting eq. (6.15) into eq. (6.13), and using the integral formula of

$$\int d^3r e^{-i\vec{q}\cdot\vec{r}} \frac{e^{-\beta r}}{r} = \frac{4\pi}{\beta^2 + q^2}, \tag{6.16}$$

the following result is obtained for $\phi(\vec{p})$,

$$\begin{aligned}\phi(\vec{p}) &= \frac{C}{(2\pi\hbar)^{\frac{3}{2}}}(8\pi\alpha)^{\frac{1}{2}}\left(\frac{1}{p^2+\alpha^2} - \frac{4}{p^2+(\alpha+\beta)^2} + \frac{6}{p^2+(\alpha+2\beta)^2}\right. \\ &\left. - \frac{4}{p^2+(\alpha+3\beta)^2} + \frac{1}{p^2+(\alpha+4\beta)^2}\right).\end{aligned} \tag{6.17}$$

Thus the differential cross section for the projectile breakup can be obtained by substituting eq. 6.17 into eq. 6.12. The calculations were done for the kinetic energies of ejectiles from 1 MeV in 1 MeV steps. The final results are expressed as a function of the excitation energies of the residual nuclei for the comparison with the experimental data, and are normalized to the experimental results. The excitation energies corresponding to the ejectile's incident energies assuming ejectiles velocities equal to the beam velocity are marked with arrows.

6.2.3 Comparison of Serber Model Calculations with Experimental Data

The calculated projectile breakup cross sections for ^{7}Li into ^{6}Li + n, and ^{7}Li into ^{6}He + p on ^{90}Zr region and ^{208}Pb region targets at E_{inc} = 30 MeV/n are given in figs. (6.2) and (6.3) together with the experimental spectra from the (^{7}Li,^{6}Li) and (^{7}Li,^{6}He) reactions. The calculations are normalized to the experimental data.

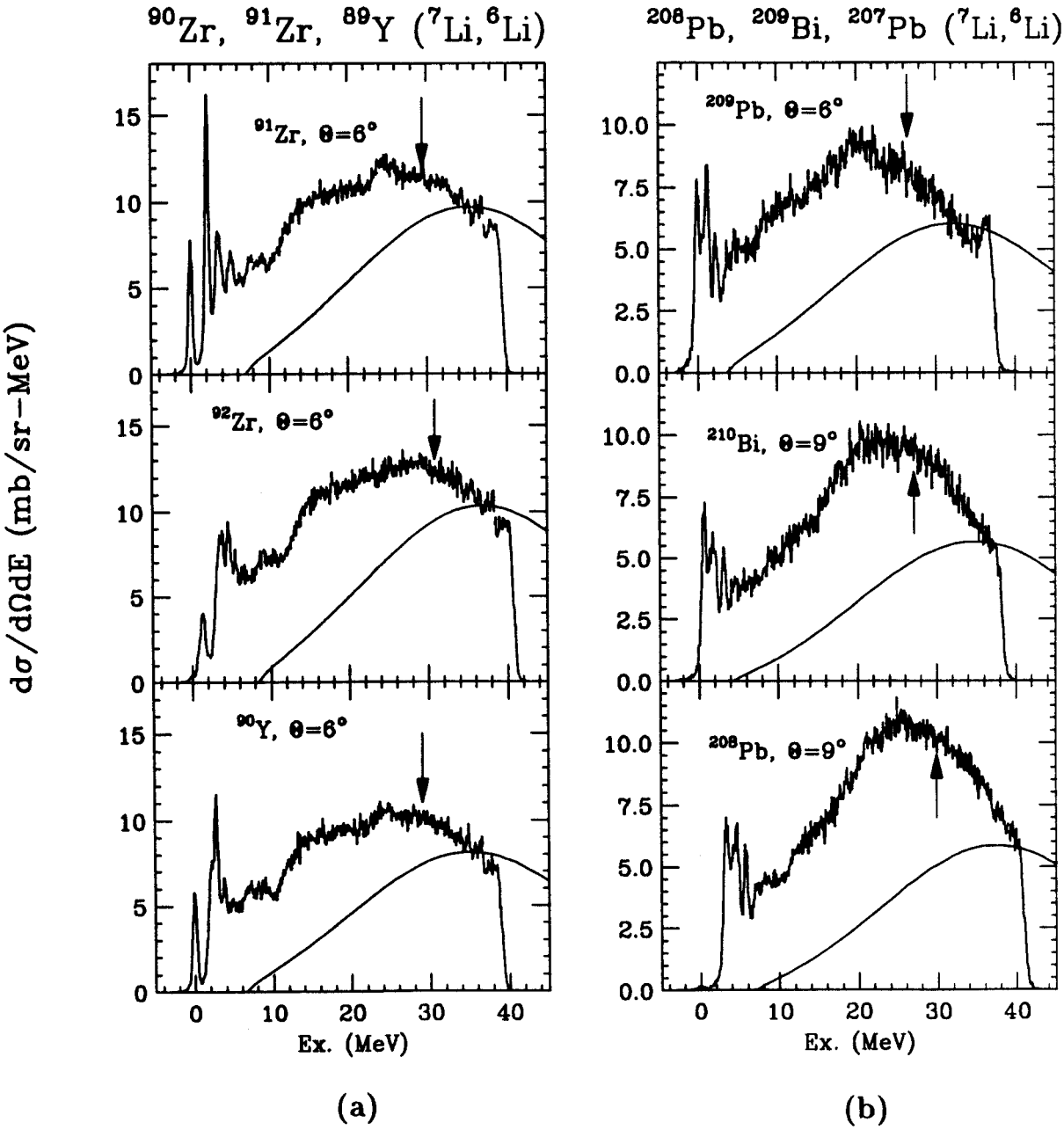

Figure 6.2: Calculated breakup cross sections of ^{7}Li (E = 30 MeV/n) into ^{6}Li + n using the Serber Model are compared with the experimental spectra. The solid lines indicate the calculated breakup cross sections which are normalized to the experimental results. The excitation energies which correspond to ^{6}Li's incident energies of the beam velocity are marked with arrows.

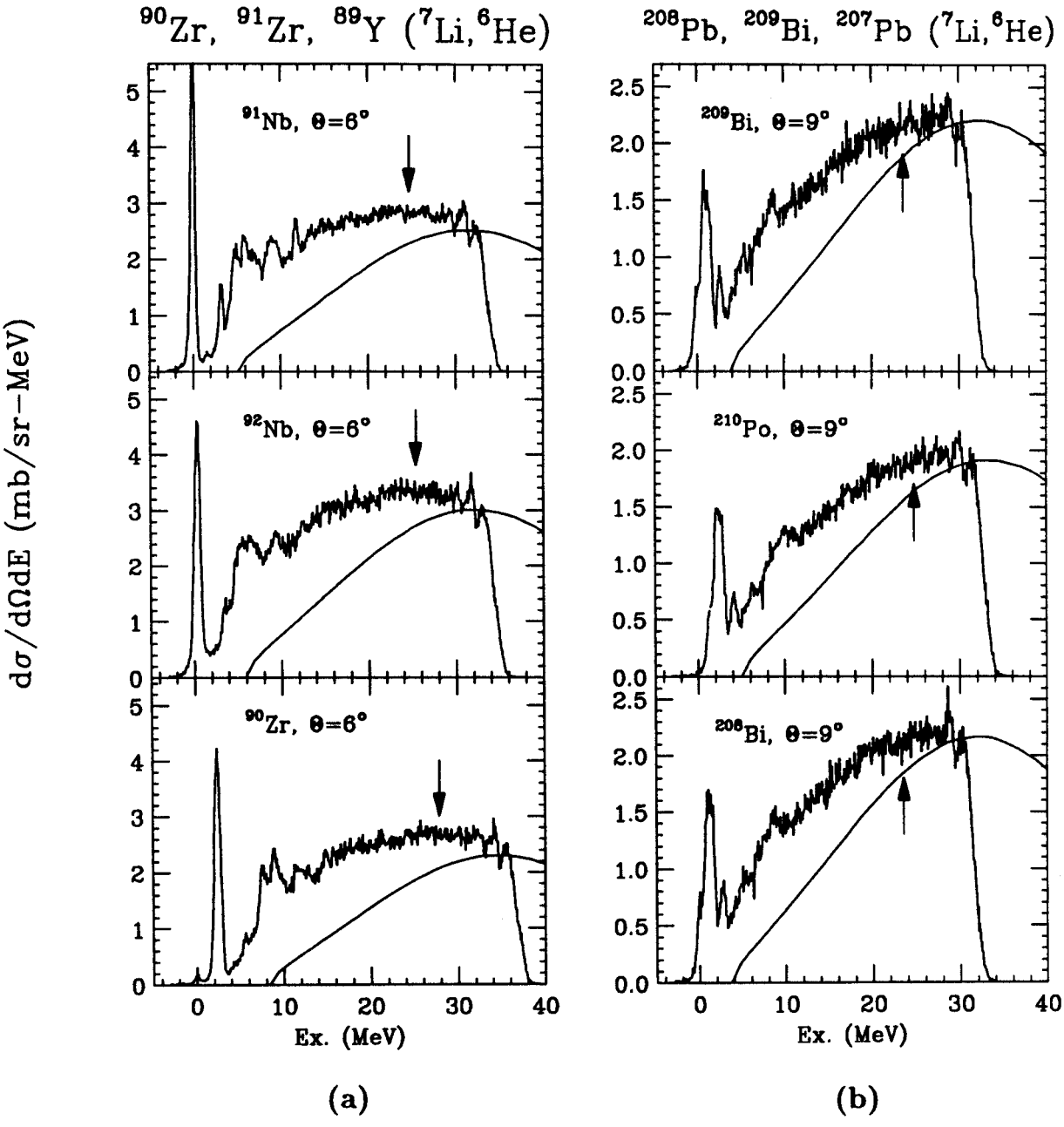

Figure 6.3: Calculated breakup cross sections of ^{7}Li (E_{inc} = 30 MeV/n) into ^{6}He + p using the Serber Model are compared with the experimental spectra. The solid lines indicate the calculated breakup cross sections which are normalized to the experimental data. The excitation energies which correspond to ^{6}He's incident energies of the beam velocity are marked with arrows.

The experimental spectra for the (^{7}Li,^{6}Li) reactions are shown out to 40 MeV of excitation energies and they are peaked at excitation energies $\sim$ 25 MeV for ^{90}Zr region targets, and at $\sim$ 20, 22 and 26 MeV for ^{208}Pb, ^{209}Bi and ^{207}Pb targets respectively. However, the calculated breakup spectra are peaked close to the incident energies of the beam velocity but smaller than them, by about 5 MeV, due to the nucleon's binding energy in the projectile. If the peaks of the experimental spectra are caused by the direct breakup of the projectile, then they should appear always at energies smaller than the energy of a ^{6}Li particle which corresponds to the beam velocity, and therefore higher in excitation energies as were seen in light ion breakup experiments [Wu 78, Wu 79, Mats 78, Mats 80] such as (d,p), (α,t), (α,^{3}He) and (^{3}He,p). But the experimental spectra observed are peaked at energies which are higher than those consultant to the beam velocity by about several MeV for lead region targets, and 3 $\sim$ 5 MeV for zirconium region targets. These differences in the peaks make it difficult to assume that the peaks of the experimental spectra are from the direct breakup of the projectile.

In fig. (6.3) for (^{7}Li,^{6}He) reactions, the experimental spectra are given out to $\sim$ 30 MeV of excitation energies. A very large fraction of the background is predicted as projectile breakup by the calculations. The calculated spectra give somewhat better agreement to the experimental spectra than the calculated spectra for the neutron stripping reactions. Except in the ^{90}Zr target, the experimental spectra are not observed up to high enough excitation energy to determine clearly where the spectrum peaks.

The ^{90}Zr(^{7}Li,^{6}He) reaction was measured out to 50 MeV excitation with two different runs using the same conditions, except for the dipole magnetic field, and connecting the two spectra together. The extended breakup cross section on the ^{90}Zr target is given in fig. (6.4). The calculated cross section is normalized to the exper-

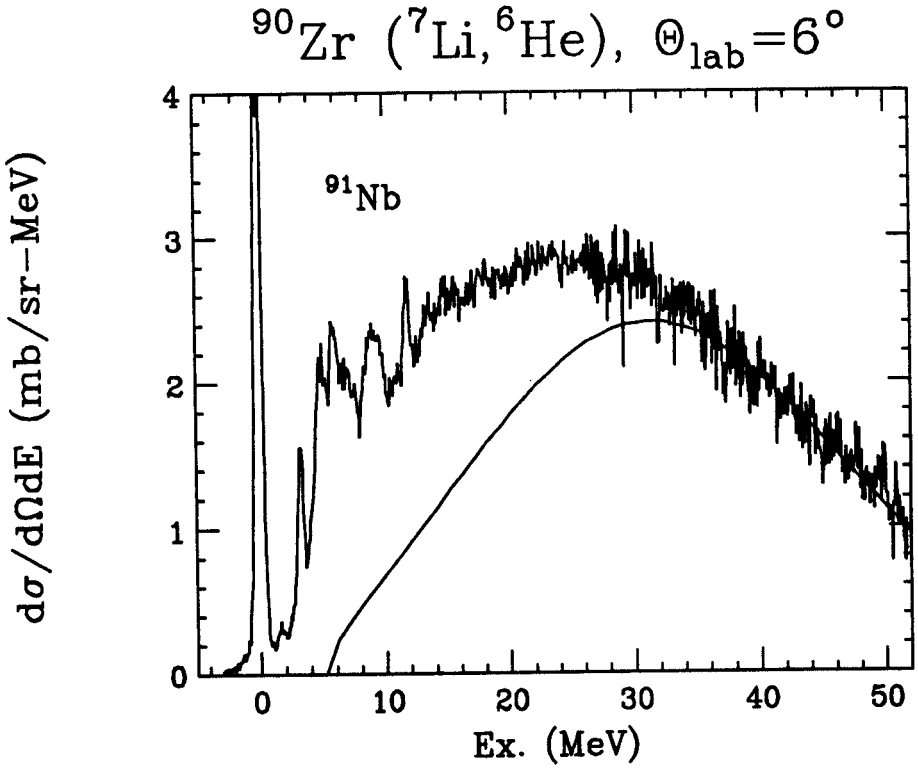

Figure 6.4: Breakup cross section calculations of ^{7}Li (E_{inc} = 30 MeV/n) into ^{6}He + p on ^{90}Zr target using Serber Model. The two spectra are connected at $Ex. \sim 26$ MeV.

imental data. From excitation energies above 35 MeV, the calculated breakup cross section agrees perfectly with the experimental spectrum. This good agreement perhaps suggests that the high lying spectra (higher than 35 MeV) are mainly the results of the projectile breakup processes rather than from the formation of the compound states. In the (^{7}Li,^{6}He) reactions on targets of ^{91}Zr and ^{89}Y, since the excitation energies are given only up to $\sim$ 35 MeV, the comparison with the calculations is more difficult. But, from the given spectra which are very similar to the spectrum from the ^{90}Zr target, the similar spectra are expected at high excitation where $Ex. \geq 35$ MeV from the ^{91}Zr and ^{89}Y targets. One more or one less nucleon in a heavy nucleus is not expected to be very important to the background at high excitation ($Ex. \geq$ 10 MeV). Even at low excitation the whole shape is not changed significantly by an extra nucleon.

In the ^{208}Pb region targets, the cross sections for the (^{7}Li,^{6}He) reactions increase continuously up to $Ex \sim 30$ MeV. The calculated breakup cross sections normalized to the experimental data explain most of the background in the given spectra. The ratios of the contributions of the calculated breakup spectra to the experimental spectra for the three ^{208}Pb region targets appears to be similar.

Since no spectra were measured at excitation energies higher than 30 MeV, it is very difficult to know whether the normalization was done correctly or not. For further investigations on this subject, it would be necessary to measure the higher excitation energy region up to 50 MeV or so, about twice the beam energy per nucleon so that the peak of the breakup processes can be seen clearly. Even though the coulomb interaction, spin-spin couplings, and the quantum states of the transferred nucleon are not considered, the simple Serber Model appears to provide reasonable agreement with the shape of the continuum above about 35 MeV excitation energy.

6.3 Single Nucleon Transfer to Continuum States Using a Semi-Classical Theory

6.3.1 Kinematics of Single Nucleon Transfer to Continuum States

A semi-classical theory which was developed by Brink and Bonaccorso [Bona 85, Bona 87, Bona 88] is used to explain the background for single nucleon stripping reactions of (^{7}Li, ^{6}Li) and (^{7}Li, ^{6}He). In this theory, the colliding nuclei are assumed to move along classical trajectories, but the transfer is calculated by quantum mechanics. In this model, a nucleon makes a transition from an initial state ψ_1 with orbital angular momentum l_1, m_1, energy ϵ_1 and potential V_1 in the projectile to a final state ψ_2 with angular momentum l_2, m_2, energy ϵ_2 and potential V_2 in the target nucleus. The amplitude for the transfer from the initial state 1 to the final state 2 becomes using the time dependent perturbation formula

$$A_{21} = \frac{1}{i\hbar}\int_{-\infty}^{\infty}\langle\psi_2 \mid V_1 \mid \psi_1\rangle dt. \tag{6.18}$$

This perturbation integral can be transformed to a surface integral over a surface Σ drawn between the two nuclei perpendicular to the line joining their centers at the point of closest approach (fig. 6.5). This surface lies between the two potentials V_1 and V_2 and which divides the space into regions R_1 and R_2, at a distance d_1 from the center of the projectile and d_2 from the target, with $d_1 + d_2 = d$. Then the matrix element can be written

$$\langle\psi_2 \mid V_1 \mid \psi_1\rangle = \int_{R_1}\psi_2^*(r,t)V_2(r,t)\psi_1(r,t)d^3r + \int_{R_2}\psi_2^*(r,t)V_1(r,t)\psi_1(r,t)d^3r. \tag{6.19}$$

The first term in eq. (6.19) can be reduced using the Schroedinger equation for ψ_1

$$\int_{R_1}\psi_2^* V_1\psi_1 d^3r = \int_{R_1}\psi_2^*(i\hbar\frac{\partial}{\partial t} + \frac{\hbar^2}{2m}\nabla^2)\psi_1 d^3r \tag{6.20}$$

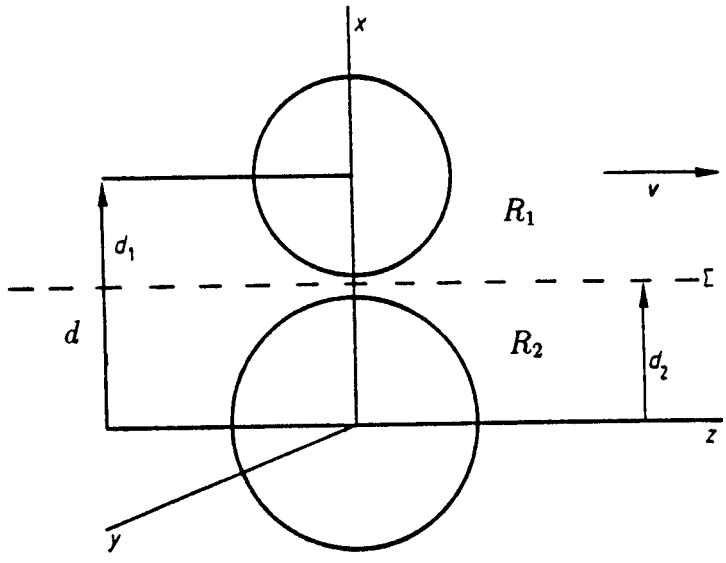

Figure 6.5: Coordinate system for transfer amplitude.

Applying Green's theorem,

$$\int_{R_1} \psi_2^* V_1 \psi_1 d^3r = \frac{\hbar^2}{2m} \int_\Sigma d\vec{S} \cdot (\psi_2^* \nabla \psi_1 - \psi_1 \nabla \psi_2^*)$$
$$+ \int_{R_1} (i\hbar \frac{\partial}{\partial t} \psi_2 + \frac{\hbar^2}{2m} \nabla^2 \psi_2)^* \psi_1 d^3r + i\hbar \frac{\partial}{\partial t} \int_{R_1} \psi_2^* \psi_1 d^3r \quad (6.21)$$

where $d\vec{S}$ is a surface element normal to R_1. If eq. (6.21) is integrated by the time between $t = -\infty$ and ∞, the third term will vanish because of no overlap between ψ_1 and ψ_2. Then the matrix element $\langle \psi_2 \mid V_1 \mid \psi_1 \rangle$ can be reduced using Schrodinger equation for ψ_2

$$\langle \psi_2 \mid V_1 \mid \psi_1 \rangle = \frac{\hbar^2}{2m} \int_\Sigma d\vec{S} \cdot (\psi_2^* \nabla \psi_1 - \psi_1 \nabla \psi_2^*)$$
$$+ \int_{R_1} \psi_2^* V_2 \psi_1 d^3r + \int_{R_2} \psi_2^* V_1 \psi_1 d^3r. \quad (6.22)$$

In a peripheral collision where the two particles approach along the z-axis with relative velocity v, the surface is parallel to the z-y plane, and the closest distance between the two particles is $d = d_1 + d_2$, there is no overlap between the potentials V_1 and V_2 and we can choose Σ so that $V_2(r,t) = 0$ for all points in R_1 on one side

of the surface, while $V_1(r,t) = 0$ for all points in R_2 on the other side. Then the last two terms in eq. (6.22) vanish and the transfer amplitude becomes [Mona 85]

$$A_{21} = \frac{\hbar}{2mi}\int_{-\infty}^{\infty} dt \int_{\Sigma} d\vec{S}\cdot(\psi_2^*\nabla\psi_1 - \psi_1\nabla\psi_2^*). \tag{6.23}$$

By using the double Fourier transform, the coordinate space wave function with respect to the coordinates y and z parallel to the surface is

$$\tilde{\psi}(x,k_y,k_z) = \int_{-\infty}^{\infty}\int_{-\infty}^{\infty} dydz\ e^{-i(yk_y+zk_z)}\psi(x,y,z). \tag{6.24}$$

The transfer amplitude was derived by Brink et. al [Mona 85, Bona 87] and after considerable algebra, the result can be written

$$A_{21} = \frac{i\hbar}{2\pi mv}\int_{-\infty}^{\infty} dk_y(\eta^2+k_y^2)^{\frac{1}{2}}\tilde{\psi}_2^*(d_2,k_y,k_2)\tilde{\psi}_1(d_1,k_y,k_1), \tag{6.25}$$

where ψ_1 and ψ_2 are bound state wave functions and have single particle energies ϵ_1 and ϵ_2 where m is the nucleon mass, $v = \sqrt{2(E_{CM}-V_{CM})/\mu}$ is the relative velocity between the two nuclei at the closest approach where μ, E_{CM} and V_{CM} are reduced mass, relative kinetic energy and Coulomb energy at the closest approach, and

$$\epsilon_l = -\frac{\hbar^2\gamma_l^2}{2m}, \qquad for\ \ l = 1,2, \tag{6.26}$$

is the binding energy and η is defined by

$$\eta^2 = k_1^2+\gamma_1^2 = k_2^2+\gamma_2^2, \tag{6.27}$$

where k_1 is the relative value of the transferred nucleon to the first nucleus and k_2 relative to the second. Then

$$\hbar(k_2-k_1) = mv. \tag{6.28}$$

The reaction Q-value is the nucleon's binding energy difference between the two nuclei

$$Q = \epsilon_1-\epsilon_2 = \frac{\hbar^2}{2m}(k_1^2-k_2^2). \tag{6.29}$$

Eqs. (6.28) and (6.29) give

$$k_1 = -(Q + \frac{1}{2}mv^2)/\hbar v \ , \quad and \quad k_2 = -(Q - \frac{1}{2}mv^2)/\hbar v. \tag{6.30}$$

The wave functions $\tilde{\psi}_1(d_1, k_y, k_1)$ and $\tilde{\psi}_2(d_2, k_y, k_2)$ are amplitudes for finding the nucleon with z-component of momentum k_1 in the first nucleus and k_2 in the second. For a peripheral reaction, d_1 and d_2 are large enough to use the Hankel function's asymptotic form for the bound initial state ψ_i with l_i, m_i and ϵ_i, and the unbound final state ψ_f with l_f, m_f and ϵ_f [Bona 88]

$$\psi_i(r) \simeq C i^l h_{l_i}^{(+)}(i\gamma r) Y_{l_i m_i}(\theta, \phi), \tag{6.31}$$

and

$$\psi_f(r) \simeq C_f \frac{i}{2}[h_{l_f}^{(+)}(k_f r) - e^{-2i\delta_{l_f}} h_{l_f}^{(-)}(k_f r)] Y_{l_f m_f}(\theta, \phi), \tag{6.32}$$

where $h_l^{(+)}$ and $h_l^{(-)}$ are Hankel functions and

$$k_f = 2m\epsilon_f/\hbar^2. \tag{6.33}$$

where ϵ_f is the kinetic energy of the transferred nucleon. The double Fourier transform of $\psi_i(r)$ and $\psi_f(r)$ are

$$\tilde{\psi}_i(x, k_y, k_z) = -C\frac{2\pi}{\gamma_x} e^{-\gamma_x |x|} Y_{l_i m_i}(\hat{k}_i), \tag{6.34}$$

$$\tilde{\psi}_f(x, k_y, k_z) = -C_f e^{i\delta_{l_f}} 2\pi \sin\delta_{l_f} \frac{e^{-\gamma_x |x|}}{\gamma_x} Y_{l_f m_f}(\hat{k}_f), \tag{6.35}$$

where $\gamma_x^2 = k_x^2 + k_y^2 + \gamma^2$, γ is related to the bound state energy ϵ in eq. (6.26), $\hat{k}_i = \vec{k_i}/|k_i|$, $k_i = -2m\epsilon_1/\hbar^2$, $\hat{k}_f = \vec{k_f}/|k_f|$ and δ_{l_f} is the phase shift for the l_f wave.

If eqs. (6.34) and (6.35) are substituted into to eq. (6.25) and integrated, then the differential transfer probability becomes [Bona 88]

$$\begin{aligned} \frac{d}{d\epsilon_f} P(l_f, l_i) &= \frac{d}{d\epsilon_f}\left(\frac{1}{2l_i + 1} \sum_{m_i m_f} |A(l_f, l_i)|^2\right) \\ &= |1 - S_{l_f}(\epsilon_f)|^2 B(l_f, l_i), \end{aligned} \tag{6.36}$$

where the probability amplitude was summed over the final angular momentum m_f and averaged over m_i.

$$B(l_f, l_i) = \frac{1}{4}\left(\frac{\hbar}{mv}\right)\frac{m}{\hbar^2 k_f}|C_1|^2(2l_f+1)P_{l_i}(X_i)P_{l_f}(X_f)\frac{e^{-2\eta R}}{\eta R}\,, \qquad (6.37)$$

P_{l_i} and P_{l_f} are Legendre polynomials of

$$X_i = 1 + 2\frac{k_1^2}{\gamma_1^2}, \qquad X_f = 2\frac{k_2^2}{k_f^2} - 1, \qquad (6.38)$$

and $R = d_1 + d_2$, a strong absorption radius, and $S_{l_f}(\epsilon_f) = e^{-2i\delta_{l_f}}$ is a reflection coefficient. This coefficient can be reduced to an optical model S matrix when the coefficient is averaged over the energies of the final compound states. Then the energy average $< S_{l_f} >$ is the S matrix for the elastic scattering of a nucleon with kinetic energy ϵ_f. Eq. (6.36) gives the probability of a transfer of a single nucleon in the orbit l_i of the projectile to the continuum state of the target as a function of the nucleon's final energy, ϵ_f.

6.3.2 Cross Section Calculations of Projectile Breakup and Compound States

The transfer probability from the initial bound state ($\epsilon_i < 0$) to a final unbound state ($\epsilon_f > 0$) can be rewritten as

$$\begin{aligned}\frac{dP(l_f, l_i)}{d\epsilon_f} &= < |1 - S_{l_f}|^2 > B(l_f, l_i) \\ &= (|1 - < S_{l_f} >|^2 + T_{l_f}) \cdot B(l_f, l_i), \end{aligned} \qquad (6.39)$$

where l_i, l_f are the initial and final angular momenta respectively, $T_{l_f} = 1 - | < S_{l_f} > |^2$, and $B(l_f, l_i)$ is explained in the previous section. The first term in eq. (6.39) $|1 - < S_{l_f} >|^2$ is for the elastic scattering of the transferred nucleon by the target. The second term T_{l_f} is due to the formation of the compound state in the target nucleus by the transferred nucleon, and includes all of the residual nucleus's excitation.

An approximate formula for the total transfer cross section can be obtained by integrating over impact parameter [Bona 88]

$$\frac{d\sigma}{d\epsilon_f} = 2\pi \int_{R_s}^{\infty} \sum_{l_f=0}^{\infty} (R - a_c) \frac{dP(R, l_f, l_i)}{d\epsilon_f} R dR \cong \pi \frac{R_s - a_c}{\eta} \sum_{l_f=0}^{\infty} \frac{dP(R_s, l_f, l_i)}{d\epsilon_f}, \tag{6.40}$$

where R_s is a strong absorption radius and a_c is a Coulomb length parameter. R_s can be obtained from the relation $kR_s = l + 1/2$, where k is the wave number of the transferred nucleon and l is the angular momentum at $|S| = 1/2$. In the real calculations, l_f was truncated at 30 because S converges to one where l is much less than 30.

In the eqs. 6.39 and 6.40, the contribution of the spin of the transferred nucleon is not appeared. The dependence of the initial and final state spins can be introduced as in refs. of [Bona 87, Hash 88]. Then the eq. 6.39 can be modified as

$$\frac{dP(l_f, l_i)}{d\epsilon_f} = \sum_{j_f} (|1 - < S_{l_f} > |^2 + 1 - | < S_{j_f} > |^2) B(j_f, j_i), \tag{6.41}$$

where

$$B(j_f, j_i) = \frac{(2j_f + 1)}{2(2l_f + 1)} (1 + R) B(l_f, l_i). \tag{6.42}$$

The factor $(2j_f + 1)/2(2l_f + 1)$ is a statistical factor which is the probability of reaching a final state j_f if all angular momentum projections are equally probable. R is a dynamical factor which depends on several variables of the transfer reaction notably the reaction Q – value and the incident energy. In a single nucleon transfer reaction, for the given channel specified (l_i, l_f), there are four possible $j-$transfers from $j_i = l_i \pm \frac{1}{2}$ to $j_f = \pm\frac{1}{2}$. The detailed derivation for R is given in ref. [Hash 88]. The result is

$$R = D(j_f, j_i) F(E) \tag{6.43}$$

Table 6.1: Coefficients $D(j_i, j_f)$

j_f \ j_i	$l_i - \frac{1}{2}$	$l_i + \frac{1}{2}$
$l_f - \frac{1}{2}$	$\frac{1}{l_i l_f}$	$\frac{-1}{l_f(l_i+1)}$
$l_f + \frac{1}{2}$	$\frac{-1}{l_i(l_f+1)}$	$\frac{1}{(l_f+1)(l_i+1)}$

where $D(j_f, j_i)$ is given in table 6.1 and

$$F(E) = -\frac{2k_1\eta}{\gamma_i^2 P_{l_i}(X_i)}\frac{dP_{l_i}(X_i)}{dX_i} \cdot \frac{2k_2\eta}{k_f^2 P_{l_f}(X_f)}\frac{dP_{l_f}(X_f)}{dX_f} \tag{6.44}$$

where X is defined in section 6.3.1.

The S-matrix can be obtained from a DWBA calculation for the nucleon elastic scattering reaction on the appropriate targets. They are dependent on the optical potential parameters and the energy of the incident particle. The optical parameters are also dependent on the incident particle's energy. Thus it is important to have good energy dependent parameters for the optical potentials. The real potentials such as volume real and spin orbit potentials should be chosen to give the correct sequence of the bound and resonance states of the target. Once they are chosen for a given energy, they may be used in the vicinity of this energy because the real parts are not so sensitive to the change of the incident energy. But the imaginary parts, such as volume imaginary and surface potentials may give a big change to the absorption probability with a small change in the potentials.

In this analysis, the real potentials are obtained by changing the input potentials smoothly to give the best sequence of the known states of the target for the given energy, and the imaginary parts are parameterized using the method of Mahaux and Sartor [Maha 89] to reproduce the correct position of the given bound state of the

Table 6.2: The optical input parameters for the neutron elastic scattering reactions on ^{90}Zr and ^{208}Pb region targets. The units for the V_R and V_{SO} are MeV, for r and a are fm.

Targets	V_R	r_R	a_R	r_I	a_I	V_{SO}	r_{SO}	a_{SO}
^{208}Pb, ^{209}Bi, ^{207}Pb	45.8	1.25	0.5	1.25	0.3	9.0	1.25	0.5
^{90}Zr, ^{91}Zr, ^{89}Y	45.8	1.25	0.5	1.25	0.3	7.5	1.25	0.5

target for the given real potentials. The optical model potential used in this analysis is

$$\begin{aligned} U(r,\epsilon_f) &= V_C - V_R f(x_R) + (\frac{\hbar}{m_\pi c})^2 V_{SO}\vec{\sigma}\cdot\vec{L}\frac{1}{r}\frac{d}{dr}f(x_R) \\ &- i[W_V(\epsilon_f) - 4a_I W_S(\epsilon_f)\frac{d}{dr}]f(x_I) \end{aligned} \tag{6.45}$$

where V_C is the coulomb potential, V_R and W_V are volume real and volume imaginary potentials, V_{SO} is the spin-orbit potential, W_S is the surface potential, $f(x_\alpha) = (1 + e^{x_\alpha})/a_\alpha$ where $x_\alpha = (r - r_\alpha A^{1/3})$, $(\frac{\hbar}{m_\pi c})^2 = 2.0fm^2$, r_α and A are radius parameter and mass of the target, and $\vec{\sigma}$ and $\vec{L}$ are spin and orbital angular momentum of the transferred nucleon respectively. In all cases α denotes real(R) or imaginary(I) part of the potentials.

The input parameters for the optical potentials to calculate the S-matrix elements for the neutron elastic scattering reactions using DWBA program are given in table 6.2. For the imaginary potentials, W_V and W_S, are used after they are obtained for the corresponding neutron's energy using eqs. (2.1), (2.3a) and (6.1a) of ref. Maha 89.

The S-matrix elements are obtained for the incident nucleon's energy from 1 MeV in 1 MeV steps for the orbital angular momentum from $l = 0$ to $l = 30$ in each step.

For the proton elastic scattering reactions, the same values are used. The calculations for the neutron transfer cross sections are done by using the eqs. (6.39) and (6.40) for the neutron's final energy (ϵ_f) from 1 MeV in 1 MeV steps. In each energy step, the cross sections are summed from $l_f = 0$ to 30 for the initial angular momentum $l_i = 1$ in the projectile. For the proton transfer, the same procedures are used. But the input values for the binding energies and reaction Q – values are used in their effective values due to the Coulomb forces.

$$\epsilon_\alpha^{eff} = \epsilon_\alpha - \frac{z_\alpha e^2}{d_\alpha}, \quad \alpha = 1,2 \tag{6.46}$$

$$Q_{eff} = \epsilon_i^{eff} - \epsilon_f^{eff} \tag{6.47}$$

where $z_{1,2}$ are the charge numbers of nucleus 1 and 2, and d_1 and d_2 are determined to satisfy the relations

$$\frac{d_1}{d_2} = \frac{A_1^{1/3}}{A_2^{1/3}}, \quad and \quad d_1 + d_2 = R_s \tag{6.48}$$

where are the mass numbers of nucleus 1 and 2. As a strong absorption radius R_s, $11.2fm$ for ^{208}Pb region targets, $8.47fm$ for ^{90}Zr region targets and $2.29fm$ for ^{7}Li are used.

6.3.3 Comparison of Semi-Classical Calculations with Experimental Data

The calculated cross sections for the reactions of (^{7}Li,^{6}Li) and (^{7}Li,^{6}He) at $E_{inc} = 30$ MeV/n on targets of ^{90}Zr, ^{91}Zr, ^{89}Y and ^{208}Pb, ^{209}Bi, ^{207}Pb are shown in figs. 6.6 and 6.7, and compared with the experimental results. Because the calculations are done for continuum states where the final neutron is in an unbound state, the calculated spectra are seen only where the excitation energies are higher than the threshold energy for decay in the residual nucleus. The dashed curve is the absorption spectrum which corresponds to the transfer to compound states and the dotted curve is the

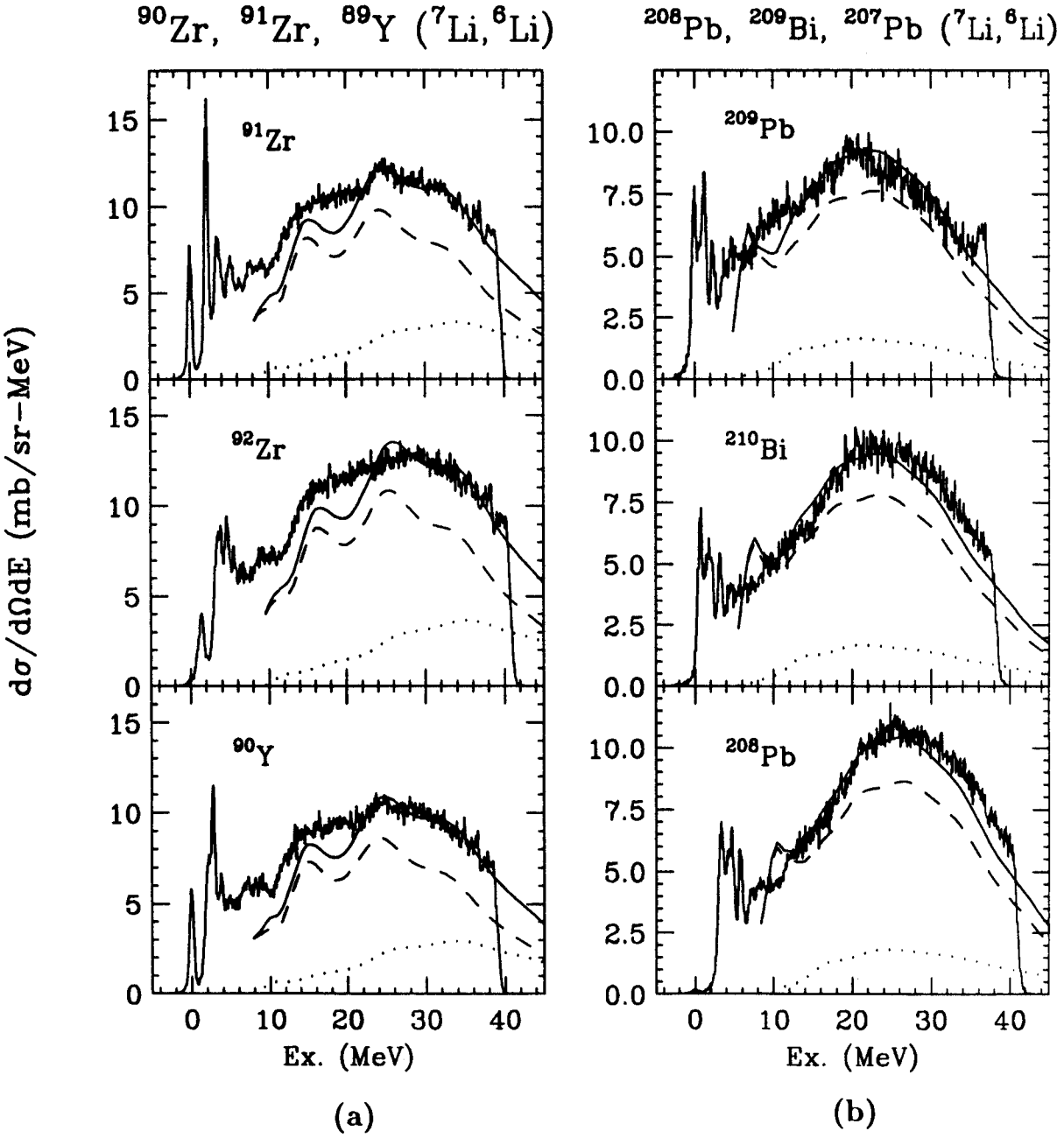

Figure 6.6: The calculated spectra of the reaction (^{7}Li, ^{6}Li) at E_{inc} = 30 MeV/n on targets of ^{90}Zr, ^{91}Zr, ^{89}Y and ^{208}Pb, ^{209}Bi, ^{207}Pb using the eqs. 6.36 and 6.37. The dashed curve is the absorption, the dotted curve is the breakup and the solid curve is the total spectrum. The spectra are normalized to the experimental results.

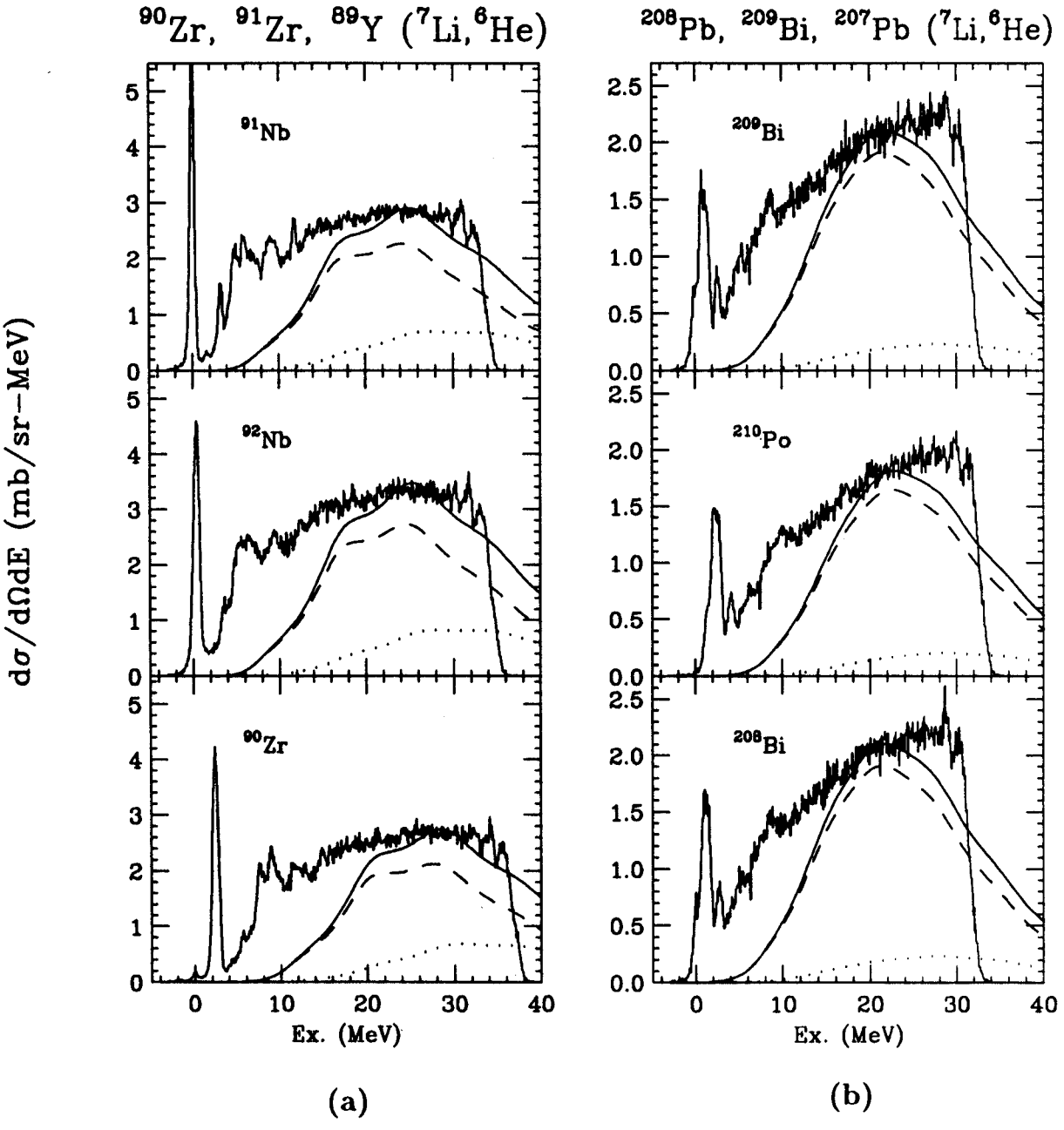

Figure 6.7: The calculated spectra of the reaction (^{7}Li, ^{6}He) at E_{inc} = 30 MeV/n on targets of ^{90}Zr, ^{91}Zr, ^{89}Y and ^{208}Pb, ^{209}Bi, ^{207}Pb using the eqs. 6.36 and 6.37. The dashed curve is the absorption, the dotted curve is the breakup and the solid curve is the total spectrum. The spectra are normalized to the experimental results.

projectile's elastic breakup spectrum. The solid curve is the sum of breakup plus absorption and should correspond to the experimental data. In all cases the calculated total cross sections are normalized to the experimental data.

In fig. 6.6.(a) for targets with masses near that of ^{90}Zr, three peaks are predicted in each spectrum. For the first peak of each spectrum, which is seen at $Ex. \sim 15$ MeV, about 50% of the strength is due to the $l_f = 6$ contribution. The contributions to the total cross sections for various l_f components are shown in fig. 6.8. The centroids of these peaks are very similar to those of the experimental results, whereas the widths of 4 MeV are about one half of the experimental results. Even though only the transfer to the single particle states is considered in the calculation, there is good agreement with the experimental data in the centroids of the peaks. This suggests that the peaks have the characteristics of single particle states rather than GR. The contribution of $l_f = 2$, which corresponds to the giant quadrupole resonance state, is very small.

For the second peak at $Ex. \sim 25$ MeV, about 60% of the strength is due to $l_f = 7$. There is very good agreement with the experimental data in the position and width, especially for the ^{91}Zr and ^{90}Y spectra. It is interesting to note that in this region of excitation energy there is little breakup predicted and it seems that the cross section is mainly due to transfer to the resonance states.

For the third peak at $Ex. \sim 32$ MeV, about 60% of the strength is due to $l_f = 8$ contribution to the sum, but the peak is not clearly seen in the experimental spectra.

The breakup predictions give smooth background curves which are peaked at excitation energies corresponding to the incident beam velocity and similar to the peaks predicted by the Serber Model. The contribution of the breakup to the sum is about 20% at excitation energies lower than 40 MeV. The breakup contribution

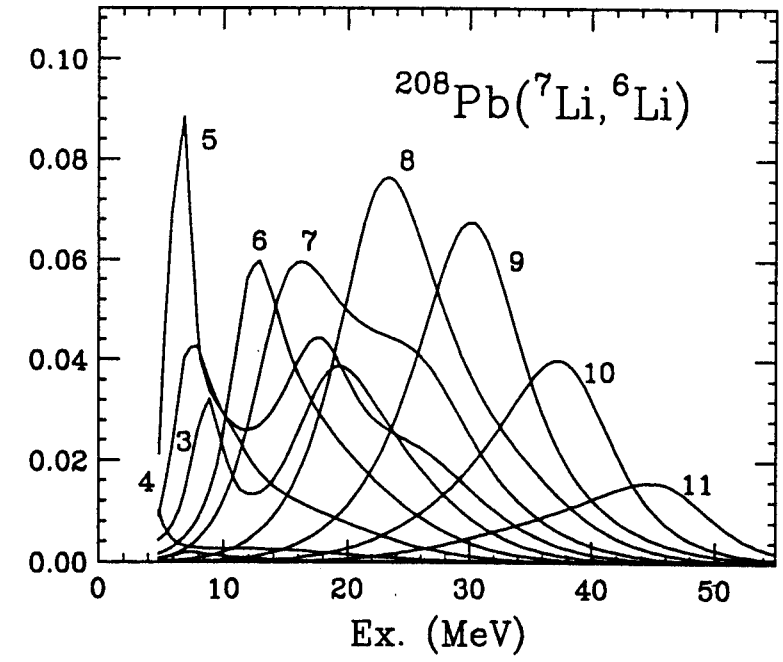

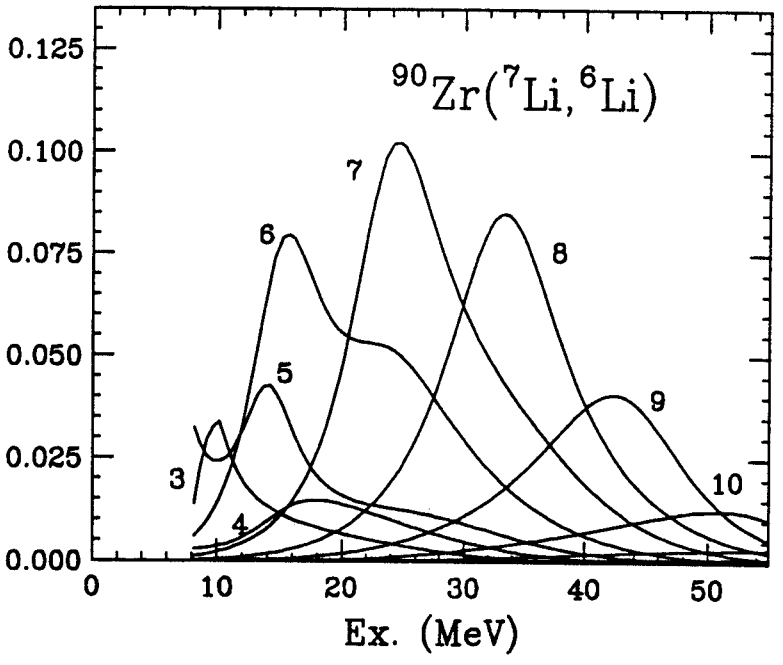

Figure 6.8: The contributions for each angular momentum component (l_f) to the total cross sections in (^{7}Li,^{6}Li) reactions at E_{inc} = 30 Mev/n predicted by Brink-Bonaccorso model. Unit is arbitrary.

becomes larger as the excitation energy increases, but still the resonance states are predicted to be dominant up to $Ex. \sim 45$ MeV.

Fig. 6.6.(b) displays the (^{7}Li,^{6}Li) reactions on the ^{208}Pb region targets. Only one peak is predicted above the smooth transfer cross section curves in each spectrum. This peak appears at $Ex. \sim 7$ MeV for the ^{209}Pb and ^{210}Bi nuclei, but it appeared at $Ex. \sim 10$ MeV in the ^{208}Pb nucleus. About 50% of the strengths of these peaks are due to the $l_f = 5$ contribution to the sum. In the experimental data the strong peaks are not seen at the same positions, instead, very weak peaks are seen at a few MeV higher excitation than the calculation predicted. The big differences, ~ 3 MeV, between the excitation energies of each peak for different targets also suggest that these peaks are from single particle states where l_f is 5. Summing the contributions for the various values of l_f results in broad peaks at $Ex. \sim 22$ MeV in ^{209}Pb and ^{210}Bi, and at $Ex. \sim 26$ MeV in ^{208}Pb in good agreement with the experimental data. In the reactions using these heavy targets, the prediction of the breakup contribution to the sum is even smaller than in the reactions using the ^{90}Zr region targets.

In fig. 6.7, the calculated cross sections for proton transfer to continuum states are displayed with the experimental data. The calculated cross sections start from zero, at the excitation energy corresponding the proton emission threshold, and increase very smoothly at low excitation. This is due to the Coulomb barrier which the proton must pass through to come out of the target nucleus. The cross section curve at low excitation shows an exponential curve of $\exp \alpha(Ex. - E_{th})$ where α, $Ex.$ and E_{th} are arbitrary constant, excitation energy and threshold energy for breakup. The shape at low excitation is completely different from the neutron transfer cross section curve where the Coulomb force does not apply. At high excitation, the curve is similar to that of the neutron transfer cross section.

In fig. 6.7.(a), the cross sections of the (^{7}Li,^{6}He) reactions for the ^{90}Zr region

targets are displayed. Three weak peaks are predicted by the calculations. The first one in each spectrum is dominated by $l_f = 6$, the second one by $l_f = 7$, and the third one by $l_f = 8$ contributions to the sum. The contributions to the total cross sections for each l_f component are shown in fig. 6.9. The predicted projectile breakup contributions are also very small as in neutron stripping reactions on the same targets. In fig. 6.10 where the spectrum is shown up to 50 MeV of excitation energy, the cross section is dominated by the process of transfer to compound states rather than the breakup process as in neutron transfer reactions.

In fig. 6.7.(b), no peak is predicted above the smooth curve. The main contributions to this curve are due to $l_f = 8, 9, 10$ and 11. The predictions on the ^{208}Pb region targets do not fit to the experimental data well. One of the explanation is that this model is very sensitive to the optical parameters and the input values may not be good for this calculation. Another one is that angle dependence is not considered in the calculations, whereas the experimental data are obtained at a particular angle.

One approach to solve the problem of the background is to obtain the pure transfer cross sections using a coincidence measurement with the ^{90}Zr(^{7}Li,^{6}He)^{91}Nb reaction, where the ^{6}He particles are detected at forward angles and the protons in an array at backward and forward angles. Coincidence of the ^{6}He with protons detected at backward angles should select only the piece of the spectra corresponding to the resonance states and should eliminate the breakup part of the spectrum, since the protons arising from the breakup of ^{7}Li will be restricted to forward angles. By measuring the ^{6}He spectra while varying the angles, the angle dependence of the absorption cross sections and the breakup cross sections can be measured.

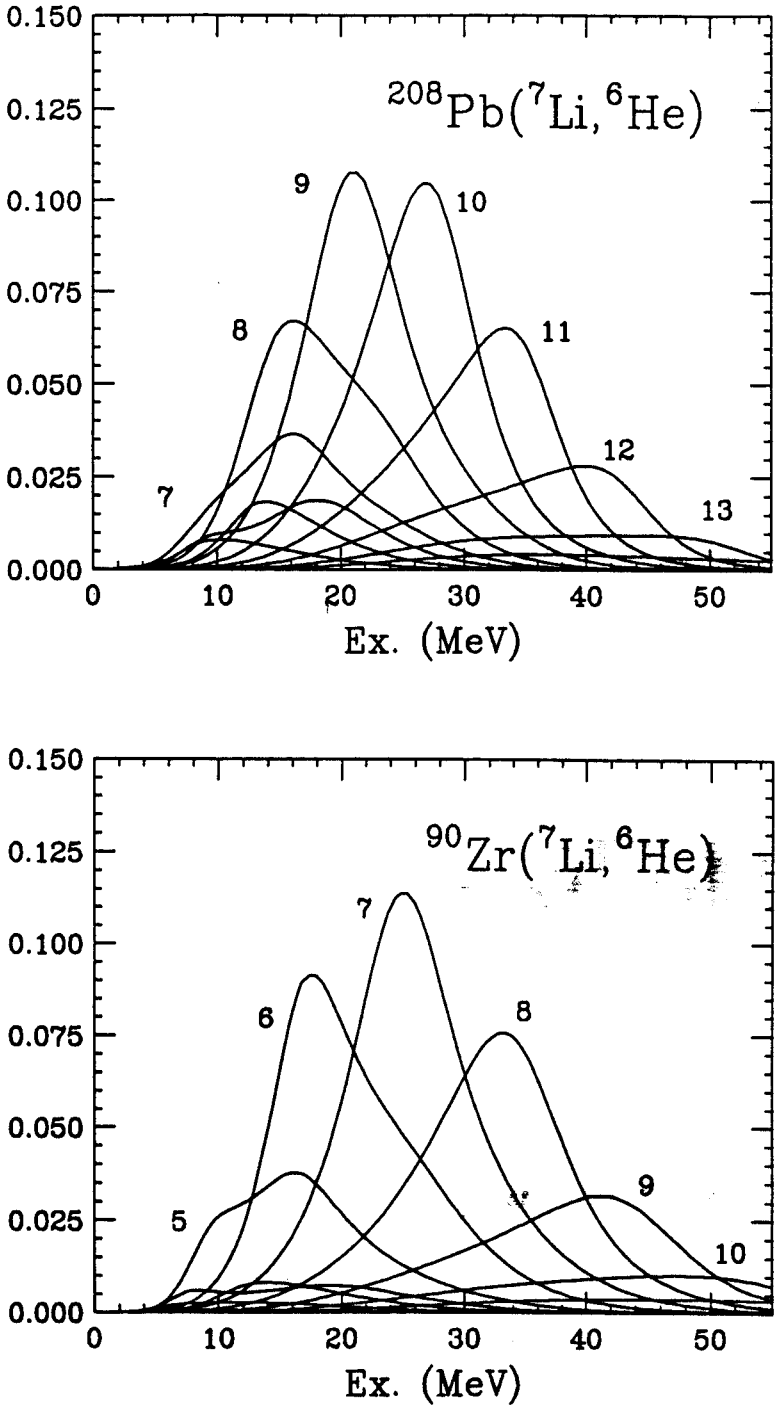

Figure 6.9: The contributions for each angular momentum component (l_f) to the total cross sections in (^{7}Li,^{6}He) reactions at E_{inc} = 30 MeV/n predicted by Brink-Bonaccorso model. Units are arbitrary.

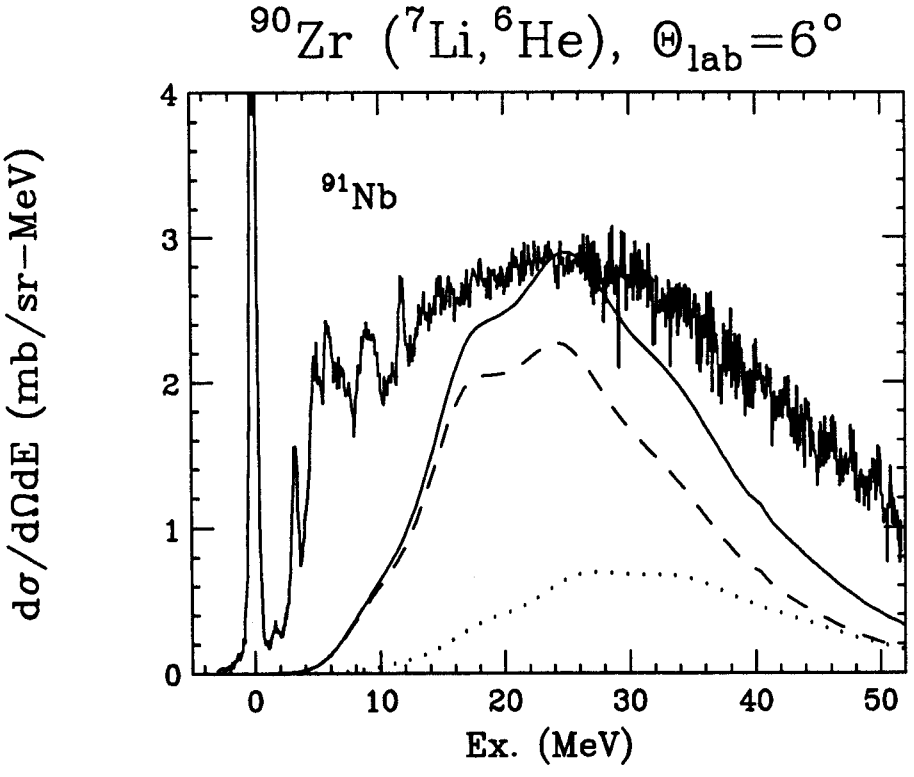

Figure 6.10: Breakup cross section of ^{7}Li (E_{inc} = 30 MeV/n) into ^{6}He + p on ^{90}Zr target using Brink-Bonaccorso model. Two spectra are connected at $Ex. \sim 26$ MeV. The dashed curve is the absorption, the dotted curve is the breakup and the solid curve is the total spectrum. The spectra are normalized to the experimental results.

6.4 Coincidence Measurement

A test run to examine the feasibility of the coincidence measurement of the products from the projectile breakup processes, and from the transfer and decay processes, was carried out. In the test run, the ^{90}Zr(^{7}Li,^{6}He) reaction with E_{inc} = 30 MeV/n was used. ^{6}He was detected in the S320 spectrograph in coincidence with two arrays of solid state detectors.

The forward array was used to set the coincidence timing using the projectile breakup of ^{7}Li $\rightarrow$ ^{6}He + p. Since the settings of the magnetic fields for ^{6}He and triton were the same, the tritons from the projectile breakup of ^{7}Li $\rightarrow$ ^{4}He + t were also detected. The forward array consisted of 5, 1cm x 1cm Si pin diodes for ΔE and CsI detectors for E (fig. 6.11). This $\Delta E - E$ arrangement allowed particle identification such as p, d, t, ^{3}He, and α (fig. 6.12).

The back angle array consisted of three, 3 x 3 cm^2 Si pin diodes. This simple detector array permitted the measurement of charged particles, mainly protons which were emitted at back angle from the excited ^{91}Nb nucleus. Time and energy spectra from the back angle detectors are shown in fig. 6.13. The back angle detector array had a total solid angle of about 0.9 sr and covered angles from about 120° to 150°. Good true to random ratios were obtained with a beam intensity of about 4 particle nano amperes (pnA).

Unfortunately after setting up the coincidence electronics, only 8 hours was available in the test run and this allowed only poor statistics to be obtained for the true coincidence spectrum. Only about 20% of the spectrum strength appeared to arise from particle unbound states.

The problems which were found in the test run can be solved or improved by changing the detecting method. Further suggestions for a future coincidence mea-

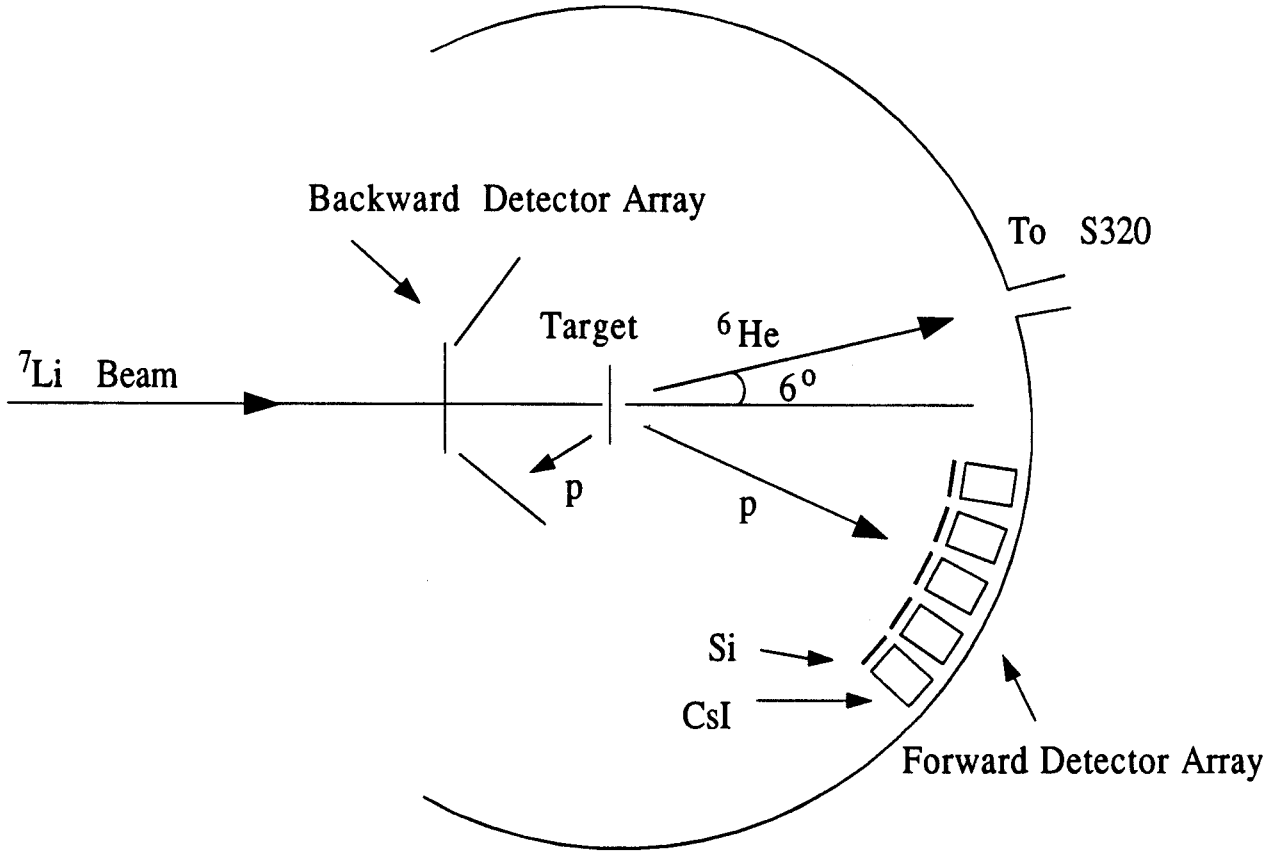

Figure 6.11: Top view for the coincidence measurement of ^{6}He and p inside a target chamber. Forward array was used to detect a proton from the breakup of ^{7}Li into ^{6}He + p, and the back array was used to detect a proton decayed from the ^{91}Nb$^* \rightarrow$ ^{90}Zr + p.

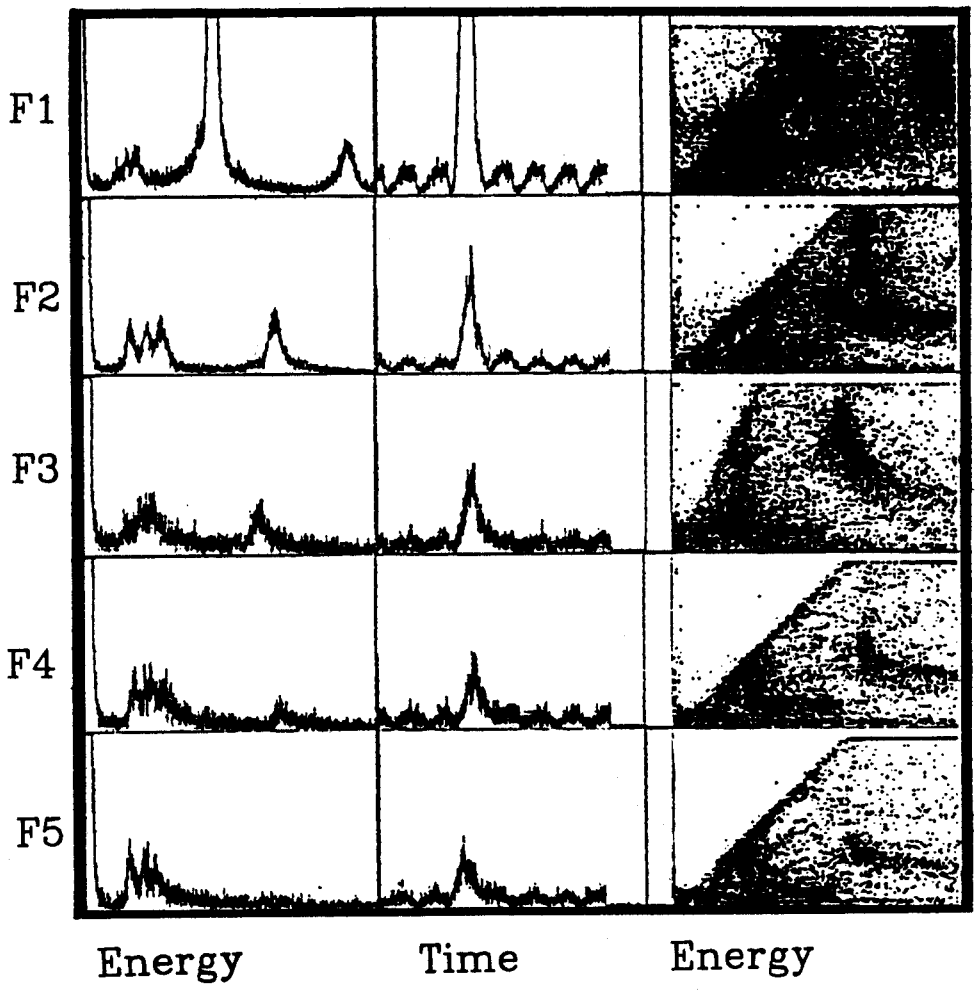

Figure 6.12: Spectra from the forward array (from F1 to F5) as functions of energy and time, and particle identification on the $\Delta E - E$ spectra from the reaction of ^{90}Zr(^{7}Li,^{6}He) at $E_{inc} = 30$ MeV/n.

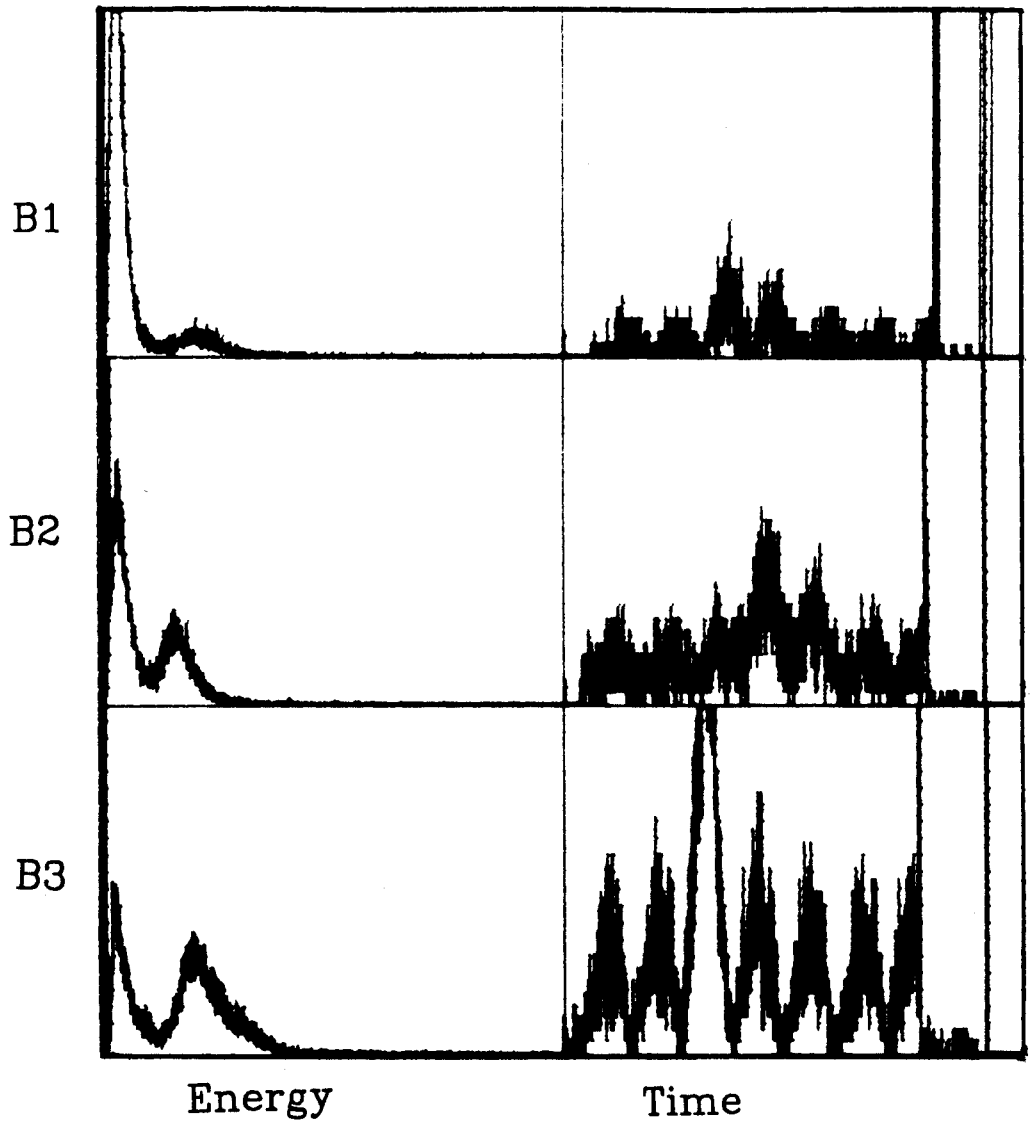

Figure 6.13: Spectra from the backward array (B1, B2 and B3) as functions of energy and time for the reaction of ^{90}Zr(^{7}Li,^{6}He) at $E_{inc} = 30$ MeV/n.

surement of the reaction ^{90}Zr(^{7}Li, ^{6}He + p) are :

- To carry out the coincidence measurement with better statistics, a longer running time is required, about 100 hours at 4 pnA.
- In each energy spectrum of the backward array, two peaks were observed (fig. 6.13). The peak of the lower energy seems to be caused by detecting the low energy electrons emitted from the target. These electrons can be blocked by placing a thin film in front of the detectors.
- Use the A1200 beam analysis device instead of the S320 spectrograph. The advantages of the A1200 are its high acceptance (about 3 times larger than the S320), enough space for the backward array, and a much higher resolving power (up to 5 times better than the S320). Particle identification in the forward direction can be done by using the two solid detectors ($Si, 0.5mm, \Delta E1 - \Delta E2$).
- By placing six, 3cm x 3cm solid detectors ($Si, 0.5mm$) in the backward direction, about 15% of the protons which are emitted isotropically by the decay process from the excited ^{91}Nb nucleus, will be detected. The counting rate will be twice than that of the test run.
- Use $\Delta E - E$ detectors for forward array to detect protons from the breakup processes and identify the particle type.

Time has been approved for this experiment at the NSCL.

Chapter 7

Results of Single Nucleon Pickup Reactions

7.1 Introduction

In this chapter, the data from the one nucleon pickup reactions (^{12}C,^{13}C) and (^{12}C,^{13}N) at E_{inc} = 30 MeV/n on targets of ^{90}Zr, ^{91}Zr, ^{89}Y, ^{208}Pb, ^{209}Bi and ^{207}Pb are reported. Data from the (^{7}Li,^{8}Li) reactions on the ^{90}Zr region targets and ^{208}Pb target are also given and compared with those from the (^{12}C,^{13}C) reactions. The ejectiles ^{13}C, ^{13}N and ^{8}Li were measured at the respective grazing angles, namely 6^o for the ^{90}Zr region targets, and 9^o for the ^{208}Pb region targets where the cross sections are large. In the (^{12}C,^{13}C) reactions, the elastically scattered ^{12}C particles were blocked by using a "finger" so as not to waste computing time by counting the unwanted elastically scattered particles.

The purpose of the pickup reactions is to study deep lying hole states and to explore the possibility of forming collective states. All the spectra are plotted as functions of the reaction Q – values and excitation energies, and are compared with each other. Overall, the spectra have much smaller backgrounds than those of the stripping reactions, but the ejectile excitation in the ^{13}C spectra and the poor energy resolution were additional problems which were not seen in the stripping reactions,

(^{7}Li,^{6}Li) and (^{7}Li,^{6}He).

Theoretically calculated single particle energy levels for ^{90}Zr and ^{208}Pb nuclei are given in fig. 7.1 to help understand the hole structures of ^{90}Zr and ^{208}Pb region nuclei [Gale 88].

7.2 ^{90}Zr, ^{91}Zr, ^{89}Y (^{12}C,^{13}C) Reactions

The energy spectra for the (^{12}C,^{13}C) reactions on the targets ^{90}Zr, ^{91}Zr and ^{89}Y at E_{inc} = 30 MeV/n and $\theta_{lab} = 6^{o}$ are given in fig. 7.2. Since a "finger" was placed in front of the focal plane detector to prevent the detection of the ^{12}C particles, ^{13}C spectra corresponding to that position were not obtained. Excitation energies, Q – values and widths of peaks observed in the ^{13}C spectra are given in table 7.1.

In the ^{13}C nucleus, the threshold energy for breakup into ^{12}C + n is 4.946 MeV and there are three bound excited states (j^{π} = $1/2^{+}$ (3.09 MeV), $3/2^{-}$ (3.68 MeV) and $5/2^{+}$ (3.85 MeV)) below this energy. These three excited states are strongly populated in the reactions on all 3 targets.

In the ^{90}Zr(^{12}C, ^{13}C)^{89}Zr reaction, peak 1 appears to be a composite of three low lying single hole states of ^{89}Zr, namely $1g_{9/2}$(ground state), $2p_{1/2}$(0.59 MeV), and $2p_{3/2}$(1.10 MeV). This peak is dominated by the $1g_{9/2}$ state rather than the other two p-shell states because the angular momentum of the $1g_{9/2}(l = 4)$ state is close to the favoured angular momentum transfer for this reaction (3 and 4$\hbar$). The $(2j+1)$ factor for the $1g_{9/2}$ state also enhances its cross section. In peak 1, no ejectile excitation contributions are observed because of the high excitation energy of the first excited state of ^{13}C.

Peak 2 (4.1 MeV) appears to be dominated by ejectile excitation. If the spectrum is compared to those from the (^{7}Li,^{8}Li) or (^{20}Ne,^{21}Ne) reactions [Fort 90], no peak is

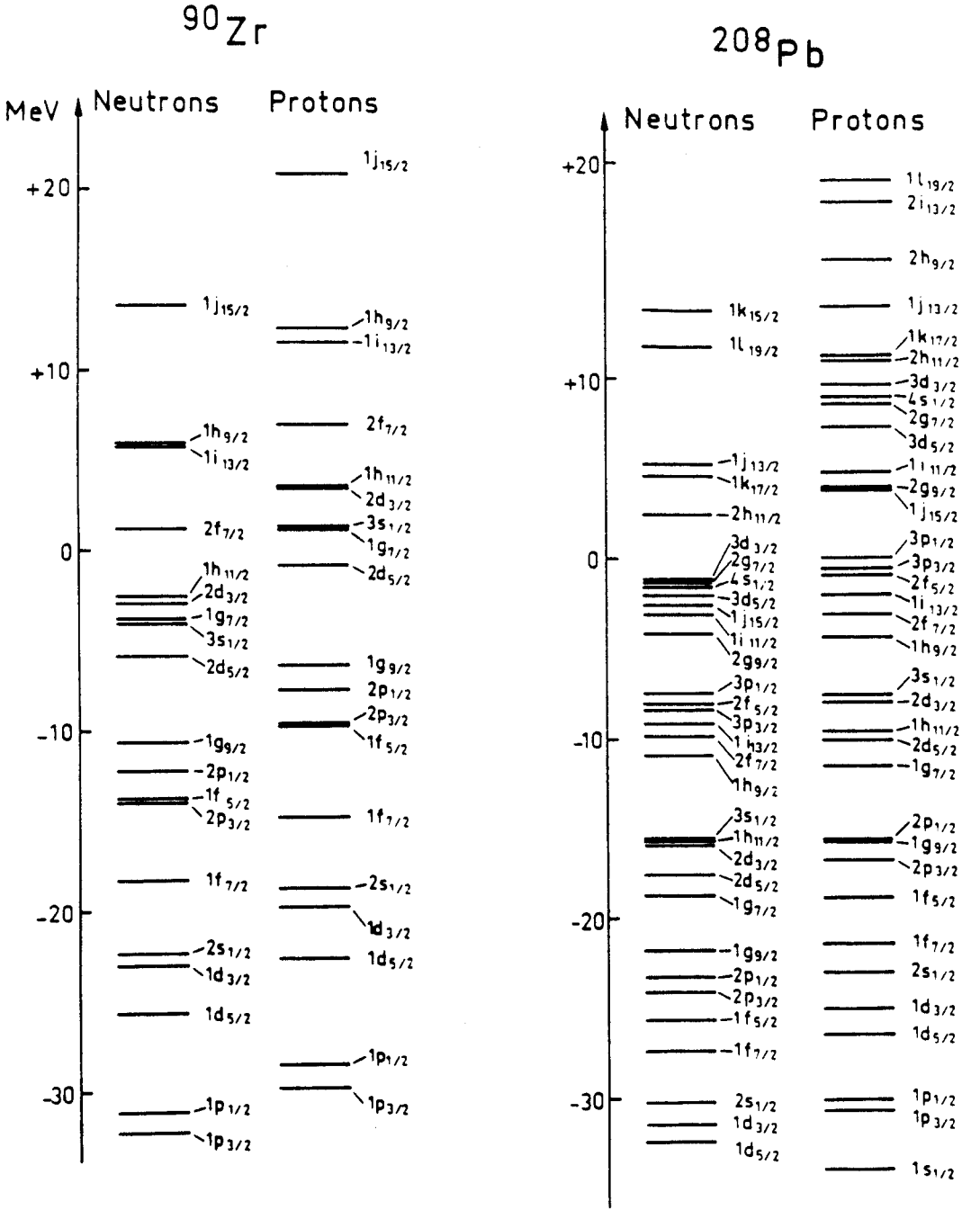

Figure 7.1: Single particle energy levels of ^{90}Zr and ^{208}Pb in a Woods-Saxon potential well [Gale 88].

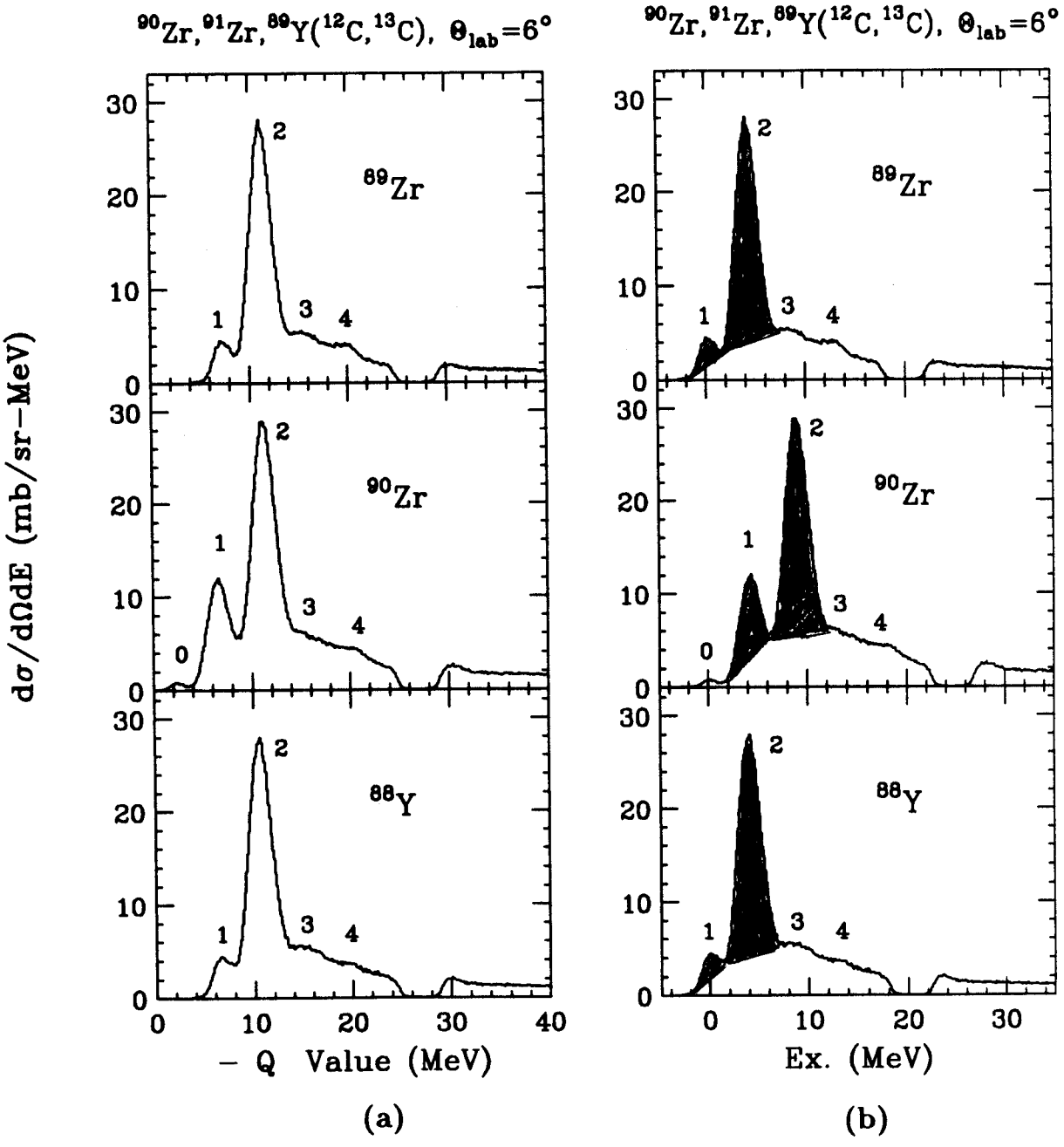

Figure 7.2: Experimental spectra of ^{90}Zr, ^{91}Zr, ^{89}Y (^{12}C,^{13}C) reactions with $E = 30$ MeV/n. The valleys seen at excitation energies about 20 MeV are produced by the "finger" used to block the elastically scattered ^{12}C. Peak 0 in the ^{90}Zr spectrum is from the pickup of an extra neutron, outside a closed shell, in a $2d_{5/2}$ state. The shaded area above the assumed background was used to obtain the cross sections for peaks 1 and 2, and to compare the positions.

Table 7.1: Excitation energies for the peaks observed in the (^{12}C,^{13}C) reactions on targets of ^{90}Zr, ^{91}Zr and ^{89}Y. Γ is the full width at half maximum, Q is the reaction Q – value for the corresponding excitation energy and units are MeV. The uncertainty is about 0.3 MeV. σ is the cross section for the shaded area in mb/sr and the uncertainty is about 20%

	$^{90}Zr(^{12}C,^{13}C)^{89}Zr$				$^{91}Zr(^{12}C,^{13}C)^{90}Zr$				$^{89}Y(^{12}C,^{13}C)^{88}Y$			
Peak #	Ex.	Γ	- Q	σ	Ex.	Γ	- Q	σ	Ex.	Γ	- Q	σ
0					0.0	1.0	2.25					
1	0.0	2	7.03	6	4.2	2.0	6.55	23	0.0	2.0	6.53	6
2	4.1	3.5	11.13	56	8.8	3.5	11.05	66	4.1	3.5	10.63	60
3	8.7		15.73		14.0		16.25		9.2		15.73	
4	13.5		19.7		18.0		20.25		13.7		20.23	

seen at about $Ex.$ = 4.1 MeV in either of these latter two reactions on ^{90}Zr. Because the excitation energy of the centroid of this peak (4.1 MeV) is higher than the ejectile's bound excited states (^{13}C ; $\frac{1}{2}^+$(3.09 MeV), $\frac{3}{2}^-$(3.68 MeV), and $\frac{5}{2}^+$(3.85 MeV)) by 0.25 to 1 MeV, there must be a mutual excitation of the ejectile's bound excited states and the residual nuclei's low lying single hole states at 0.59 and 1.10 MeV. The 1 MeV energy resolution makes it difficult to give more detailed description of this peak.

Peaks 3 and 4 (8.7 and 13.5 MeV respectively), appear to arise from the deep hole states. In the light ion transfer reaction, ^{90}Zr($\vec{p}, d$) [Kasa 83] at E_{inc} = 90 MeV, two peaks were also observed at similar excitation energies to those of peaks 3 and 4. At around 9.5 MeV excitation energy in the ^{90}Zr(^{20}Ne,^{21}Ne) reaction, a very weak peak is also seen at an excitation energy similar to that of peak 3. Comparing these excitation energies with the theoretically calculated single particle energies (see fig. 7.1), peak 3 corresponds to the $1g_{9/2}, 1f_{5/2}$ and $2p_{3/2}$ hole states, and peak 4 corresponds to the $1f_{7/2}$ hole state.

In the ^{91}Zr(^{12}C, ^{13}C)^{90}Zr reaction, the spectrum is slightly different from the other two spectra. Peak 0 arises from the pickup of the outmost neutron in the $2d_{5/2}$ state with no ejectile excitation. As both the first excited states in ^{13}C (3.09 MeV) and in the residual nucleus (1.76 MeV) are reasonably well separated from peak 0, no ejectile excitation or excited state of the residual nucleus contributes to this peak.

Peak 1 is much more strongly populated compared to the reactions with the ^{90}Zr and ^{89}Y targets, and the ratio of peak 1 to peak 2 is much bigger than the other two cases. This may be accounted for by the superposition of the two different peaks resulting from the pickup of neutrons from the two different states. When the outmost $2d_{5/2}$ neutron is transferred to the bound excited states in ^{13}C, the centroid of the ejectile excitation energy will be around 3.70 MeV. If a neutron in the $2g_{9/2}$ state of the ^{90}Zr target is transferred to the ejectile in its ground state, the excitation energy

will be 4.77 MeV which corresponds to the difference in neutron's binding energy between the $2d_{5/2}$ and $2g_{9/2}$ states. Since the two peaks (3.70 MeV and 4.77 MeV) are not resolved, they form a single peak at around 4.2 MeV. Compared with the other two spectra, peak 1 is dominated by the ejectile excitation.

Peak 2 is very similar to that of the ^{90}Zr(^{12}C,^{13}C) reaction in the Q – value and the cross section. This peak appears to arise from the mutual excitation resulting when a neutron in the $2g_{9/2}$ shell is transferred to bound excited states in ^{13}C as in the reaction with the ^{90}Zr target. The excitation energy difference between peak 1 (4.2 MeV) and peak 2 (8.8 MeV) is about 4.6 MeV, which is larger than in the other two spectra by 0.6 MeV. This is because peak 1 is not a single peak but a combination of two peaks at 3.7 MeV and 4.77 MeV which gives the centroid at 4.2 MeV, while peak 1 from the reaction with the ^{90}Zr or ^{89}Y target is a single peak arising from the residual nucleus only.

Peaks 3 and 4 are very similar to those of the reaction with the ^{90}Zr target but are very weak for all 3 targets. They appear at almost the same reaction Q – values. The presence of one neutron in the $2d_{5/2}$ state does not seem to affect these peaks.

In the reaction ^{89}Y(^{12}C,^{13}C)^{88}Y, the spectrum is very similar to that of the ^{90}Zr(^{12}C,^{13}C) reaction. All four peaks occur at very similar reaction Q – values. This suggests that the peaks are formed with the same components as in the reaction with the ^{90}Zr target. The couplings of the proton hole of $\pi(2p_{1/2})^{-1}$ to the neutron holes in ^{88}Y nucleus does not appear to change the spectrum significantly.

The broadening due to $p-h$ or $h-h$ interactions is not visible in these spectra. Because of ejectile excitation, the exact strengths of single hole states or coupling strengths between the hole and particle states are difficult to disentangle in the (^{12}C,^{13}C) reactions.

7.3 ^{90}Zr, ^{91}Zr, ^{89}Y (^{7}Li,^{8}Li) Reactions

The energy spectra from the ^{90}Zr, ^{91}Zr, ^{89}Y (^{7}Li,^{8}Li) reactions at E_{inc} = 30 MeV/n and θ_{lab} = 6° are shown in fig. 7.3. The purpose of carrying out these reactions is to compare the spectra with those from the (^{12}C,^{13}C) reactions, and thus help to determine which structures arise from excitation in the residual nucleus and which from ejectile excitations. Since the threshold energy for breakup of ^{8}Li into ^{7}Li + n is 2.03 MeV, there is only one bound excited state, at $Ex.$ = 0.98 MeV.

In the ^{90}Zr(^{7}Li, ^{8}Li)^{89}Zr reaction, only two peaks are observed. Peak 1 (ground state) arises from the pickup of a neutron in the $1g_{9/2}$ state. The second peak (1.14 MeV) appears to be a composite of an ejectile excitation (1^+, 0.98 MeV) and the residual nucleus excitation, mainly a $2p_{3/2}$ (1.10 MeV), and $1f_{5/2}$ (1.45 MeV), which are both single hole states. The $2p_{1/2}$ (0.59 MeV) state is likely to be weakly excited because of the spin-flip process and the small value of $2j + 1$. No other peaks are observed at excitation energies higher than 3 MeV. In particular, the strong peak seen in the ^{90}Zr(^{12}C,^{13}C) reaction at $Ex.$ = 4.1 MeV is not seen in the ^{8}Li spectrum. This suggests that the peak of $Ex.$ = 4.1 MeV in the ^{13}C spectrum arises from the ejectile excitation.

In the ^{91}Zr(^{7}Li, ^{8}Li)^{90}Zr reaction, four peaks are observed. Peaks A and B arise from the pickup of a single neutron in the $2d_{5/2}$ state, leaving ^{8}Li in the ground state for peak A, and in an excited state (1^+, 0.981 MeV) for peak B. From the comparison of peaks A and B, the ejectile excitation in ^{8}Li is less than in ^{13}C. In fig. 7.3.(a), where the spectra are plotted as a function of reaction Q – values, peaks 1 and 2 of all three spectra appear at almost the same positions, while peaks A and B shift to lower energy by 4.56 MeV. But in fig. 7.3.(b), where the spectra are plotted as a function of excitation energies, peaks 1 and 2 are shifted to higher excitation energies

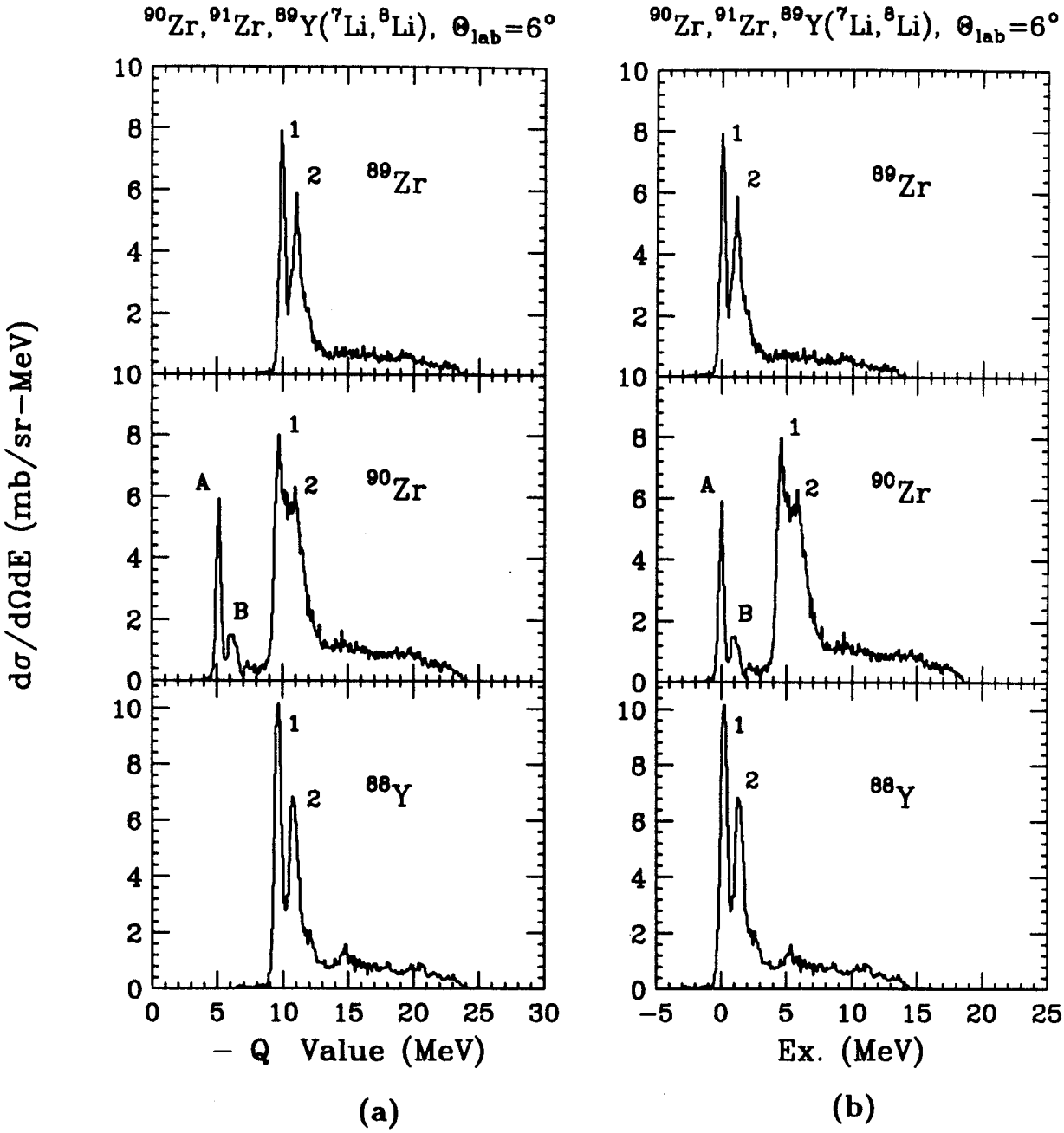

Figure 7.3: Experimental spectra from the ^{90}Zr, ^{91}Zr, ^{89}Y (^{7}Li,^{8}Li) reactions at E = 30 MeV/n. Peak A of the ^{90}Zr spectrum arises from the pickup of a neutron in the $2d_{5/2}$ state and peak B arises from the ^{8}Li's excitation (1^{+}).

compared to peak 1 from the same reaction on the ^{90}Zr target by 4.56 MeV. Peak 1 (4.56 MeV) arises from the pickup of a neutron in the $1g_{9/2}$ state, as in the reaction with the ^{90}Zr target. Then the $1g_{9/2}$ hole state couples to the single neutron particle state, $2d_{5/2}$, and forms many states, with j^{π} ranging from 2^+ to 7^+. Peak 2 (5.70 MeV) is obtained by pickup of a neutron at the same state as in the ^{90}Zr(^{7}Li,^{8}Li) reaction, with some ejectile excitation. Then the neutron particle state $2d_{5/2}$ couples to the hole state, and makes the hole state split into many states, which are not separated clearly from peak 1. The existence of the neutron in the $2d_{5/2}$ state outside the closed shell does not change the shape of the spectrum substantially, but makes the peaks a little wider, keeping the total strength the similar.

In the ^{89}Y(^{7}Li, ^{8}Li)^{88}Y reaction, two strong peaks (at 0.2 and 1.32 MeV) and a very weak peak (at about 5.5 MeV) are observed. The spectrum of ^{88}Y is very similar to that of ^{89}Zr. The only difference is that the ^{89}Y nucleus has one less proton in the $2p_{1/2}$ state than the ^{90}Zr nucleus. Peak 1 (0.20 MeV) arises from the pickup of a single neutron in the $1g_{9/2}$ state. This neutron hole state $1g_{9/2}$ couples to the proton hole state $2p_{1/2}$ and forms 4^- (ground state) and 5^- (0.232 MeV) states which are not resolved in this experiment. The centroid of these two states is at 0.2 MeV. Peak 2 appears at an excitation energy of 1.32 MeV. The energy difference between peak 1 and peak 2, and the ratio of their relative strengths are almost the same as in the other two spectra. A very weak peak, seen at an excitation energy of about 5.5 MeV, is not seen in the other two reactions at the corresponding reaction Q – values. It is not clear whether this peak arises from the residual nucleus's structure or not.

Overall, no deep lying hole state was excited in the (^{7}Li,^{8}Li) reaction. The cross section for the ^{90}Zr(^{7}Li,^{8}Li) is smaller than the other two reactions by about 15%. This probably can be accounted for by the uncertainties for the thicknesses of the targets. The presence of one extra particle or hole outside a closed shell appears to

make little difference to the structures observed in the residual nucleus.

7.4 ^{208}Pb, ^{209}Bi, ^{207}Pb (^{12}C,^{13}C) and ^{208}Pb(^{7}Li,^{8}Li) Reactions

The energy spectra from the ^{208}Pb, ^{209}Bi, ^{207}Pb (^{12}C,^{13}C) and ^{208}Pb(^{7}Li,^{8}Li) reactions at E_{inc} = 30 MeV/n are shown in figs. 7.4 and 7.5. The ejectiles, ^{13}C and ^{8}Li were measured at the grazing angles $\theta_{lab} = 9°$. The favoured angular momentum for the (^{12}C,^{13}C) reaction is $l = 6$, and for the (^{7}Li,^{8}Li) reaction is $l = 3$ and 4. The spectra, for all three targets, have very similar shapes. Excitation energies, Q - values and widths of peaks observed in the ^{13}C spectra are given in table 7.2.

In the ^{208}Pb(^{12}C,^{13}C)^{207}Pb reaction, three broad peaks (at $Ex.$ = 1.14, 5.8 and 10.05 MeV respectively) are seen. In fig. 7.4.(a), plotted versus reaction Q - values, peak 1 ($Ex.$ = 1.14 MeV) has almost the same Q - value (within 0.1 MeV) as peak 1 of the other two reactions. This suggests that these peaks are caused by the pickup of neutrons from the same levels which are the single hole states ($3p_{1/2}$(0.00), $2f_{5/2}$(0.57 MeV), $3p_{3/2}$(0.90 MeV) and $2i_{13/2}$(1.63 MeV)). No ejectile excitation contributes to peak 1 because ^{13}C's first excited state energy (3.09 MeV) is much higher than the energy of peak 1. As the ground state of ^{13}C is $p_{1/2}$ ($l = 1, j = l - 1/2$) a high spin state with no spin-flip process is preferable. From these conditions for preferable transfer, $2f_{5/2}(l = 3, j = l - 1/2)$ and $2i_{13/2}(l = 6, j = l + 1/2)$ states seem to be equally dominant. The ground state ($3p_{1/2}$) of the ^{207}Pb nucleus is not strongly populated due to the small factor of $(2j + 1)$ and small angular momentum transfer ($l = 1$) compared to the favoured large angular momentum transfer ($l = 6$).

The excitation energy of peak 2 ($Ex.$ = 5.80 MeV) is somewhat high to be assumed as a pure ejectile excitation. It appears to be formed by mutually excited

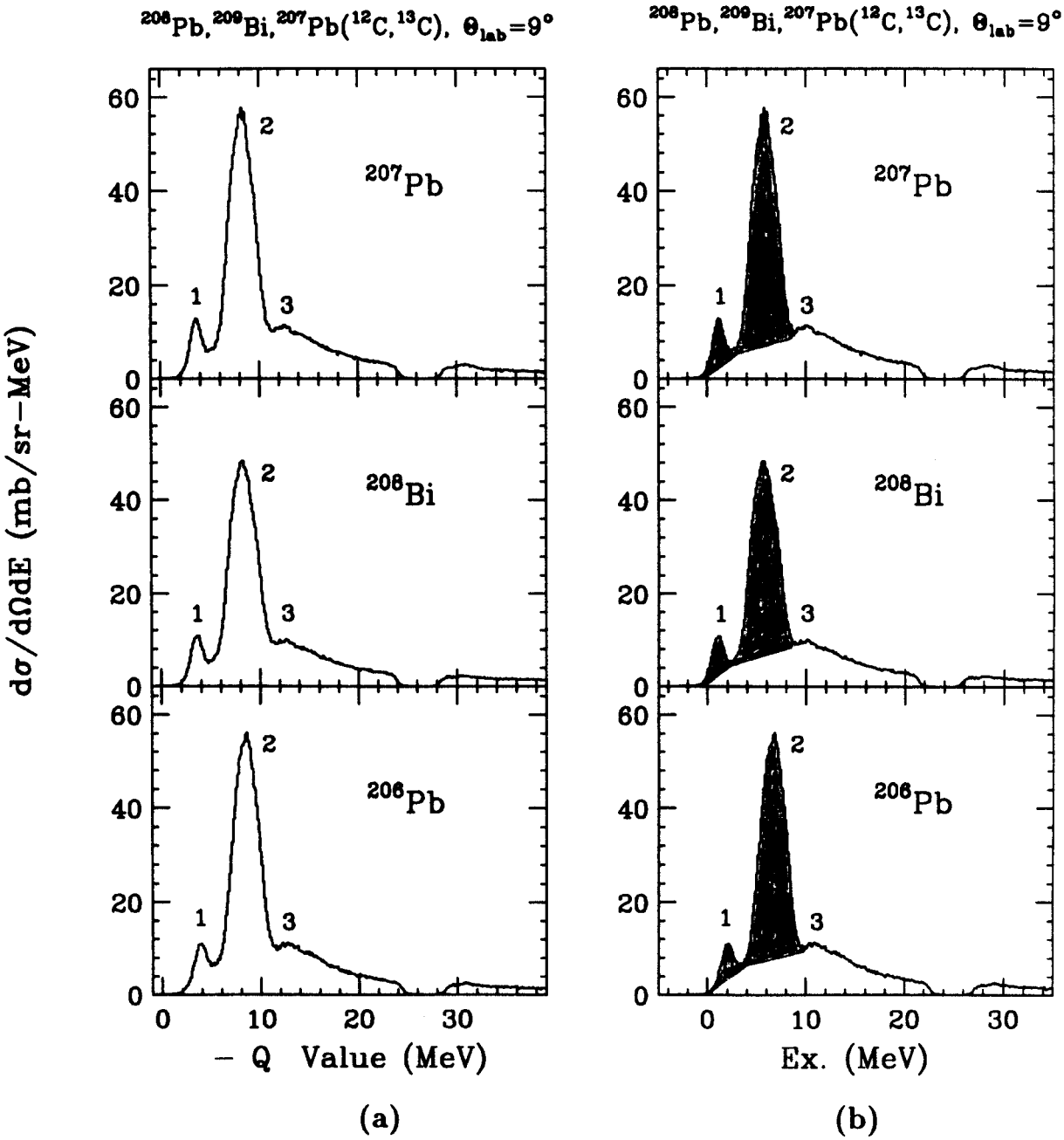

Figure 7.4: Experimental spectra of ^{208}Pb, ^{209}Bi, ^{207}Pb (^{12}C,^{13}C) reactions with E_{inc} = 30 MeV/n. The valleys seen at excitation energies 20 MeV are produced by the "finger" to block the elastically scattered ^{12}C. The shaded area above the assumed background was used to obtain the cross sections for peaks 1 and 2, and to compare the positions.

Table 7.2: Excitation energies for the peaks observed in the (^{12}C,^{13}C) reactions on targets of ^{208}Pb, ^{209}Bi and ^{207}Pb. Γ is the full width at half maximum, Q is the reaction Q – value for a corresponding excitation and the units are MeV. The uncertainty is about 0.3 MeV. σ is the cross section for the shaded area in mb/sr and the uncertainty is about 20%.

	^{208}Pb(^{12}C,^{13}C)^{207}Pb				^{209}Bi(^{12}C,^{13}C)^{208}Bi				^{207}Pb(^{12}C,^{13}C)^{206}Pb			
Peak #	Ex.	Γ	- Q	σ	Ex.	Γ	- Q	σ	Ex.	Γ	- Q	σ
1	1.14	1.7	3.56	16	1.12	1.7	3.63	12	2.16	1.7	3.95	12
2	5.80	3.5	8.22	160	5.70	3.5	8.21	115	6.80	3.5	8.59	160
3	10.05	2.0	12.47		10.12	2.0	12.63		11.00	2.0	12.79	

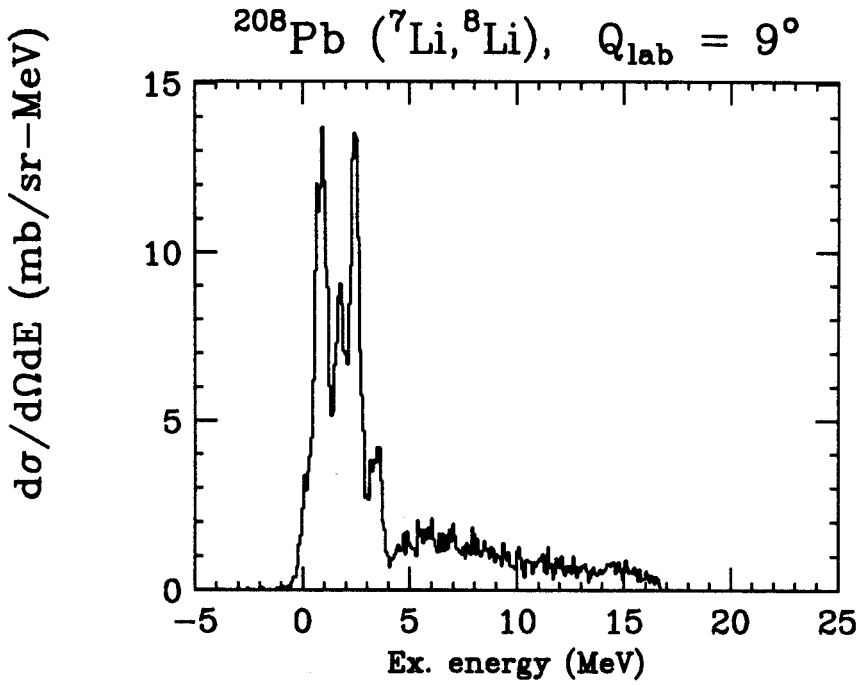

Figure 7.5: Experimental spectrum of ^{208}Pb(^{7}Li,^{8}Li) reaction at $E = 30$ MeV/n.

states of ^{13}C ($1p_{1/2}$(3.09 MeV), $1p_{3/2}$(3.68 MeV), and $1d_{5/2}$(3.84 MeV)) and ^{207}Pb ($1i_{13/2}$(1.63 MeV), $2f_{7/2}$(2.33 MeV), and $1h_{9/2}$(3.41 MeV)). Peaks 2 in all three reactions have almost the same reaction Q – values and they seem to be formed by the pickup of neutrons in the same states in each target, and with some ejectile excitation. Considering the maximum transfer matching conditions, the most dominant transitions are likely to be from the $1i_{13/2}$ and $2f_{7/2}$ states in ^{208}Pb, $1p_{3/2}$ and $1d_{5/2}$ states in ^{13}C.

In the experiment done with the (^{20}Ne,^{21}Ne) reaction at $E_{inc} = 30,25$ MeV/n [Fort 90], two large peaks are observed at excitation energies of 2.5 and 6.5 MeV where the threshold energy for breakup of ^{21}Ne is 6.76 MeV. These two peaks are very similar to peak 1 and peak 2 of the present experiment, except that they are higher in excitation energies by about 1.4 and 0.8 MeV respectively. The differences of the excitation energies of the peaks from the present experiment can be accounted for by the different energy levels in the two ejectiles, ^{13}C and ^{21}Ne.

While in the ^{208}Pb(^{7}Li,^{8}Li) reaction, low lying states are resolved clearly, which correspond to peak 1 of the (^{12}C,^{13}C) reaction. A very weak bump is observed in the spectrum at excitation energies between 5 and 8 MeV (fig. 7.5) which are likely to be from the $2f_{7/2}$, $1h_{9/2}$ and $1h_{11/2}$ states (see fig. 7.1), where a strong peak 2 was observed in the ^{208}Pb(^{12}C,^{13}C) reaction. From the comparisons of the ^{13}C spectrum with the spectra of ^{8}Li, ^{21}Ne and the (^{12}C,^{13}C) reaction on the ^{90}Zr region targets, peak 2 of ^{13}C spectrum appears to be dominated by the ejectile excitation and little is contributed by the real structure of ^{207}Pb.

Peaks 3 are seen weakly in all three reactions at almost the same reaction Q – values, at about 12.5 MeV, and they have very similar strengths and shapes. They seem to show some of the inner hole structure of ^{208}Pb region nuclei. But, it is not clear whether the strength of these peaks is due to the residual nucleus's inner

hole states or mutual excitation. In the experiments of (^{20}Ne,^{19}Ne) at $E_{inc} = 25, 30$ MeV/n [Fort 90], (^{7}Li,^{8}Li) (this experiment), and ^{208}Pb(^{12}C,^{13}C) done at $E_{inc} = 101$ MeV [Oert 84], no peak was observed at corresponding excitation energies of about 10 MeV.

In the ^{209}Bi(^{12}C, ^{13}C)^{208}Bi reaction, the spectrum is very similar to that of the ^{208}Pb(^{12}C,^{13}C) reaction. Three broad peaks are observed at almost the same excitation energies and the reaction Q – values with those from the ^{208}Pb target, and the difference of the reaction Q – values between the ground states, 0.09 MeV,is not recognizable in the spectrum. ^{209}Bi has an extra proton in $1h_{9/2}$ state outside the closed shell nucleus ^{208}Pb. The coupling of this proton to the neutron hole states does not seem to change the shape of the spectrum or the centroid of the peaks.

In the ^{207}Pb(^{12}C,^{13}C)^{206}Pb reaction, the whole spectrum is shifted to higher excitation energy compared to the spectra of the reactions from the ^{208}Pb or ^{209}Bi targets, by about 1 MeV. The ^{207}Pb nucleus has a single neutron in the $3p_{1/2}$ state and the reaction Q – value to pickup this neutron is higher by about 0.7 MeV than that to pickup a neutron in a paired state of the ^{208}Pb and ^{209}Bi nuclei. Except for this unpaired $3p_{1/2}$ neutron, all the processes of the pickup a neutron seemed to have the similar reaction Q – values. The single neutron in $3p_{1/2}$ state couples to an inner neutron hole state produced by a neutron pickup reaction, but the couplings appeared not so strong enough as to observe any significant change in the spectrum.

For all (^{12}C,^{13}C) reactions on the ^{90}Zr and ^{208}Pb region targets examined here, the predominance of ejectile excitation makes the investigation of deep lying single hole states in the residual nuclei difficult. In the (^{7}Li,^{8}Li) reaction, ejectile excitation is not so serious as in the ^{13}C spectra, but the deep lying hole states are not excited as much as in the ^{13}C spectra.

7.5 ^{90}Zr, ^{91}Zr, ^{89}Y (^{12}C,^{13}N) Reactions

The energy spectra for the (^{12}C,^{13}N) reactions on targets ^{90}Zr, ^{91}Zr and ^{89}Y with E_{inc} = 30 MeV/n at θ_{lab} = 6° are shown in fig. 7.6. Because the threshold energy for breakup into ^{12}C + p (1.94 MeV) is lower than the excitation energy of the first excited state (2.37 MeV), there is no bound excited state in ^{13}N, and thus no ejectile excitation contributes to the ^{13}N spectra. The favoured angular momentum transfers for this reaction are $2\hbar$ and $3\hbar$, and no spin-flip process is preferable. Excitation energies, reaction Q - values and widths for the observed peaks are given in table 7.3.

In the ^{90}Zr(^{12}C, ^{13}N)^{89}Y reaction, a strong peak is seen at low excitation ($Ex.$ ~ 1.58 MeV) and a broad weak peak is observed at medium excitation ($Ex.$ ~ 6.56 MeV). The widths are about 3 MeV for both peaks. Since there is no ejectile excitation, these peaks arise from the real structure of the residual nucleus. Peak 1 (1.58 MeV) arises from the excitation of the low lying hole states $2p_{1/2}$(ground state), $1g_{9/2}$(0.91 MeV), $2p_{3/2}$(1.51 MeV) and $1f_{5/2}$(1.75 MeV) (see fig. 7.1) [Fort 90, Gale 88]. The ground state is observed very weakly on the side of the large peak 1. Considering the two transfer matching conditions (Δl = 2 and 3, and no spin-flip process), the most dominant contribution very likely comes from the $1f_{5/2}$ state.

Peak 2 (6.56 MeV) appears to arise from the pickup of a $1f_{7/2}$ proton. Since there is only one proton hole state ($1f_{7/2}$) near $Ex.$ = 6.56 MeV (see fig. 7.1), the $1f_{7/2}$ state accounts for most of the cross section between the excitation energies of 4 MeV and 12 MeV. In the ^{90}Zr(d,^{3}He) reaction done with E_d = 52 MeV [Stui 80], two sharp peaks were observed at $Ex.$ = 5 and 6.8 MeV above a broad large peak. But in the present experiment, these peaks are not resolved. Similar peaks were also observed in the reaction ^{90}Zr(^{20}Ne,^{21}Na) with E = 25,30 MeV/n at $Ex.$ ~ 7 MeV [Fort 90]

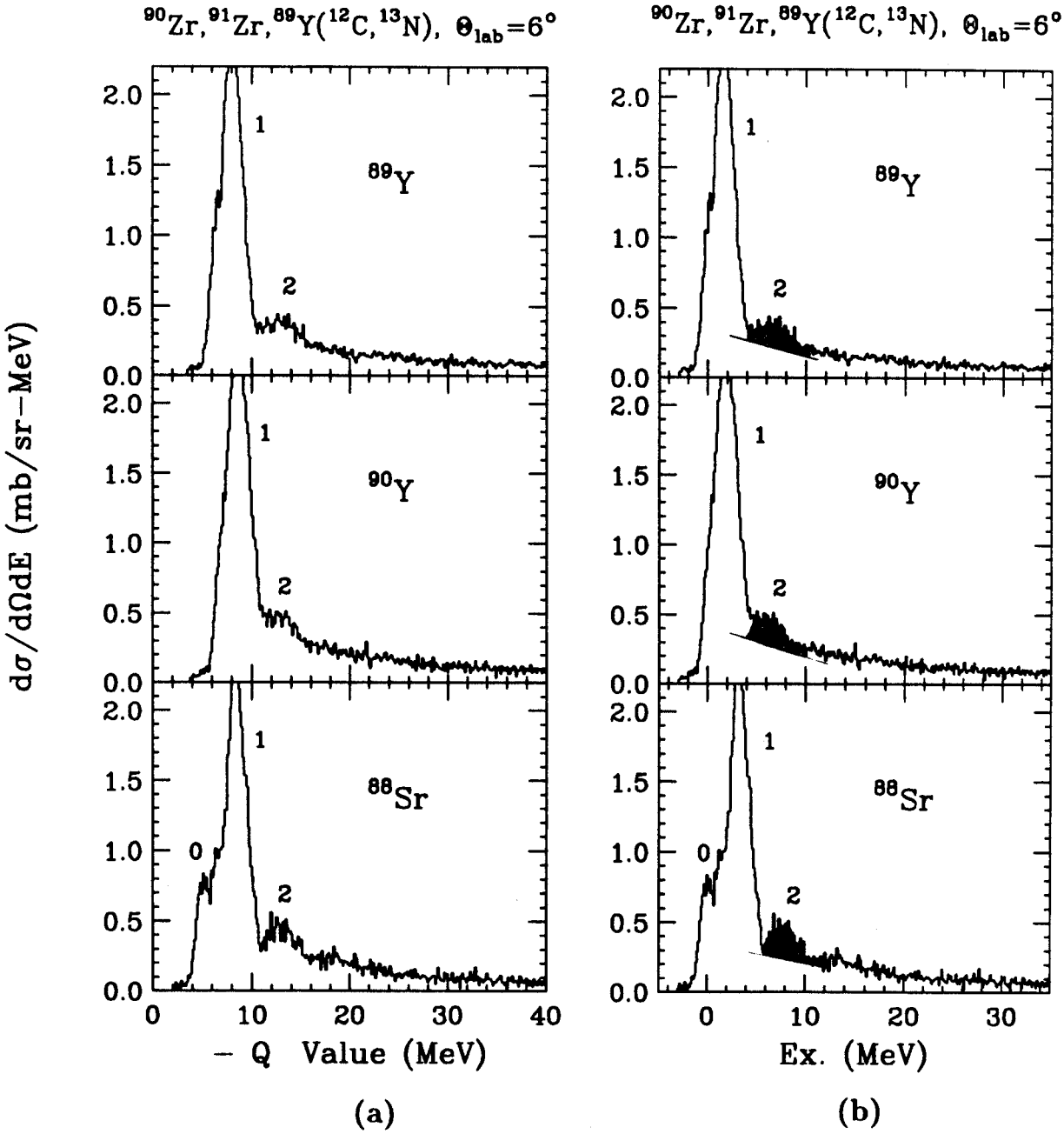

Figure 7.6: Experimental spectra of ^{90}Zr, ^{91}Zr, ^{89}Y (^{12}C,^{13}N) reactions with $E = 30$ MeV/n. The shaded area above the assumed background was used to obtain the cross sections for peaks 2, and to compare the positions.

Table 7.3: Excitation energies for the observed peaks in the (^{12}C,^{13}N) reactions on targets of ^{90}Zr, ^{91}Zr and ^{89}Y. Γ is the full width at half maximum, Q is the reaction Q – value for the corresponding excitation energy and units are MeV. The uncertainty is about 0.3 MeV. σ is the cross section for the shaded area in mb/sr and the uncertainty is about 20%.

	^{90}Zr(^{12}C,^{13}N)^{89}Y				^{91}Zr(^{12}C,^{13}N)^{90}Y				^{89}Y(^{12}C,^{13}N)^{88}Sr			
Peak #	Ex.	Γ	- Q	σ	Ex.	Γ	- Q	σ	Ex.	Γ	- Q	σ
0									0.00	1.5	5.13	
1	1.58	3.0	7.99		1.87	3.0	8.63		3.28	3.0	8.41	
2	6.56	3.5	12.97	1.0	6.09	3.5	12.84	0.9	7.90	3.0	13.03	0.9

where the excitation energies are some higher than in the present experiment. The differences might be caused by the low lying excitation ($1d_{5/2}$, 0.33 MeV) of the ejectile ^{21}Na, while there is no ejectile excitation in ^{13}N. The high energy tail ($Ex. \geq 10$ MeV) can be explained by the pickup of a deep lying proton in the *sd* shell (see fig. 7.1).

The spectrum for the ^{91}Zr(^{12}C,^{13}N)^{90}Y reaction is very similar to that of the reaction with the ^{90}Zr target. When a proton in the $2p_{1/2}$ state is picked up, the $2d_{5/2}$ neutron state couples to the proton hole state ($2p_{1/2}$) and forms a doublet. One member of this doublet is the ground state (2^-), which is shifted to lower energy by 1.87 MeV from peak 1, and the contribution of the ground state to peak 1 is not as clear as in the ^{90}(^{12}C,^{13}C) reaction. Peaks 1 and 2 appeared to be formed by the same hole states as in the reaction with ^{90}Zr target. Significant change in the spectrum due to the coupling between the $2d_{5/2}$ neutron and proton holes is not seen.

In the ^{89}Y(^{12}C, ^{13}N)^{88}Sr reaction, the ground state (peak 0) is shifted to lower energy from the centroid of peak 1 by 3.28 MeV, and it is separated from peak 1 enough to be recognizable as an independent peak. ^{89}Y has one less proton in the $2p_{1/2}$ state compared to ^{90}Zr or ^{91}Zr. The ground state is formed by pickup of a $2p_{1/2}$ proton as in the reactions on the ^{90}Zr and ^{91}Zr targets. But the reaction Q – value for the ground state in the ^{89}Y target is much higher than in the other two targets, by about 1.28 and 1.62 MeV respectively, because the $2p_{1/2}$ proton in ^{89}Y is not paired. This phenomenon is similar to the pickup of a neutron in the $3p_{1/2}$ state seen in the (^{12}C,^{13}C) reactions on targets of ^{208}Pb, ^{209}Bi and ^{207}Pb. Thus the whole spectrum is shifted to higher excitation energy. Peak 2 of this spectrum, which has an excitation energy of 7.9 MeV, appears to be slightly narrower than those from the other two targets, while the total cross section for peak 2 is about the same in all 3 reactions.

The mechanism of forming peak 2 is not understood clearly. This peak is seen in a previous study which the authors designated as "giant resonance like structure"

[Stui 80]. But, from the comparison of the reaction Q – values and excitation energies, the broad peaks 2 show the characteristics of single hole states rather than giant resonance states.

7.6 ^{208}Pb, ^{209}Bi, ^{207}Pb (^{12}C,^{13}N) Reactions

The energy spectra for (^{12}C,^{13}N) reactions on the targets ^{208}Pb, ^{209}Bi and ^{207}Pb with $E_{inc} = 30$ MeV/n at $\theta_{lab} = 9^o$ are shown in fig. 7.7. Excitation energies, reaction Q – values and widths for the observed peaks are given in table 7.4. The favoured angular momentum transfers for this reaction are $2\hbar$ and $3\hbar$. In each reaction, three peaks are observed.

In the ^{208}Pb(^{12}C,^{13}N)^{207}Tl reaction, one strong peak and two weak broad peaks are observed. Peak 1 is observed at an excitation energy of 1.08 MeV with a width of 3 MeV. Similar peaks are also observed in the reactions on ^{209}Bi and ^{207}Pb targets at similar reaction Q – values. This peak appears to consist of the excitation of many low lying states such as $3s_{1/2}$, $2d_{3/2}$, $1h_{11/2}$ and $2d_{5/2}$ states at 0.0, 0.35, 1.35 and 1.67 MeV excitation energy respectively. Individual states are not resolved due to the small energy gap between the states compared to the experimental resolution ($\sim$ 1 MeV).

Peak 2, seen at about 5.4 MeV excitation with a width about 4 MeV, can be accounted for by the hole states $2p_{1/2}$, $1g_{9/2}$, and $2p_{3/2}$. The main contribution seems to be from the $1g_{9/2}$ state due to the large factor of $(2j+1)$. A similar peak centered at 5.4 MeV of excitation energy was also observed in the ^{208}Pb(^{17}O,^{18}F) reaction at $E_{inc} = 376$ MeV [Fern 87].

A very broad peak is seen at excitation energies ranging from 10 to 24 MeV. Peaks at similar excitation are also observed in the reactions with ^{209}Bi and ^{208}Pb targets

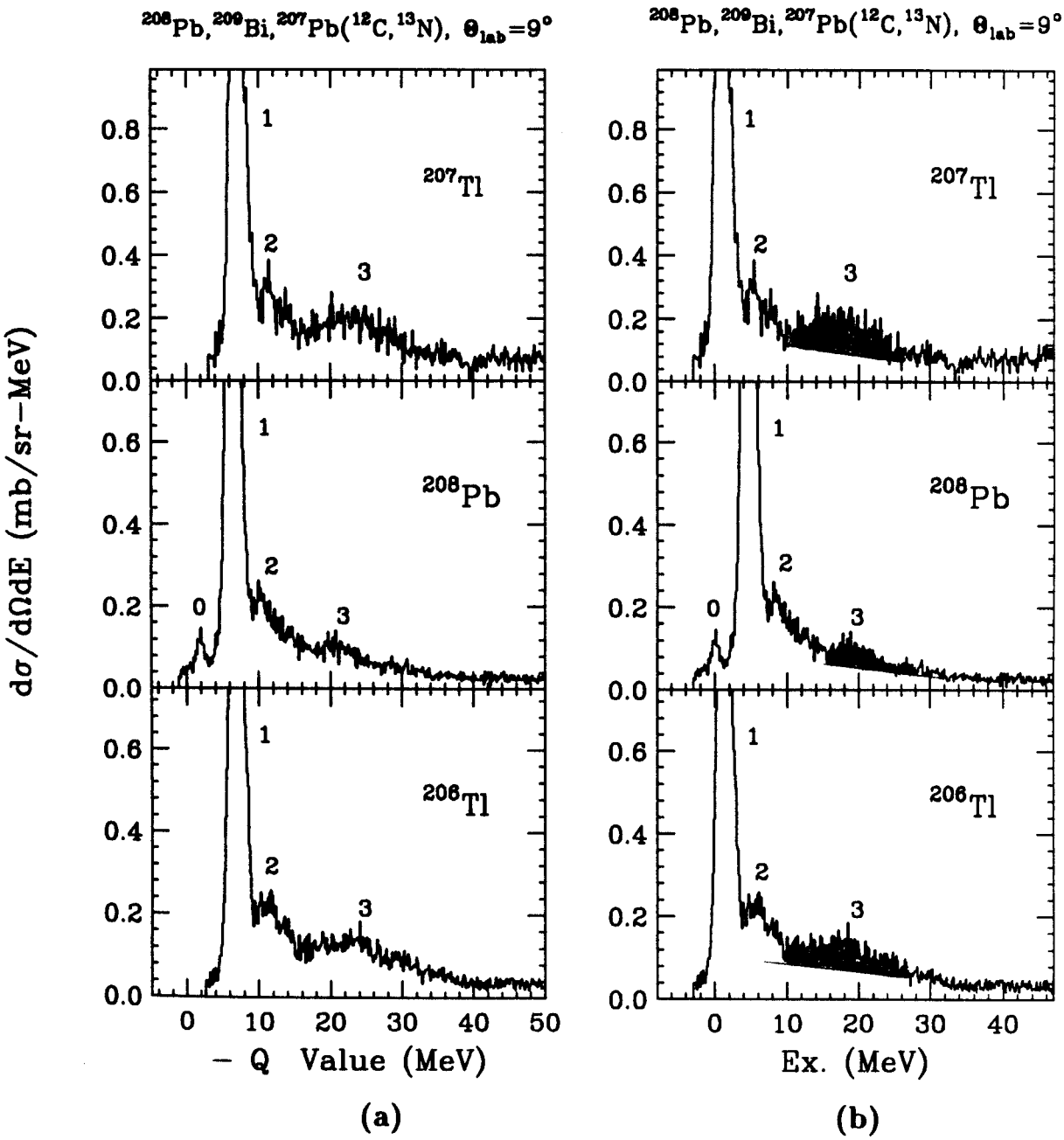

Figure 7.7: Energy spectra of ^{208}Pb, ^{209}Bi, ^{207}Pb (^{12}C,^{13}N) reactions with E = 30 MeV/n. The shaded area above the assumed background was used to obtain the cross sections for peaks 3, and to compare the positions.

Table 7.4: Excitation energies of the peaks observed in the (^{12}C,^{13}N) reactions on targets of ^{208}Pb, ^{209}Bi and ^{207}Pb. Γ is the full width at half maximum, Q is the reaction Q – value for the corresponding excitation and units are MeV. The uncertainty is about 0.3 MeV. σ is the cross section for the shaded area in mb/sr and the uncertainty is about 20%.

	^{208}Pb(^{12}C,^{13}N)^{207}Tl				^{209}Bi(^{12}C,^{13}N)^{208}Pb				^{207}Pb(^{12}C,^{13}N)^{206}Tl			
Peak #	Ex.	Γ	- Q	σ	Ex.	Γ	- Q	σ	Ex.	Γ	- Q	σ
0					0.00	1.0	1.86					
1	1.08	3.0	7.15		5.00	3.0	6.86		1.41	3.0	6.95	
2	5.40	4.0	11.41		8.30	4.0	10.17		5.70	4.0	11.24	
3	17.50	8.0	23.57	1.3	18.50	4.0	20.36	0.6	18.00	8.0	23.54	1.2

in this experiment, but were not observed in the experiments of ^{208}Pb(^{20}Ne,^{21}Na) at E_{inc} = 25,30 MeV/n [Fort 90], ^{209}Bi(^{20}Ne,^{21}Na) at E_{inc} = 48 MeV/n, and ^{209}Bi(^{36}Ar,^{37}K) at E_{inc} = 42 MeV/n [Fras 89]. This structure is not understood at this point.

In the ^{209}Bi(^{12}C,^{13}N)^{208}Pb reaction, four peaks are observed. The ground state (0^+) is obtained by pickup of an $1h_{9/2}$ proton. This state is shifted to lower energy by 5.0 MeV from the centroid of peak 1. Peak 1 is similar to those in the ^{206}Tl and ^{207}Tl spectra in Q – values and widths, but peaks 2 and 3 appear at lower energy (Q – value) by about 1 and 3 MeV respectively compared to the other spectra. The relative energy between peak 1 and peak 2 is about 3.3 MeV, which is smaller than that of the values in the ^{207}Tl spectrum, namely 4.3 MeV. The shapes and the widths of peaks 1 and 2 are very similar in all three spectra. But peaks 3 appear to be slightly different. Peak 3 in the ^{208}Pb spectrum is weaker than peaks 3 of the other two spectra, and is only about half the width. The presence of a $1h_{9/2}$ proton outside the closed shell not only shifted the position of peaks 2 and 3 but also changed the relative energy between peaks 1 and 2, and the width and strength of peak 3.

In the ^{207}Pb(^{12}C,^{13}N)^{206}Tl reaction, the spectrum is very similar to that of ^{208}Pb(^{12}C,^{13}N) reaction. Peaks seen in this reaction can be explained in the same way as in the reaction with the ^{208}Pb target, with the exception of the extra coupling between the neutron hole state ($3p_{1/2}$) and the inner proton hole states. One neutron hole in the $3p_{3/2}$ state did not change the spectrum significantly from that of the ^{208}Pb(^{12}C,^{13}N) reaction, but only shifted the ground state to lower energy by about 0.5 MeV.

When peaks 1 and 2 of all three reactions are compared as functions of reaction Q – values, they appear at similar positions (within 1.3 MeV). This suggests that peaks 1 and 2 of all three reactions are composed mainly of single hole states.

But the comparison for peaks 3 suggests a different result. In each reaction, the width of peak 3 is very large. From the single particle energy levels given in fig. 7.1, $1f_{5/2}$ and $1f_{7/2}$ states may account for this broad peak. This conclusion is also supported by an $(e, e'p)$ experiment [Gale 89]. If peak 3 is a broad single hole state, the reaction Q – value of the peak should not change much from having an extra particle or hole state outside the closed nucleus, while the excitation energy may change due to the shift of ground state energy. On the other hand, if peak 3 is the result of collective motion, the excitation energy should not change much, whereas the reaction Q – value may change [see chap. 4].

The reaction Q – values of the centroid of the peaks of the (^{12}C,^{13}N) reaction are 23.57, 20.36 and 23.54 MeV on ^{208}Pb, ^{209}Bi and ^{207}Pb targets respectively. The reaction Q – value for the ^{209}Bi target is lower than those for the other two targets by about 3.2 MeV. While the corresponding excitation energies are 17.5, 18.5 and 18.0 MeV respectively. The excitation energy for the ^{208}Pb residual nucleus is higher than those for the other two residual nuclei by 1.0 and 0.5 MeV, which are within the resolution limit of this reaction, about 1 MeV. This comparison shows that some of the characteristics of peaks 3 are closer to those of GR states than single particle states.

Chapter 8

Summary

8.1 Summary

Experiments to investigate high lying single particle and hole states were performed at Michigan State University using the K500 superconducting cyclotron. The purpose of the experiments was to study heavy ion single nucleon transfer reactions including the underlying background at high excitation, and to solve a particular question viz. whether the broad peaks, observed in some recent neutron stripping reactions on targets of ^{90}Zr, ^{208}Pb, ^{207}Pb, and ^{209}Bi [Olme 78, Mass 86, Fras 87, Fort 90, Lhen 91], are GR states or single particle states.

Projectiles and targets were chosen based on the requirements to distinguish the nature of the broad peaks. For projectiles, ^{7}Li and ^{12}C were chosen, because the resulting ejectiles such as ^{6}Li, ^{6}He, ^{8}Li, ^{13}N and ^{13}C have very low threshold energies for breakup or no bound excited states except ^{13}C. For the targets, two *even – even* nuclei ^{208}Pb and ^{90}Zr, and their neighboring *even – odd* nuclei, ^{207}Pb, ^{209}Bi, ^{89}Y and ^{91}Zr were chosen.

The reactions used were (^{7}Li,^{6}Li), (^{7}Li,^{6}He), (^{7}Li,^{8}Li), (^{12}C,^{13}C), and (^{12}C,^{13}N) with $E_{inc} = 30$ MeV/n. For the (^{7}Li,^{8}Li) reactions, a limited number of targets were used due to the limited beam time available. The reaction products were analyzed us-

ing the S320 broad range magnetic spectrograph and detected by the standard focal plane detector system (two resistive wire position counters, two ionization chambers, and a plastic scintillator). In the (^{12}C,^{13}C) reactions, elastically scattered ^{12}C particles were blocked by using a "finger". Data obtained were analyzed using the program *SARA*. Particles were cleanly identified using the two dimensional spectra of $\Delta E.vs.E$ and $TOF.vs.POS$.

Shell model calculations were carried out on ^{208}Pb region targets in order to estimate the coupling strengths of $p-p$, $h-h$, and $p-h$, and to observe how the characteristics of the single particle states at high excitation, such as the centroid, width, and strength of the single particle states, depend on these couplings. The results showed that the single particle states, split into multiplets by an extra particle or hole in the target, were spread over several MeV. However, the centroid energies of the multiplets were shifted by at most a few hundred keV from the values of the single particle states. The calculations were compared with the experimental data in chap. 3, and they agreed within a few hundred keV. The results provided evidence that the presence of an extra particle or hole outside a closed shell nucleus does not change the absolute energies significantly, but it may change the excitation energies.

The method used to distinguish GR states and single particle states was described in chap. 4. In GR excitations, the motion is collective, many particles are involved, and the excitation energies vary smoothly with the mass [Youn 76]. There should be no significant change in the excitation energy for a change in mass (A) of 1 unit. In this experiment, giant quadrupole resonances were observed in the reactions ^{90}Zr, ^{91}Zr, ^{89}Y (^{12}C,^{12}C) at E_{inc} = 30 MeV/n. No differences were found in their characteristics, such as the excitation energies and widths. On the other hand, in single particle states, only a few particles are involved, and the excitation energies may vary drastically with the mass. The reaction Q – value is not expected to change

much, at most by a few hundred keV, due to $p-p$ or $p-h$ interactions, as was shown in the shell model calculations. The comparison of the reaction Q – values and excitation energies for certain states provides evidence for the nature of the states.

This method was applied to the broad peaks observed in single nucleon transfer reactions on ^{90}Zr region targets, and ^{208}Pb region targets separately, both for neutron and proton transfer reactions in chapters 5 and 7.

One nucleon stripping reactions were discussed in chap. 5. The spectrum of each reaction was plotted, for ^{90}Zr and ^{208}Pb region targets separately, as a function of both the reaction Q – values and excitation energies. A preference for the high spin states with no spin-flip was observed.

In the (^{7}Li,^{6}Li) reactions with $even-odd$ targets, the couplings between the single particle states and the target's ground state changed the shapes of the peaks of the single particle states significantly at low excitation energies ($Ex. \leq 10$ MeV) for both ^{90}Zr and ^{208}Pb region nuclei. But they did not shift the centroid of the multiplet significantly as indicated in the figures plotted versus reaction Q – values.

In each spectrum with ^{90}Zr region targets, a large broad peak at about $Ex. = 14$ MeV, was observed. The comparisons of the reaction Q – values and excitation energies for these broad peaks showed that the broad peaks have the characteristics of single particle states.

A similar phenomenon was observed in the same reaction on ^{208}Pb region targets. In each spectrum, a weak broad peak was observed at around $Ex. = 10$ MeV. The comparison of the Q – values and excitation energies suggested that the broad peaks arise from the single particle states. The strengths for the broad peaks were much weaker than in the reactions using ^{20}Ne, α, and ^{36}Ar projectiles at similar incident energy per nucleon.

In the (^{7}Li,^{6}He) reactions with ^{90}Zr region targets, the spectra were very similar. The presence of an extra proton particle or hole in the targets did not change the overall shape of the spectra, but some peaks at low excitation were changed significantly in the widths.

In the (^{7}Li,^{6}He) reactions with ^{208}Pb region targets, the broad peaks seen at around 9 MeV of excitation energies appeared at almost the same reaction Q – values, but differed in their excitation energies by about 1.3 MeV. This result again suggests that these broad peaks have the characteristics of single particle states.

Substantial background appeared in all the stripping reactions studied and made it difficult to observe structures at high excitation. An attempt was made to explain the background by calculating the projectile breakup cross section using the theoretical models in chap. 6. Among the many theoretical models, the Serber model, and a semi-classical model developed by Brink and Bonaccorso were used. The Serber model does not match the shape of the experimental spectra except at very high excitation energy ($>$ 35 MeV) in proton stripping reaction. The Brink-Bonaccorso model, does match the shape of the experimental spectra for neutron stripping reactions very well although it does not agree with the shape for the proton stripping case.

The Brink-Bonaccorso model predicted that only about 20% of the total continuum arose from projectile breakup, and the rest of the continuum was predicted to come from the formation of the compound states in the (^{7}Li,^{6}Li) reactions for both ^{90}Zr and ^{208}Pb region targets. The shape of the total cross sections agreed very well with the experimental data for the neutron transfer reactions. But predictions for the (^{7}Li,^{6}He) reactions did not agree well with the experimental data. One possible explanation is that the optical parameters might not be very good for this calculation. Another possibility is that the angle dependence was not considered in the calculation, whereas the experimental data were obtained at a particular angle. It would be

useful to have angle dependent predictions.

The results of the pickup reactions are presented in chap. 7. In the (^{12}C,^{13}C) reactions, substantial ejectile excitation was observed both for ^{90}Zr and ^{208}Pb region targets. The presence of ejectile excitation made it difficult to explore the deep lying hole states. The comparison of the reaction Q – values and excitation energies for the peaks suggested that all the peaks had the characteristics of single hole states.

However, in proton pickup reactions of (^{12}C,^{13}N) on the ^{208}Pb region targets, the experiment suggested a different result. Broad peaks seen at the (^{12}C,^{13}N) reactions on the ^{208}Pb, ^{209}Bi and ^{207}Pb targets, have centroids at reaction Q – values of 23.57, 20.36 and 23.54 MeV, and excitation energies of 17.50, 18.50 and 18.00 MeV respectively. From the comparison of the Q – values and excitation energies, the characteristics of these peaks appear to be closer to those of the GR states than the single hole states. But, it is not very clear whether the GR states were really formed or not, because the peaks are so broad that uncertainties are large. More investigation on this subject is required for the clear understanding.

Bibliography

[Alfo 70] W. P. Alford, J. P. Schiffer and J. J. Schwartz, Phys. Rev. C 3, 860(1970)

[Baym 58] B. F. Bayman, A. S. Reiner and R. K. Sheline, Phys. Rev. Vol.115, 1627(1958)

[Becc 87] F. D. Becchetti, D. A. Roberts, J. W. Janecke, A. Nadasen, C. A. Ogilvie and J. S. Winfield, Annual Report of NSCL, 100(1987)

[Bert 76] F. E. Bertrand, Ann. Rev. Nucl. Sci. 26, 457(1976)

[Bert 81] F. E. Bertrand, Nucl. Phys. A 354, 129c(1981)

[Bert81a] F. E. Bertrand, E. E. Gross, D. J. Horen, J. R. Wu, J. Tinsley, D. K. McDaniels, L. W. Swenson and R. Liljestrand, Phys. Lett. Vol. 103B, 326(1981)

[Bing 70] C. R. Bingham and M. L. Halbert, Phys. Rev. C 2, 2297(1970)

[Bohr 69] A. Bohr and B. R. Mottelson, "Nuclear Structure", Vol.1, 1969

[Bona 85] A. Bonaccorso, G. Picolo and D. M. Brink Nucl. Phys. A 441, 555(1985)

[Bona 87] A. Bonaccorso, D. M. Brink and L. Lo Monaco J. Phys. G 13, 1407(1987)

[Bona 88] A. Bonaccorso and D. M. Brink, Phys. Rev. C 38, 1776(1988)

[Bona 91] A. Bonaccorso and D. M. Brink, Phys. Rev. C 44, 1559(1991)

[Brin 72] D. M. Brink, Phys. Lett. 40B, 37(1972)

[Chom 86] Ph. Chomaz, J. Phys. (Paris) Colloq. 47, C4-155(1986)

[Chom 90] Ph. Chomaz, N. Frascaria, S. Fortier, S. Gales, J. P. Garron, H. Laurent, I. Lhenry, J. C. Roynette, J. A. Scarpaci, T. Suomijarvi, N. Alamanos, A. Gillibert, G. Crawley, J. Finck, G. Yoo, A. Van der Woude, Annual Report, IPN-Orsay 63(1990)

[Craw 73] G. M. Crawley, E. Kashy, W. Lanford and H. G. Blosser, Phys. Rev. C 8, 2477(1973)

[Duff 86] J. E. Duffy, Ph. D. Thesis, Michigan State University, unpublished, (1986)

[Fern 87] M. A. G. Fernandes, F. E. Bertrand, R. L. Auble, R. O. Sayer, B. L. Burks, D. J. Horen, E. E. Gross, J. L. Blankenship, D. Shapira, and M. Beckerman, Phys. Rew. C 36, 108(1987)

[Finc 82] J. E. Finck, Ph. D. Thesis, Michigan state University, unpublished, (1982)

[Fink 73] G. Finkel, D. Ashery, A. I. Yavin, G. Bruce and A. Chaumeaux, Nucl. Phys. A 217, 197(1973)

[Fort 90] S. Fortier, S. Gales, S. M. Austin, W. Benenson, G. M. Crawley, C. Djalali, J. S. Winfield and G. Yoo, Phys. Rev. C 41, 2689(1990)

[Fox 85] R. Fox, Au. A. Vander Molen, B. Pollack and T. Glynn, IEEE Trans. on Nucl. Sci., Vol. NS-32, 1286(1985)

[Fox 89] R. Fox, Au. A. Vander Molen IEEE Trans. on Nucl. Sci., Vol. NS-36, 1608(1989)

[Fras 87] N. Frascaria et al., IPN - Orsay, Rapport Annuel, 41(1987)

[Fras87a] N. frascaria, Y. Blumenfeld, Ph. Chomaz, J. Garron, J. Jacmart, J. Roynette, T. Suomajarvi and W. Mittig, Nucl. Phys. A 474, 253(1987)

[Fras 89] N. Frascaria et al., Proposal for GANIL exp., (1989)

[Fuch 82] H. Fuchs, Nucl. Ins. and Meth. 200, 361(1981)

[Gale 85] S. Gales, C. P. Massolo, S. Fortier and J. P. Shapira, Phys. Rev. C 31, 94(1985)

[Gale 88] S. Gales, Ch. Stoyanov and A. I. Vdovin, Phys. Rep. 166, 125(1988)

[Gale 89] S. Gales, IPNO-DRE-89-43, IPN Orsay (1989)

[Gale 91] S.Gales, Private communications.

[Goan 72] R. E. Goans and C. R. Bingham, Phys. Rev. C, 5, 914(1972)

[Hash 88] H. Hashim and D. M. Brink, Nucl. Phys. A476, 107(1988)

[Herl 72] G. H. Herling and T. T. S. Kuo, Nucl. Phys. A 181, 113(1972)

[Hodg 80] P. E. Hodgson, "Groth Points in Nuclear Physics", Pergamon Press, (1980)

[Gerl 75] E. Gerlic, J.Kallne, H. Langevin-Joliot, J. Vande Viele and G. Duhamel, Phys. Lett. 57B, 338(1975)

[Kasa 83] J. Kasagi, G. M. Crawley, E. Kashy, J. Duffy, S. Gales, E. Geric and D. Friedsel, Phys. Rev. C 28, 1065(1983)

[Knop 70] K. T. Knopfle and M. Rogge, Nucl. Phys. A 159, 642(1970)

[Lanf 74] W. A. Lanford and G. M. Crawley, Phys. Rev. C 9, 646(1974)

[Lhen 91] I. Lhenry, T. Suomijarvi, Y. Blumenfeld, Ph. Chomaz, N. Frascaria, J. P. Garron, J. C. Roynette, J. A. Scarpaci, D. Beaumel, S. Fortier, S. Gales, H. Laurent, A. Gillibert, G. Crawley, J. Finck, G. Yoo and J. Barreto, RIKEN-AF-105, 317(1991)

[Ma 73] Chin W. Ma and William W. True Phys. Rev. 8, 2313(1973)

[Maha 89] C. Mahaux and R. Sartor, Nucl. Phys. A 493, 157(1989)

[Mass 86] C. P. Massolo, F. Azaiez, S. Gales, S. Fortier, E. Gerlic, J. Guillot, E. Hourani, and J. M. Maison, Phys. Rev. C 34, 1256(1986)

[Mats 78] N. Matsuoka, A. Shimizu, K. Hosono, T. Saito, M. Kondo, H. Sakaguchi, Y. Toba, A. Goto and F. Ohatani and N. Nakanishi, Nucl. Phys. A 311, 187(1978)

[Moha 91] M. Mohar, Ph. D. Thesis, Michigan State University, unplished, (1991)

[Mats 80] N. Matsuoka, M. Kondo, A. Shimizu, T. Saito, H. Sakaguchi, A. Goto and F. Ohtani Nucl. Phys. A 337, 269(1980)

[Mcgr 75] J. B. Mcgrory and T. T. S. Kuo, Nucl. Phys. A 247, 283(1975)

[Meij 85] R. J. de Meijer and R. Kamermans, Rev. od Mod. Phys. Vol. 57, 147(1985)

[Merm 88] M. C. Mermaz, E. Tomasi-Gustafsson, B. Berthier, R. Lucas, J. Gastebois, A. Gillibert, A. Boucenna, L. Kraus, I. Linck, B. Lott, R. Rebmeister, N. Schulz, J. C. Sens, and C. Grunberg, Phys. C 37, 1942(1988)

[Merm 87] M. C. Mermaz, B. Berthier, J. Barrette, J.Gastebois, A. Gillibert, R. Lucas, J. Matuszek, A. Miczaika, E. Van Renterghem, T. Suomijarvi, A. Boucenna, D. Disdier, P. Gorodetzky, L. Kraus, I. Linck, B. Lott, V. Rauch, R. Rebmeister, F. Scheibling, N. Schulz, J. C. Sens, C. Grunberg and W. Mittig, Z. Phys. A 326, 353(1987)

[Mona 85] L. Lo Monaco and D. M. Brink, J. Phys. G 11, 935(1985)

[Lim 73] T. K. Lim, Phys. Lett. 44 B, 341(1973)

[Ohls 65] G. G. Ohslen, Nucl. Ins. and Meth. 37, 240(1965)

[Olme 78] C. Olmer, M. Mermaz, M. Buenerd, C. K. Gelbke, D. L. Hendrie, J. Mahoney, D. K. Scott, M. H. Macfarlane and S. C. Pieper, Phys. Rev. C 18, 205(1978)

[Oert 84] W. von Oertzen, H. Lettau, H. G. Bohlen and D. Fick, Z. Phys. A 315, 81(1984)

[OXBA 88] B. A. Brown, A. Etchegoyen and W. D. M. Rae, MSU NSCL Report Num. 524, (1988)

[Ring 80] P. Ring and P. Schuk, "The nuclear many body problem", Springer-Verlag, 1980

[S320 90] H. Plicht and J. Winfield, "THE S320 SPECTROGRAPH MANUAL", (1990)

[Sara 90] B. Sherrill and J. Winfield, "THE SARA DATA ANALYSIS PROGRAM", (1990)

[Serb 48] R. Serber, Phys. Rev. 72, 1008(1948)

[Sher 85] B. M. Sherrill, Ph. D. Thesis, Michigan State University, Dept. of Physics, unpublished, 1985

[Stui 80] A. Stuibrink, G. J. Wagner, K. T. Knopfle, Liu Ken Pao, G. Mairle, H. Riedesel, K. Schindler, V. Bechtold and L. Friedrich, Z. Phys. A 297, 307(1980)

[Suom 89] T.Suomijarivi, D. Beaumel, Y. Blumenfeld, Ph. Chomaz, N. Frascaria, J. Garron, J. Jacmart, J. Roynette, J. Barrette, J. Berthier, B. Fernandez, J. Gastebois, P. Roussel Chomaz, W. Mittig, L. Kraus and I. Link, Nucl. Phys. A 491, 314(1989)

[Suom 90] T.Suomijarivi, D. Beaumel, Y. Blumenfeld, Ph. Chomaz, N. Frascaria, J. Garron, J. Roynette, J. Barrette, J. Scarpaci, B. Fernandez, J. Gastebois, W. Mittig, Nucl. Phys. A 509, 369(1990)

[Ture 88] P. Turek, A. Kiss, A. Djaloeis, C. Mayer-Boricke, M. Rogge and S. Wiktor, J. Phys. G : Nucl. Phys. 14, 771(1988)

[Vour 69] G. Vourvopouros and J. D. Fox, Phys. Rev. Vol.177, 1558(1969)

[Warb 91] E. K. Warbuton and B. A. Brown, Phys. Rev. C 43, 602(1991)

[Winf 91] J. S. Winfield, private communication

[Woud 87] Van Der Woude, Prog. in Part and Nucl. Phys. Vol.18, 217(1987)

[Wu 78] J. R. Wu, C. C. Chang and H. D. Holmgren Phys. Rev. Lett. 40, 1013(1978)

[Wu 79] J. R. Wu, C. C. Chang and H. D. Holmgren Phys. Rev. C 19, 370(1979)

[Yama 81] T. Yamagata, S. Kishimoto, K. Yuasa, K.Iwamoto, B. Saeki, M. Tanaka, T Fukuda, I. Miura, M. Inoue and H. Ogata, Phys. Rev. C 23, 937(1981)

[Youn 76] D. H. Youngblood, J. M. Moss, C. M. Rozsa, J. D. Bronson, A. D. Batcher and D. R. Brown, Phys. Rev. C 13, 994(1976)

[Zism 73] M. S. Zisman, F. D. Becchetti, B. G. Harvey, D. G. Kovar, J. Mahoney and J. D. Sherman, Phys. Rev. C 8, 1866(1973)